Spring August 2014

The Roles of Myosin XI and ROP in Moss Tip Growth

Graham M. Burkart
University of Massachusetts - Amherst

The Roles of Myosin XI and ROP in Moss Tip Growth

A Dissertation Presented
by

GRAHAM M. BURKART

Submitted to the Graduate School of the
University of Massachusetts, Amherst, in partial fulfillment
of the requirements for the degree of

DOCTOR OF PHILOSOPHY

May 2014

Plant Biology Graduate Program

The Roles of Myosin XI and ROP in Moss Tip Growth

A Dissertation Presented

by

GRAHAM M. BURKART

Approved as to style and content by:

_____
Magdalena Bezanilla, Chair

_____
Tobias I. Baskin, Member

_____
Samuel P. Hazen, Member

_____
Patricia Wadsworth, Member

_____
Elsbeth L. Walker, Program Head
Plant Biology Graduate Program

ACKNOWLEDGEMENTS

Ever since I was little, I have been interested in finding out why and how things work. The moment I decided that I wanted to work on plants was when I first read about phytoremediation and two aspects of working on plants really struck me then. The fact that plants can't move means that they have evolved methods for surviving toxic environments that animals are able to move away from, and the concept of bioengineering plants to perform specific tasks. I started thinking about how plants are able to accomplish and regulate all of the complex processes that are required of them both at the level of individual cells and as an organism. This fueled my fascination for cellular and molecular biology, but there are so many people to thank for helping me along the way.

Thanks to all of my family for their support. My dad has always credited my passion for science solely to my mother, but both my dad and my sister have always been supportive of my interest in science even if they do not understand what I am talking about when I explain my work to them. I would like to thank my friends for their support and reminding me that sometimes you need to just relax and let the brain cool down for a bit. Special thanks to my very good friends Harmeet and Katie, who helped me immeasurably in going back to school after my mother passed away. To my undergraduate advisor, Jeanne Harris, thank you for letting me get my first taste of working in the lab, encouraging me to apply for graduate school, and specifically recommending UMass.

To my graduate advisor, Magdalena Bezanilla, thank you so much for the opportunity to work in your lab. I really appreciate that your door has always been

open and that you have maintained such a positive, encouraging, and fun environment in the lab. You have set such an excellent standard to strive for and have been a fantastic mentor. I would also like to thank the other members of my committee, Tobias Baskin, Sam Hazen and Patricia Wadsworth for excellent suggestions as well as reminding me that no matter how much I have learned and understand, I can always dig deeper and learn even more.

Last but certainly not least, I want to thank all of the Bezanilla lab members I have had the privilege of working with over my time here. Thanks to Luis, Julie, and Paula for welcoming me to the lab and helping me get started working with moss. To Robert and Kelli, for being the best across-the-bench neighbors and transformation teammates I could ask for. To Ming, thanks for helping me through my first protein extractions and western blots. To Heidi, thanks for your no nonsense attitude and your spot-on impression of Shelly. To Peter, thanks to you for your company watching hockey games, bringing great Belgian beer over for said games, and your looks of disgust at some classic American food combinations and drinks. To Shu-zon, thanks for being the quiet and sane balance to all of the loud and crazy that the rest of the lab creates. Lastly I would like to thank all of the wonderful undergraduates that have come through the lab, especially Katie and Alexis, who I have depended on so much to help me with my projects in the lab.

ABSTRACT

THE ROLES OF MYOSIN XI AND ROP IN MOSS TIP GROWTH

MAY 2014

GRAHAM M. BURKART, B.S., UNIVERSITY OF VERMONT

Ph.D, UNIVERSITY OF MASSACHUSETTS, AMHERST

Directed by: Professor Magdalena Bezanilla

Because of the large number of myosin XI and ROP genes found in many angiosperms, it has been difficult to determine their precise role with respect to tip growth. In contrast, there are only two myosin XI genes in four *ROP* genes in the moss *Physcomitrella patens*, and within each family the proteins are nearly identical. To determine their role in tip growth using a loss-of-function approach, I used RNA interference (RNAi) and found that both of these proteins are essential for tip growth.

I discovered that the two myosin XI genes are functionally redundant, since silencing of either gene does not affect tip growth. However, simultaneous silencing of both myosin XIs results in severely stunted plants composed of small rounded cells. Consistent with a role in tip growth, I show that a functional, full-length fusion of mEGFP to myosin XI accumulates at a subcortical, apical region of actively growing protonemal cells. Myosin XI RNAi plants also appear to have decreased cellulose in the cell wall, suggesting a role in secretion of cellulose synthases.

I demonstrate that RNAi of the moss *ROP* family yields plants consisting of small spherical cells, similar to myosin XI RNAi, indicating that ROP is also essential

for tip growth. Interestingly, alteration of a *ROP* genomic locus impacts the expression of the other ROP genes indicating that there might be a mechanism for regulating overall *ROP* expression. I found that silencing ROP increases cortical actin dynamics but does not appear to have a specific affect on the microtubule cytoskeleton. Further investigation found that ROP recruits class II formins to the cell cortex where they actively nucleate and elongate actin filaments. Loss of ROP also causes a decrease in intracellular adhesion. Unlike myosin XI RNAi plants, examination of the crystalline cellulose content of the cell wall shows that the deposition of the cell wall is not inhibited in the absence of ROP. Taken together my findings suggest that ROP defines a membrane region where myosin XI delivers secretory vesicles containing cellulose synthase and other materials needed to build new cell wall during tip growth.

TABLE OF CONTENTS

Page

LIST OF TABLES

Table **Page**

LIST OF FIGURES

Figure **Page**

CHAPTER 1

INTRODUCTION

Mechanisms of plant cell expansion

Plant growth occurs through the processes of cell division and expansion. The expansion of plants cells is driven by turgor pressure. With no system of control in place cells would exhibit isotropic growth, equal expansion in all directions. However, expansion is predominantly anisotropic. Plant cells mechanically control expansion via the cell wall, a complex extracellular network of cross-linked sugars, proteins and ions. Delivery of new plasma membrane and cell wall material must be coordinated with the loosening of the existing cell wall for turgor driven expansion to occur. Many plant cells control the direction of expansion by controlling the deposition of cellulose microfibrils. Cellulose microfibrils have the tensile strength of steel and when oriented along one axis, limit expansion on this axis. This encourages expansion along the perpendicular axis and enables plants to generate elongated cell shapes.

A subset of plant cells uses a different mechanism to generate elongated, filamentous cells. In this mechanism, which is commonly referred to as tip growth, new membrane and cell wall material is secreted to the apical region of the plasma membrane. This requires coordination of exocytosis, endocytosis, ion gradients and cytoskeletal components (Hepler et al., 2001; Cheung and Wu, 2008; Craddock et al., 2012). Tip growth is the predominant method of expansion in pollen tubes, root

hairs, and the filamentous tissues (protonemata and rhizoids) of ferns and mosses. The elongation of pollen tubes is required for fertilization to occur and propagate the species. Root hairs and rhizoids are important for obtaining nutrients and water from the soil. Because these cell types are essential for plant growth and propagation, tip growth is an essential process in all land plants. While important factors for tip growth have been identified, the molecular basis for this process is still poorly understood.

Tip growing cells have a vesicle-rich apical region known as the clear zone due to the absence of larger organelles such as plastids or vacuoles. The clear zone is an area of active exocytosis and endocytosis, containing endoplasmic reticulum and Golgi bodies (Derksen et al., 1995; Lancelle and Hepler, 1992). In angiosperm pollen tubes, the clear zone is somewhat defined by reverse fountain cytoplasmic streaming, where the cytoplasm flows towards the cell tip along the cortex and then flowing inward just before the tip and heading back towards the base of the cell (Lovy-Wheeler et al., 2007). In gymnosperm pollen, the streaming pattern is reversed, but flow in both directions depends on the actin cytoskeleton regardless of the streaming pattern (de Win et al., 1996; Justus et al., 2004; Vidali et al., 2001). In contrast, comparatively slow growing moss protonemata do not display cytoplasmic streaming (Furt et al., 2012) so this process is not crucial for tip growth, but may be associated with faster growth rates.

Research in a variety of systems has demonstrated that the actin cytoskeleton is critical for tip growth, as it is thought to regulate where and when cell wall material is secreted. In general, tip growing cells have actin longitudinally

oriented along the cell shank (Cheung and Wu, 2008; Era et al., 2009; Lovy-Wheeler et al., 2005). At the base of the clear zone there is a highly dynamic cortical actin structure that dissipates towards the tip of the cell where the actin becomes more cytoplasmic and less dense (Cheung and Wu, 2008; Era et al., 2009; Lovy-Wheeler et al., 2005). In cellular processes involving actin, the actin cytoskeleton does not act as a static scaffold, rather constant turnover of actin filaments as well as formation of higher order actin bundles occurs. In contrast to microtubules, which are dynamically unstable polymers capable of spontaneous polymerization and depolymerization, the regulation of filamentous actin dynamics requires actin binding proteins. Additionally, control of where actin is assembled or disassembled is often controlled upstream by small GTPases and their effectors (Jaffe and Hall, 2005).

Numerous studies have demonstrated that changes in expression or loss of actin binding proteins involved in filament severing, nucleation, and bundling impact tip growth and actin organization. The Bezanilla lab has demonstrated that actin binding proteins such as profilin, actin depolymerizing factor (ADF), and formin are essential for polarized growth (Vidali et al., 2009b; Vidali et al., 2007; Augustine et al., 2008). However, not all actin binding proteins are essential for tip growth. Mutations in subunits of the actin related protein (Arp) 2/3 complex, which generates new actin filaments, result in reduced and wavy growth as well as branching of arabidopsis root hairs (Mathur et al., 2003a; Mathur et al., 2003b). Silencing of the Arpc1 member of this complex in moss does not lead to a loss of tip

growth, but does result in an inability to differentiate into new cell types (Harries et al., 2005).

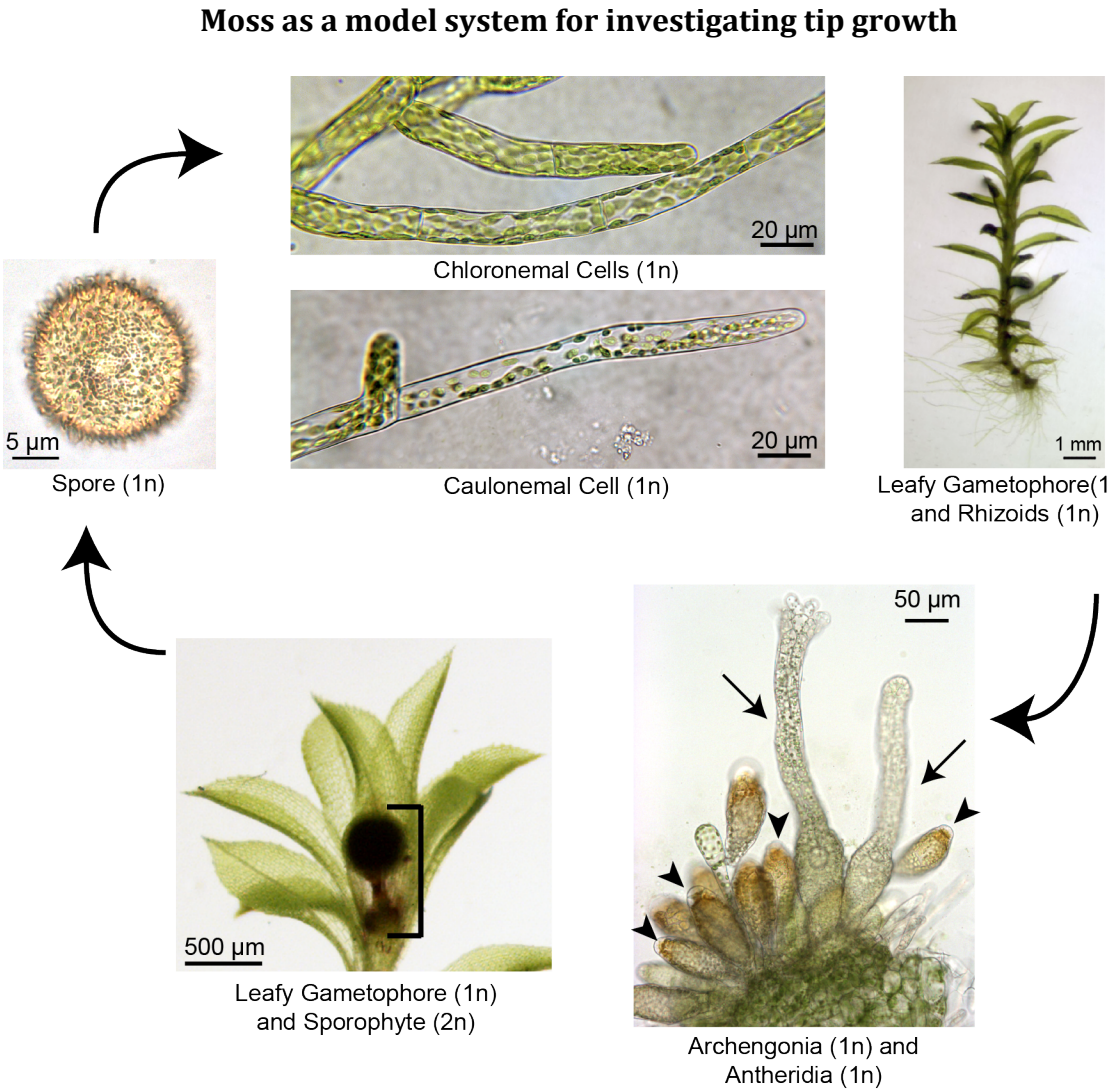

Figure 1.1. *Physcomitrella patens* life cycle. Cell types are labeled below images. Haploid (1n) and diploid (2n) tissues are indicated. Straight arrows point to archegonia, and arrowheads point to antheridia. Archegonia and antheridia develop near the apex of the gametophore. A bracket marks the sporophyte. Image modified from Prigge and Bezanilla, 2010.

The moss *Physcomitrella patens* is an ideal model system for studying tip growth. Moss tissue at most any stage of the life cycle (Figure 1.1) can be homogenized to induce dedifferentiation and regeneration of protonemal filaments,

ensuring a constant and abundant supply of tip growing cells. Haploid moss spores germinate to form filamentous outgrowths known as protonemata. The protonemal tissue is composed entirely of two types of tip growing cells, chloronemata and caulonemata. Chloronemal cells are the basal cell type as they are the first to emerge from the spore. Typically chloronemal cells have a higher chloroplast density and grow slower compared to caulonemal cells, which develop seven days after spore germination. Through tip growth and filament branching these protonemal filaments provide a network for acquiring nutrients. As the plant matures, some branching sites form a bud that gives rise to the gametophore, a central shoot containing leafy structures known as phyllids. The gametophore is anchored by forming rhizoids. The antheridium and archegonium (male and female organs, respectively), both form upon the same gametophore and fertilization by the motile sperm generates the sporophyte, the only diploid tissue throughout the life cycle. The sporophyte undergoes meiosis to generate haploid spores to complete the cycle (Figure 1.1).

Because the predominant part of the life cycle is haploid and the genome has been sequenced (Rensing et al, 2008), moss is an ideal system for reverse genetics approaches. It is also the only land plant known to undergo efficient homologous recombination when transformed with DNA, allowing for targeted gene knockouts and replacements (Schaefer and Zryd, 1997). In addition, almost all tissues in *Physcomitrella patens* are a single cell layer thick, making moss a good system for subcellular imaging. Establishment of a rapid transient RNAi assay in moss (Bezanilla et al., 2005) allows for loss of function studies to be performed on

essential genes as well as functionally redundant gene families (Figure1.2). This RNAi assay uses a stable line expressing a nuclear localized GFP-β-glucoronidase fusion protein (NLS-GFP-GUS). RNAi constructs contain inverted sequence repeats from GUS and the gene(s) of interest (Figure 1.2). When the RNAi construct is transiently expressed in the NLS-GFP-GUS line the inverted sequence repeats fold back to form double stranded RNA, silencing the NLS-GFP-GUS trancripts in addition to those of the gene(s) of interest. Plants undergoing active gene silencing are identified by loss of the nuclear GFP:GUS signal (Figure 1.2). Tip growth phenotypes can be observed within one week of transformation, allowing for quick assessment of loss of function phenotypes of single genes or entire gene families.

In moss protonematal cells, the cortical actin cytoskeleton is highly dynamic, with filament polymerization, depolymerization, translocation, bundling, and severing events occurring on the second time scale. Moss plants defective in actin filament severing and plants treated with the actin stabilizing drug jasplakinolide have severely reduced actin dynamics (Augustine et al., 2008; Vidali et al., 2010). Moss protoplasts regenerated on media containing latrunculin B, which inhibits actin filament polymerization by binding actin monomers, are unable to generate tip-growing cells (Harries et al., 2005). It is generally thought that the apical actin is essential for vesicle transport and regulates the location and rate of cell wall material deposition. However, our understanding of the coordination and regulation of actin during tip growth is far from complete.

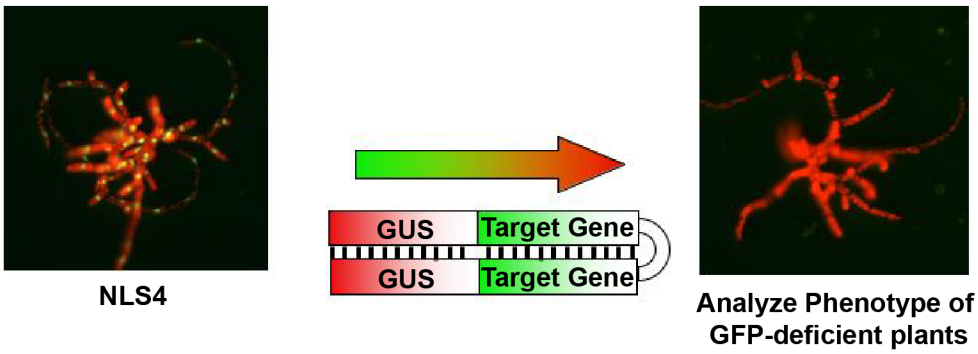

Figure 1.2. Transient RNAi assay. A fluorescence micrograph of a stable moss line (NLS4; image on left) that expresses nuclear localized-GFP-GUS, red is the chlorophyll autofluorescence. Protoplasts from the NLS4 line are transformed with an RNAi construct that generates double-stranded RNA containing inverted-repeats of sequences from GUS as well as gene(s) of interest linked by a loop region. Double-stranded RNA triggers the RNAi pathway, which silences transcripts complementary to the double-stranded RNA sequence. Double-stranded RNA silences the nuclear localized-GFP-GUS sequence as well as the gene(s) of interest. Plants actively silencing the nuclear GFP reporter are easily distinguishable from non-silenced plants because they lack green nuclei (image on right). This allows loss-of-function analysis of the target gene(s). The plant on the right is derived from a single protoplast after 1 week of growth.

Here, I will be investigating the role of two gene families in moss, class XI myosins and a family of small Rho-like GTPases called Rho of plants (ROP). Both have been shown to affect polarized growth of root hairs or pollen tubes in seed plants. However in seed plants, both of these proteins are members of large gene families, which has made assessing their functions challenging. Previous studies have mainly used dominant negative mutations, over-expression or deletions of a subset of gene family members. The powerful genetic tools available in moss have allowed me to use a loss-of-function approach to characterize the function of these two gene families in tip growth.

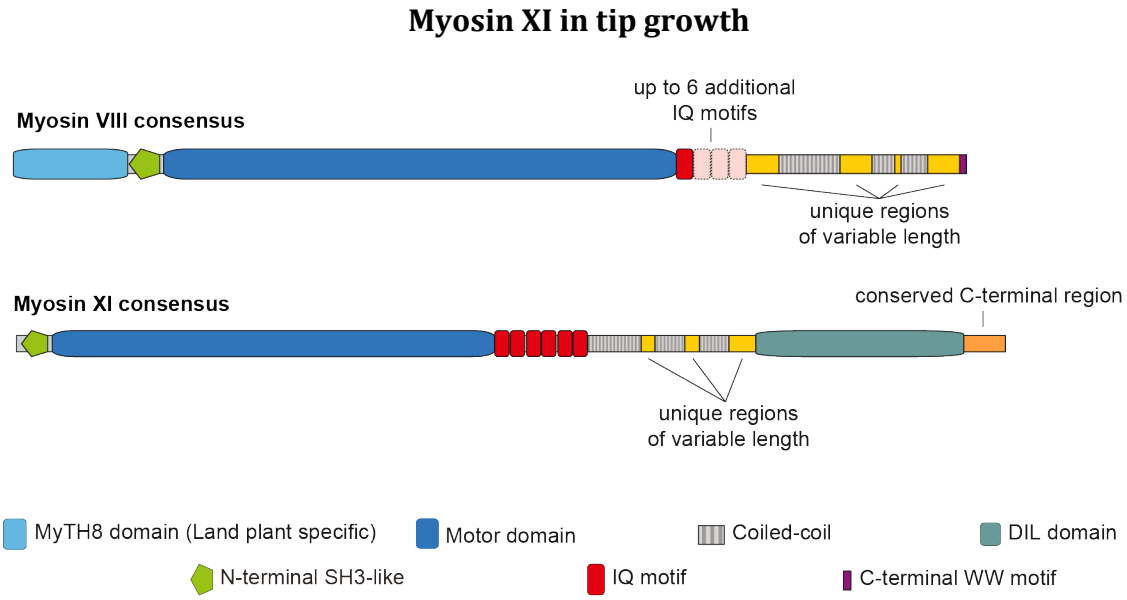

Figure 1.3. Domain structures of plant myosins. Consensus domain structures of myosin VIII (top) and myosin XI (bottom) were reached by comparing the gene families across the plant lineage. Domains are color coded according to the key. Image modified from Muhlhausen and Kollmar, 2013.

It is generally accepted that tip growth is achieved by deposition of membrane and enzymes for cell wall synthesis to the growing region of the cell. This deposition is thought to occur by transporting vesicles along actin filaments to the cell apex. Thus, one role for the actin network is to act as a highway for myosin-mediated transport of secretory vesicles, thereby regulating the location and rate of cell wall material deposition. Land plants have two families of myosins: class VIII and class XI. While both classes have in common the N-terminal SH3-like domain, a motor domain, IQ motifs, and coiled-coil regions, additional domains differentiate between the two myosins (Figure 1.3). Class VIII myosins have a MyTH8 domain that is unique to land plants and also a C-terminal WW motif. The C-terminus of class XI myosins has a DIL domain that is similar to the secretory vesicle binding

domains of class V myosins in yeast (Sattarzadeh, et al., 2011) (Figure 1.3). The conserved C-terminal region is thought to interact with the DIL domain (Muhlhausen and Kollmar, 2013). Class XI myosins are most similar to class V myosins from animals and fungi (Mooseker and Cheney, 1995), in which homology is highly conserved throughout the protein, from the motor to the globular tail domain (Li and Nebenfuhr, 2007). Based on this striking similarity and the fact that class V myosins are known to be responsible for vesicle transport, class XI myosins have been considered the best candidates for carrying out polarized secretion in plant cells.

In support of this, myosin XIs have been shown to be necessary for cytoplasmic streaming and subcellular organelle transport in vascular plants and the Characean algae (Shimmen and Yokota, 2004; Avisar et al., 2012). Analyses of knockout lines and dominant negative approaches has implicated a subset of these myosins in organelle transport and root hair elongation (Ojangu et al., 2007; Peremyslov et al., 2008; Prokhnevsky et al., 2008). Some mutants also have stunted root hairs, although polar outgrowths are still present (Ojangu et al., 2007; Peremyslov et al., 2008; Prokhnevsky et al., 2008). More recent work has implicated myosin XI in the transport of secretory vesicles on actin (Peremyslov et al., 2012; Peremyslov et al., 2013), and in regulating nuclear movement and shape (Tamura et al., 2013). Loss of multiple myosin XI genes causes progressively worse defects in plant development and actin organization (Peremyslov et al., 2010; Ojangu et al., 2012). The dominant-negative approach, which relies on over-expression of the tail domain of myosin XI, has been used to investigate global loss of myosin XI function

(Sparkes et al., 2008). It is expected that over-expression of the tail domain will sequester critical tail-interacting proteins. These studies have lead to somewhat contradictory results (Reisen and Hanson, 2007; Sparkes et al., 2008), which may result from different levels of over-expression. In addition, the myosin tails may sequester other essential molecules, thus further confusing the analysis.

Prior to the work in this thesis, the localization of full-length myosin XI in live plant cells was not known. Using antibody localization in fixed cells, a subset of myosin XIs have been found to be associated with peroxisomes (Hashimoto et al., 2005), while others have been identified on the endoplasmic reticulum (Yokota et al., 2008) and at the tip of pollen tubes (Yokota et al., 1995). *In vivo* studies analyzed the localization of fluorescently tagged globular tail (Li and Nebenfuhr, 2007; Reisen and Hanson, 2007; Sattarzadeh et al., 2011; Sattarzadeh et al., 2013) or head domains (Walter and Holweg, 2008), but not a full-length molecule. Fluorescent tail constructs localize to peroxisomes, and at a lower frequency to Golgi and mitochondria (Li and Nebenfuhr, 2007; Reisen and Hanson, 2007). In contrast, expression of the motor domain of myosin XI accumulates on actin filaments (Walter and Holweg, 2008). These contradictory results underline the importance of using the entire molecule to accurately assess subcellular localization.

Functional characterization of myosin XI has also been challenging due to the large number of isoforms present in many plants. For example, in arabidopsis there are thirteen class XI myosins (Reddy and Day, 2001; Peremyslov et al., 2008). Moss offers a simpler system to investigate myosin XI function and regulation; in contrast to the 13 isoforms present in arabidopsis, there are only three myosin XI genes in

moss. In chapter 2, I describe my contributions to our published work (Vidali et al., 2010) analyzing the role of myosin XI in tip growth using RNAi to simultaneously silence all myosin XI genes expressed in protonemata.

ROP in tip growth

ROPs are a plant-specific family of small GTPases. ROPs act as molecular switches: they are active in a GTP-bound state and after hydrolysis of GTP to GDP they are inactive. In their active state, ROPs have been shown to moderate a number of cellular processes (Craddock et al., 2012). Small GTPases have highly conserved structural motifs required for nucleotide binding and hydrolysis as well as membrane localization. In particular, ROP has five motifs (G1-G5) that are highly conserved in animal and fungal Rho GTPases (Figure 1.4). The catalytic GTPase domain consists of three structural motifs: switch I, switch II, and the phosphate-binding loop (p-loop). During GTP binding and hydrolysis, the switch I and II motifs undergo conformational changes. G1 contains the p-loop, which binds α and β phosphate groups (Paduch et al., 2001; Berken, 2006). Mutations in the P-loop impact hydrolysis and nucleotide exchange capability. The G2 motif is switch I and binds magnesium ions as well as effector molecules such as GTPase activating proteins (GAPs) when in the GTP bound conformation (Paduch et al., 2001; Spoerner et al., 2001). Switch II (G3) binds γ phosphate groups along with magnesium ions (Zheng and Yang, 2000). Just downstream of switch II there is a potential phosphorylation site (Zheng and Yang, 2000). The G4 and G5 loops are involved in nucleotide binding (Paduch et al., 2001). Lying between the G4 and G5

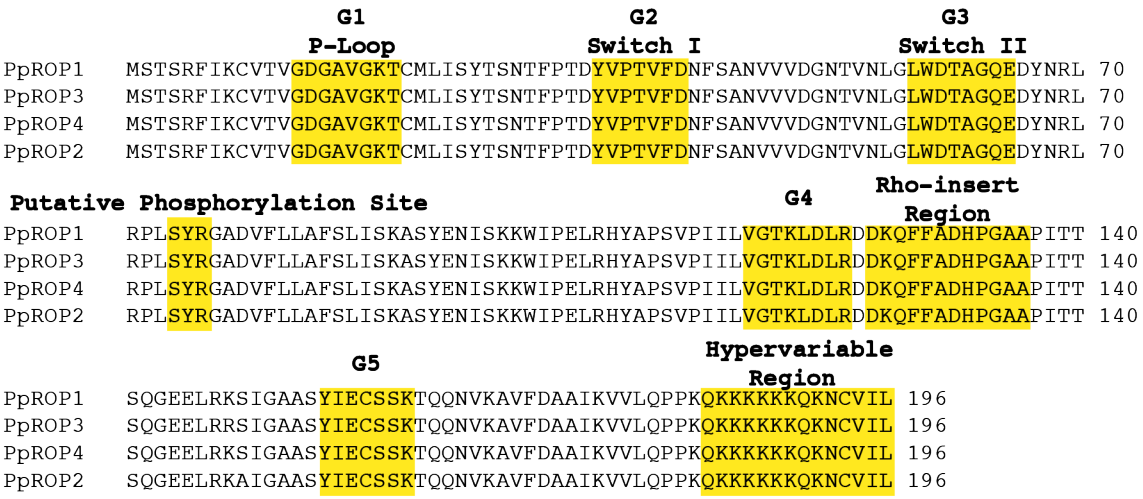

Figure 1.4. Highly conserved funtional domains in *Physcomitrella patens ROP* gene family. G1-G3 domains form the catalytic GTPase domain. The G1 domain binds phosphate groups. The conformations of the G2 and G3 domains change depending on whether ROP is bound to GTP or GDP. A putative phosphorylation site exists downstream of the G3 domain. The G4 and G5 domains are involve in nucleotide binding. Rho insert region is a sequence unique to Rho GTPases for family specific interactions. The hypervariable region determines the type of lipid modification that happens at the the C-terminus.

loops is the Rho-insert region, a region that is unique to Rho GTPases and is required for interaction with guanine nucleotide dissociation inhibitors (RhoGDIs) (Wu et al., 1997). Located at the C-terminus of ROP is a hypervariable region that determines membrane localization by lipid modification (Zheng and Yang, 2000). ROPs are divided into two types based on the lipid modification, which allows for attachment to the plasma membrane; type I ROPs are prenylated by geranylgeranylation while type II ROPs are attached by S-acylation (Sorek et al., 2007). Only type I ROPs are found in moss.

Numerous studies have examined the impact of ROP on tip growth. Much of this has been accomplished through the use of constitutively active and dominant negative mutants. Over-expression of constitutively active ROP causes ballooning tips in pollen tubes (Gu et al., 2006; Li et al., 1999; Jones et al., 2002; Fu et al., 2002). Over-expression of dominant-negative ROPs causes inhibition and arrest of growth

in both root hairs and pollen tubes (Li et al., 1999; Jones et al., 2002; Fu et al., 2002; Fu et al., 2001). ROP has also been linked to the regulation of calcium influxes at the tip (Li et al., 1999; Gu et al., 2005). ROP has been repeatedly reported to localize to the apical cell membrane in both pollen tubes and root hairs of various species through the use of GFP-ROP fusion proteins as well as immunolocalization (Gu et al, 2003; Molendijk et al., 2001). Arabidopsis *ROP2* has also been localized to the exit sites of the endoplasmic reticulum using immunolocalization (Zhang et al., 2010). These studies have suggested that ROP is critical for tip growth, and potentially defines a membrane domain for deposition of secretory vesicles.

While there is evidence that ROP is a master regulator for cell polarity and tip growth, there have been a limited number of studies investigating ROP loss-of-function mutants (Venus and Oelmuller, 2013, Singh et al., 2012). Phenotypes arising from expression of constitutively active and dominant negative mutant forms can be difficult to interpret since they might arise from titrating out ROP interactors, rather than a direct result of ROP activity. I investigated the role of ROP in the regulation of tip growth in moss using a loss-of-function approach. Moss is an excellent system for this approach because there are only four ROP genes compared to eleven in arabidopsis (Winge et al, 2000), making a loss-of-function approach more manageable. Another reason moss is a great system for studying ROP function is because in seed plants ROP is involved in many different processes in many different plant tissues, while young moss tissue is entirely composed of tip growing cells. This facilitates focusing specifically on the role of ROP in tip growth.

Numerous studies have examined the impact of ROP on actin dynamics and tip growth. Over-expression of constitutively active ROP causes delocalization of apical actin (Gu et al., 2006; Li et al., 1999; Jones et al., 2002; Fu et al., 2002). Over-expression of dominant-negative ROPs disrupts and inhibits apical actin formation in both root hairs and pollen tubes (Li et al., 1999; Jones et al., 2002; Fu et al., 2002; Fu et al., 2001). While changes in actin structures have been observed in previous studies, a quantitative analysis of the dynamic state of the actin cytoskeleton has not been performed.

Studies in arabidopsis have discovered that some ROPs are involved in deposition or disassembly of microtubules (Xu et al., 2010; Oda and Fukuda, 2012; Lin et al, 2013). Based on what has been reported, it seems that there is somewhat of a division of labor amongst arabidopsis ROPs with specific genes regulating either the actin or microtubule cytoskeletons. Since the four moss ROPs are virtually identical, it raises the question of whether they are capable of regulating both actin and microtubules. While microtubules do not play an essential role in tip growth, I can readily generate loss-of-function mutants to investigate the effect of the absence of ROP on the microtubule cytoskeleton.

To further study the role of ROP in tip growth, I investigated proteins that interact with ROP. There are two families of plant specific ROP effectors that have been identified: ROP-interacting CRIB motif containing proteins (RICs) and interactors of constitutively active ROP/ROP-interactive partners (ICRs/RIPs) (Wu et al., 2001; Lavy et al., 2007; Li et al., 2008). In arabidopsis, ICR1/RIP1 was shown to bind SEC3A, a component of the exocyst complex (Lavy et al., 2007), linking ROP

to exocytosis. However, I found no ICRs/RIPs in moss. *AtRIC4*, *AtRIC3* and *AtRIC1* are ROP effectors that during the formation of lobes in arabidopsis leaf pavement cells, regulate the actin (*AtRIC4* and *AtRIC3*) and microtubule (*AtRIC1*) cytoskeletons (Xu et al., 2010). Unfortunately, RNAi of the sole *RIC* in moss does not have a polarity phenotype, suggesting that this interaction with ROP either does not occur in moss or RIC is an effector for a different cellular process. Since these known effectors of ROP are absent in moss or have no tip growth phenotype when silenced, I focused on investigating the proteins that control the activity of ROP.

ROP activity is regulated by cycling between the active (GTP bound) and inactive (GDP bound) conformations (Figure 1.5). Small GTPase superfamilies have family specific regulators of the GTPase activity. Rho guanine nucleotide exchange factors (RhoGEFs) activate ROP by facilitating the exchange of free GTP for bound GDP, activating ROP. The active GTP-ROP form can interact with downstream effectors. Deactivation of ROP is carried out through GTPase activating proteins (RhoGAPs), which induce the native GTPase activity of ROP. A third class of protein, guanine nucleotide dissociation inhibitors (RhoGDIs) remove inactive ROP from the membrane so that it can be recycled and moved to where ROP activity is required (Klahre et al., 2006; Carol et al., 2005). Confirming their regulatory roles, over-expression of RopGEFs results in depolarized growth while over-expression of tobacco RhoGDI and RhoGAP lead to inhibition and arrest of pollen tube growth (Gu et al., 2006; Klahre et al., 2006; Carol et al., 2005). These three proteins are thought to regulate the level and localization of active ROP in the cell, confining ROP signaling to the apical membrane during tip growth.

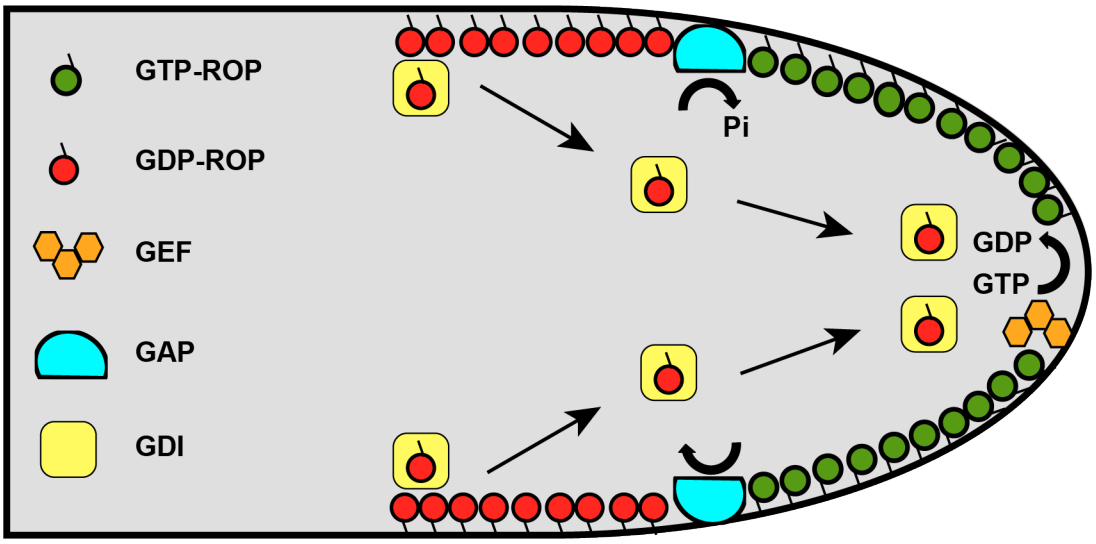

Figure 1.5. Current model of the regulation of ROP activity during tip growth. Inactive ROP (red) releases GDP and binds GTP to become active (green) when interacting with GEF (orange). As active ROP approaches the shank of the cell it is inactivated by hydrolyzing GTP to GDP when it interacts with GAP (blue). Inactive ROP is removed from the membrane by GDI (yellow) and kept inactive as it is recycled back to the tip where it can be reactivated.

My objective in this thesis is to build upon the current understanding of tip growth in plants. To accomplish this, I examined how myosin XI and ROP are involved in this process using a whole gene family loss-of-function approach. The powerful molecular tools available in moss allowed me to examine how these proteins affect the actin cytoskeleton. By studying the regulators of ROP activity, I am able to examine how mis-regulation of ROP impacts tip growth. Together, my findings reveal links between essential polarized growth components that give insight as to how tip growth is accomplished at the molecular level in plants.

CHAPTER 2

THE ROLE OF MYOSIN XI IN TIP GROWTH

P. patens has three myosin XI genes

Detailed analysis of the *P. patens* genome revealed the presence of eight myosin motor domains. On the basis of sequence similarity with other plant myosins, three can be assigned to class XI and five to class VIII. No other sequences related to the myosin motor domain are present in the genome. I investigated whether these three myosin XI motor domains are expressed using reverse transcriptase-PCR of protonemal mRNA. Only myoXIa and myoXIb are detectably expressed and will be the focus of this study. Both of these have all sequences encoding domains present in canonical myosin XI proteins.

The intron-exon distribution of the moss myosin XI genes are conserved with that of arabidopsis *MYA1* (Figure 2.1). In both cases, the ATG codon is located at the end of the first exon; this characteristic is also conserved in *MYA1*. The 5' and 3' untranslated regions (UTRs) were assigned based on the presence of EST sequences. The intron-exon boundaries are conserved between the *MYA1* gene and both moss myosin genes. The main differences are that *MYA1* has significantly shorter introns and has one less exon, which appears to be due to a fusion of the corresponding exons 35 and 36 of the *P. patens* myosin genes. At the nucleotide level, the moss myosin open reading frames are 88% identical to each other; at the protein level they are 94% identical (98% similar). When compared with *MYA1* across the whole molecule, the moss proteins are 63% identical (79% similar).

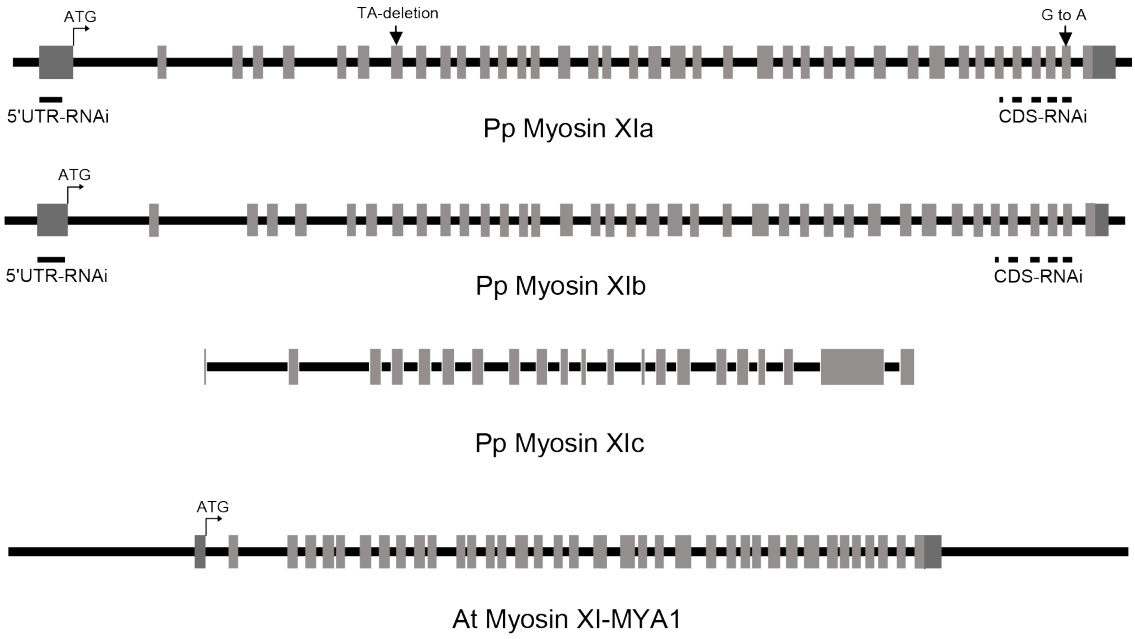

Figure 2.1 Schematic diagram of myosin XI genes. Exon sequences are represented by light grey boxes and intron sequences by black lines. The untranslated regions are represented by dark grey boxes. Intron-exon boundaries were determined by comparing the cDNA and genomic sequences. Sites used to design the RNAi constructs are indicated by black lines underneath the exons. The sites for the two variants observed in the transcripts are indicated by arrows. Scale bar is 1000bp.

A full-length cDNA (pdp20423) encoding myoXIa was obtained from one of the EST collections (http://moss.nibb.ac.jp/). Sequencing revealed that pdp20423 contains two sequence variants not present in the genomic sequence. I verified the genomic sequence by sequencing PCR products spanning the regions encompassing the variants. The first variant is a two-base pair deletion after position 807, which generates a premature stop codon after amino acid 270 (Figure 2.1). The second variant is a missense mutation, resulting in a change from threonine to alanine at position 1477. To ensure that these sequence variants are present in the mRNA pool and not the result of reverse transcription infidelity, I sequenced cDNA synthesized from protonemal mRNA. For variant 1, I identified one of three cDNA fragments

containing the genomically encoded sequence. For variant 2, I sequenced eleven cDNA fragments, but none contained the genomically encoded sequence. However, inspection of EST sources revealed the presence of at least one clone containing the genomic sequence (EST- BJ960751.1). Although the threonine to alanine change is located at a residue conserved in many myosin XIs, an alanine substitution does not affect myosin XI function during tip growth (see below).

Myosin XI is essential for protonemal tip growth

To investigate the role of myosin XI in tip growth, I used RNAi to silence the expression of myoXIa and myoXIb in one-week-old moss plants, which develop entirely from tip-growing protonemal cells. I used a previously established robust system for fast gene silencing in *P. patens* in which a reporter line expressing a GFP fusion of GUS with a nuclear localization signal is used to report on the activity of gene silencing (Bezanilla et al., 2005). This reporter line has a strong nuclear GFP signal that is suppressed by the expression of GUS inverted repeats. Using silencing constructs containing sequences of GUS fused to a gene of interest enables the monitoring of gene suppression. This system has been used successfully to silence the expression of single genes and entire gene families (Vidali et al., 2007; Augustine et al., 2008; Vidali et al., 2009b).

Our lab generated an RNAi construct, myoXIa+bCDS, that contains regions of the coding sequence of both myoXIa and myoXIb (Figure 2.1). These regions were located at the carboxy terminus of the protein sequence, where the two molecules are slightly more divergent and in particular, are divergent from other myosins, plausibly preventing any silencing of class VIII myosins. I transformed the RNAi

construct into moss protoplasts, and allowed single protoplasts to regenerate into whole plants for one week. Expression of myoXIa+bCDS in one-week-old plants causes a loss of growth polarity (Figure 2.2A) The plants lacking nuclear GFP fluorescence are severely stunted and composed of small, spherical cells, demonstrating that myosin XI is essential for tip growth.

To quantify the morphological changes produced by silencing of myosin XI, I evaluated two parameters: plant area and solidity. Area is estimated by the thresholded chlorophyll autofluorescence acquired from images of individual silenced plants. Solidity is a unit-less parameter defined as the ratio of area over convex hull area. The convex hull area is calculated from the shape of the thresholded chlorophyll autofluorescence. Solidity values approaching one correspond to rounder, more solid objects in which the area and convex hull area are similar. Solidity values approaching zero correspond to more branched structures. Since control plants are highly branched and elongated, the solidity value provides a sensitive measure of the degree of polarization. Silencing of myosin XI significantly reduces the total area of plants with a concomitant increase in solidity (Figure 2.2B).

To determine if the two myosin XI isoforms are functionally redundant with respect to tip growth, specific RNAi constructs were generated, targeting sequences from the 5'UTR of each gene. Expression of either myoXIa5'UTR or myoXIb5'UTR has no effect on plant size or polarity (Figure 2.2A, B). Importantly, expression of an RNAi construct containing the 5’UTR sequences from both myoXIa and myoXIb,

myoXIa+b5'UTR, phenocopies the coding sequence construct, generating small plants with a high solidity value (Figure 2.2A, B).

To ensure that myosin XI transcripts were silenced in GFP-deficient plants, I picked plants lacking GFP fluorescence and isolated RNA. I performed real time RT-PCR analysis with primers specific for the myoXIa and myoXIb transcripts. In plants transformed with the control RNAi construct, myoXIa is expressed 60-200 fold higher than myoXIb (Figure 2.2C, D). When transformed with myoXIa+bCDS or myoXIa+b5'UTR, the total myosin XI transcript levels are reduced by 52% or 69%, respectively (Figure 2.2C), with the majority of the reduction detected in the myoXIa transcript. Since I did not observe a phenotype when silencing only myoXIa with the myoXIa5'UTR construct, I hypothesized that myoXIb transcript levels are elevated to compensate for the loss of myoXIa. To test this, I used quantitative real time RT-PCR to measure levels of myosin XI transcripts in plants transformed with either myoXIa5'UTR or myoXIb5'UTR, the RNAi constructs specific for each gene. In the myoXIa5'UTR transformed plants, I detected a 90% reduction in the myoXIa transcript, and a concomitant 690% increase in the myoXIb transcript (Figure 2.2D). These data support the conclusion that two myosin XI genes are functionally redundant and suggest that there is a threshold level of myosin XI transcript required for tip growth. Interestingly, in control plants the myoXIa transcript is present at levels far above the apparent threshold.

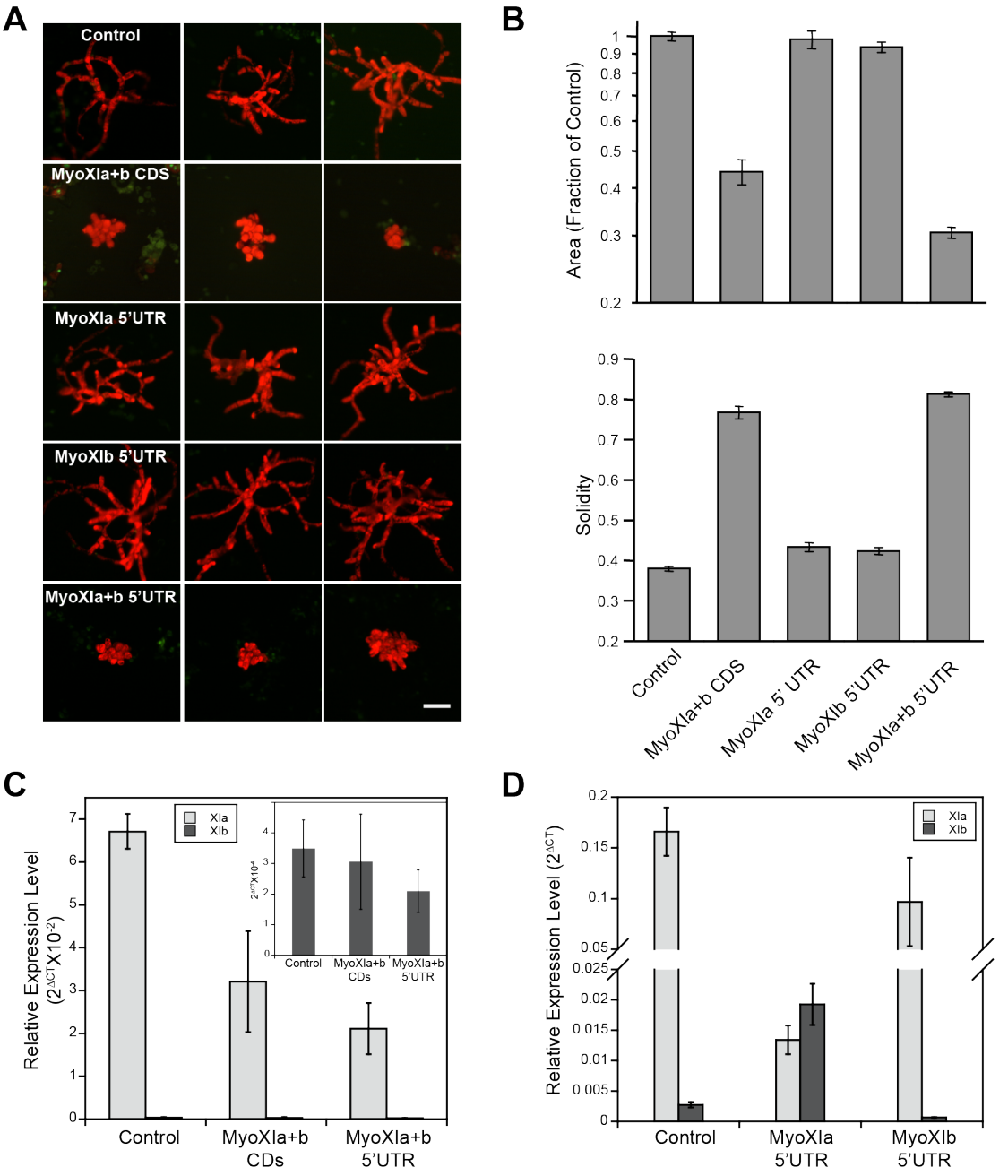

Figure 2.2. Myosin XI is essential for tip growth. **(A)** Representative chlorophyll autofluorescence images of one-week old plants; the absence of nuclear GFP signal indicates that they are undergoing active gene silencing. The RNAi constructs present in the plants are indicated. Scale bar is 100 µm. **(B)** Quantification of the RNAi induced phenotype (Control, n=175; MyoXIa+bCDS, n=85; MyoXIa5'UTR, n=50; MyoXIb5'UTR, n=50; MyoXIa+b5'UTR, n=150). Error bars represent SEM. **(C)** and **(D)** Relative expression levels of MyoXIa (light grey) and MyoXIb (dark grey) normalized to Ubiquitin10 as determined by real time RT-PCR of RNA isolated from one week old plants transformed with the indicated constructs. Inset in C: relative expression level of MyoXIb normalized to Ubiquitin10.

Myosin XI-RNAi can be rescued with a single myosin XI gene

Complementation of loss-of-function phenotypes establishes the specificity of the observed RNAi phenotype and is also a powerful test of purposefully modified sequences. Here I first tested whether expression of myoXIa cDNA from an exogenous promoter rescued the myoXIa+b-5'UTR-induced phenotype. This transient complementation assay enables evaluation of constructs within one week of transformation, and because large numbers of plants can be easily analyzed, the assay is statistically robust. I tested for rescue with the myoXIa cDNA variants I identified as well as the genomically encoded myoXIa cDNA. The Thr to Ala variant (myoXIa (TtoA)) substantially rescued myoXIa+b-5'UTRwhen expressed from the 35S promoter, and importantly, the level of complementation is identical to the rescue achieved with the genomically encoded sequence (myoXIa) (Figure 2.3A, B). As expected, the stop codon variant (MyoXIa(STOP)) did not rescue myoXIa+b-5'UTR (Figure 2.3A, B). I also tested for rescue with different strength promoters driving myoXIa (TtoA). Using the same amount of plasmid for comparison, I found that the promoter does not affect complementation: cDNAs driven by the relatively moderate strength 35S or the strong maize ubiquitin promoters produce similar levels of rescue (Figure 2.3A, B).

To evaluate whether myosin expression level affects the degree of rescue, I performed complementation studies using different amounts of the rescuing plasmid. I found the degree of rescue had a roughly hyperbolic dependency on the amount of plasmid (Figure 2.3C, D). Low levels of myoXIa plasmid (<5 μg) partially rescue the loss of function phenotype, creating small plants with spherical

branching cells. Intermediate levels of plasmid (5-10 μg) produce plants with an intermediate phenotype; cells are more elongated but several of the branching cells maintain their spherical appearance. To obtain full and consistent rescue, 15 μg of myoXIa is required. Interestingly, I did not find a detrimental effect of up to 60 μg of plasmid, suggesting that moss can either tolerate high myosin XI levels or its transient expression is regulated.

Myosin XI localizes to the cell apex

To gain insight into myosin XI function, I investigated its localization during growth. I fused three tandem monomeric enhanced green fluorescent proteins (mEGFPs) (3xmEGFP) to the N-terminus of myoXIa. I chose to use tandem mEGFPs to increase the signal to noise ratio, enabling prolonged observation by confocal microscopy. In addition, I used the maize ubiquitin promoter instead of the 35S promoter because it expresses consistently in all protonemal cell types, particularly the apical cell (Saidi et al., 2005; Vidali et al., 2009a). I generated a stable line expressing 3xmEGFP-myoXIa in the NLS-GFP-GUS background (GFP-myoXI). Using the GFP-myoXI line, I first determined whether the tagged myosin is functional by performing RNAi experiments. The 3xmEGFP-myoXIa construct lacks the endogenous 5'UTR sequence and hence should be insensitve to the myoXIa+b5'UTR construct. Demonstrating functionality, the GFP-myoXI line is indistinguishable from controls in area and morphology when the endogenous myosin XIs are silenced (Figure 2.4A, B). Moreover, transforming with myoXIa+bCDS, which targets both the endogenous and the tagged myosin XIs, phenocopies the myosin XI-RNAi

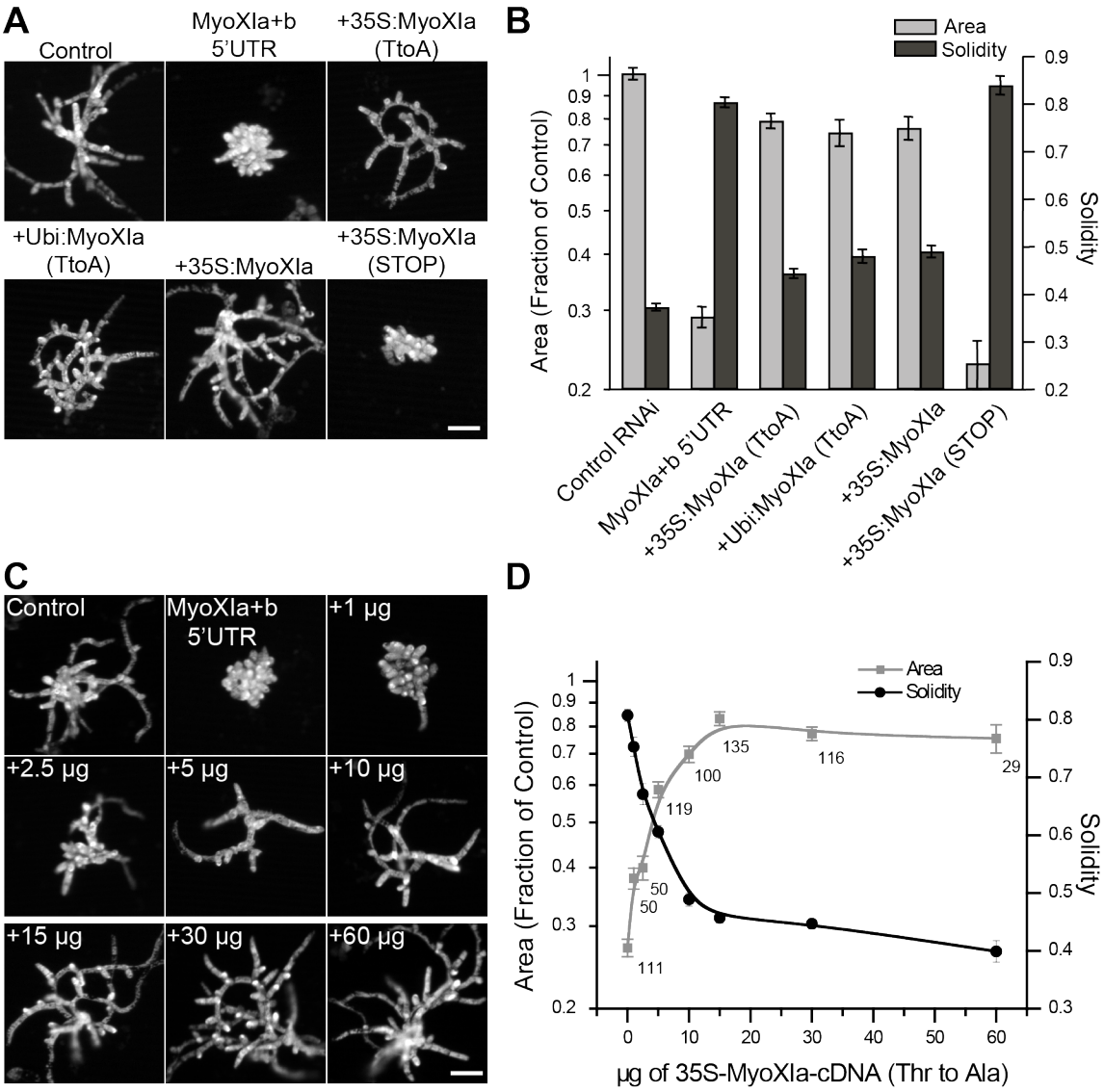

Figure 2.3. Transient complementation of myosin XI-RNAi. **(A)** Representative images of one week old plants visualized by chlorophyll autofluorescence. The complementing construct used to rescue myoXIa+b 5'UTR is indicated after the plus sign. Rescue experiments were carried out with 30 µg of complementing plasmid. Scale bar is 100 µm. **(B)** Quantification of the degree of rescue by the complementing plasmids (Control, n=117; MyoXIa+b5'UTR, n=111; +35S:MyoXIa(TtoA), n=91; +Ubi:MyoXIa(TtoA), n=50; +35S:MyoXIa, n=43; +35S:MyoXIa(STOP), n=25). Error bars represent standard error of the mean. No statistical significance of the comparison of the means found (+35S:MyoXIa(TtoA) vs +Ubi:MyoXIa(TtoA): area p=0.6340, solidity p=0.2586; +35S:MyoXIa(TtoA) vs +Ubi:MyoXIa: area p=0.9974, solidity p=0.0987; MyoXIa+b 5'UTR vs +35S:MyoXIa(STOP): area p=0.08891, solidity p=0.5355). Note that promoter strength and the threonine to alanine mutation have no effect on rescue, but the deletion that introduces a stop codon can not rescue. **(C)** Representative images of one week old plants visualized by chlorophyll autofluorescence. The amount of 35S-MyoXIa-cDNA (TtoA) plasmid is indicated. Scale bar is 100 µm. **(D)** Quantification of the dependence of polarized growth on the levels of myosin XI. Numbers next to the data points indicate the number of plants analyzed. Error bars represent standard error of the mean. For these data 117 plants were analyzed for the control, with an average area of 1.000 +/- 0.0294 and solidity 0.3684 +/- 0.0072.

phenotype (Figure 2.4A, B). These data demonstrate that 3xmEGFP-myoXIa is fully functional.

To ensure that the tagged myosin XI construct was silenced, I measured levels of GFP fluorescence in the GFP-myoXI plant transformed with control, myoXIa+b5'UTR, and myoXIa+bCDS constructs. I observed that the GFP fluorescence was reduced by 70% in the myoXIa+bCDS plants but not affected in the myoXIa+b5'UTR plants (Figure 2.4C). To confirm that the GFP fluorescence is not altered in plants with a similar phenotype, I silenced class II formins in the GFP-myoXI line. Formin2 RNAi plants are of similar size and shape to myosin XI RNAi plants (Vidali et al., 2009b). In these plants, I observed similar levels of GFP fluorescence as the control and myoXIa+b5'UTR plants (Figure 2.4C), demonstrating that the phenotype observed in the myoXIa+bCDS plants is due to loss of myosin XI.

By confocal microscopy, the 3xmEGFP-myoXIa fluorescent signal is diffuse and cytosolic, but accumulates at the tips of growing caulonemal, chloronemal and branching cells, (Figure 2.5A, C, D). In the absence of growth, this accumulation is not observed. Sometimes the fluorescence accumulation forms a well-defined spot near the cell apex (see arrow in figure 2.5A). This spot is not static: in time-lapse sequences, it moves from one side of the cell apex to the other and becomes more or less distinct. To distinguish between fluctuations in signal intensity versus changes in the focal plane, I collected a series of optical sections, minimizing time between images, and made maximum projections (Figure 2.5A). This approach confirmed

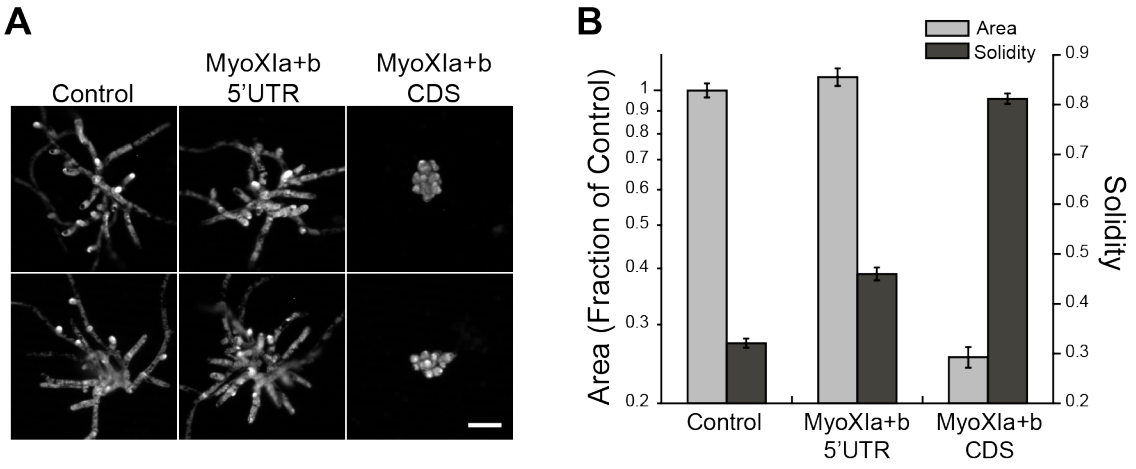

Figure 2.4. The tagged 3xmEGFP-myoXIa is functional. **(A)** Representative images of one-week old plants visualized by chlorophyll autofluorescence. Two images are shown for each condition. A stable line expressing 3xmEGFP-myosin XIa was transformed with the indicated RNAi constructs. Scale bar is 100 μm. **(B)** Quantification of the growth phenotype resulting from the expression of the RNAi constructs 100 plants were analyzed for each condition; Adjusted P values are shown for rejecting equivalence of means. Control vs. MyoXIa+b5'UTR: area p=0.9073, solidity p<0.0001; Control vs. MyoXIa+bCDS: area p<0.0001, solidity p<0.0001). Note the normal phenotype in plants transformed with myoXIa+b 5'UTR but a clear loss of growth with myoXIa+bCDS. **(C)** Quantification of GFP fluorescence from one-week old GFP-myoXI plants expressing the indicated RNAi constructs. 3xmEGFP-myoXIa is reduced by 70% in plants transformed with MyoXIa+bCDS. (Control, n=44; MyoXIa+b5'UTR, n=40; MyoXIa+bCDS, n=26; Formin2 RNAi, n=9).

that the apical fluorescent spot changes both in position and intensity (Figure 2.5A). Interestingly actin also forms a similar focal accumulation at the tip (Figure 2.5B). This apical localization along with the requirement of myosin XI for tip growth suggests that myosin XI's role in this process is to drive secretion to the site of tip growth.

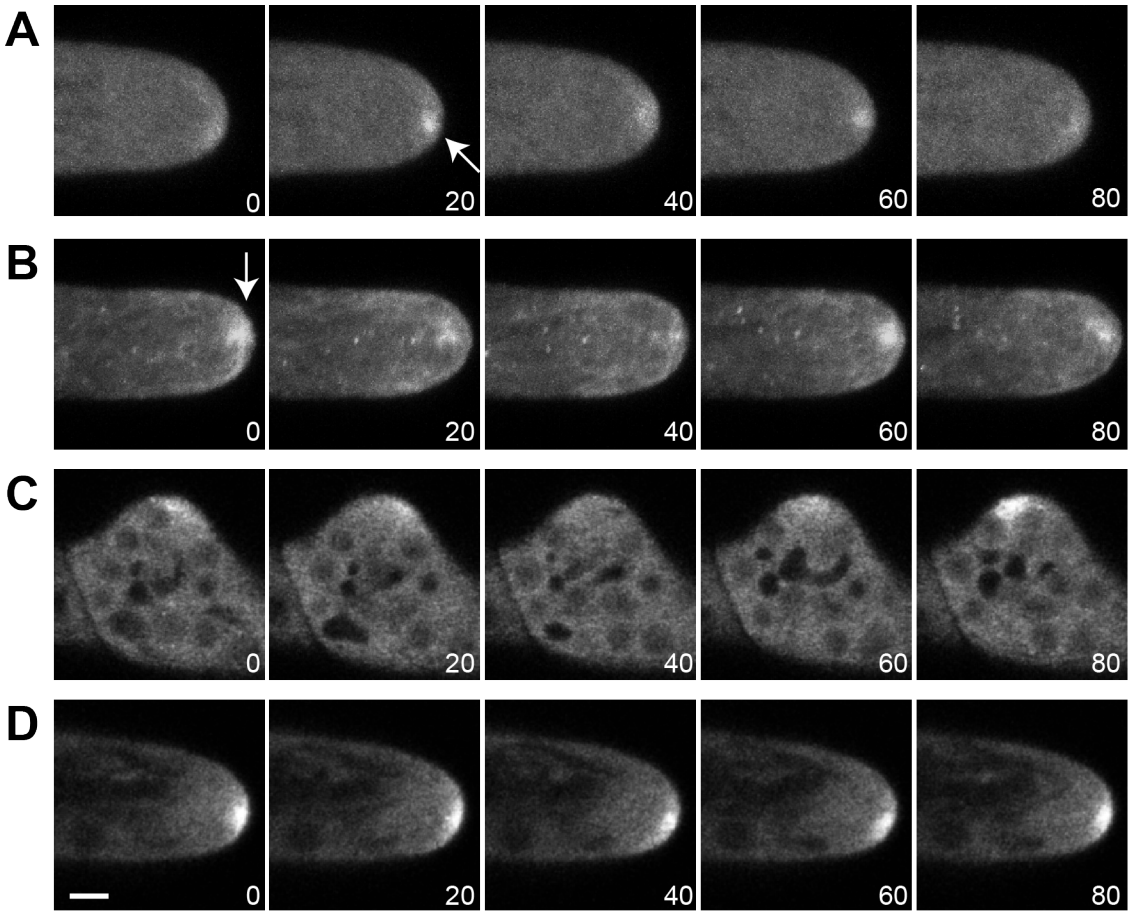

Figure 2.5. Time-lapse imaging of tagged myosin XI and F-actin. **(A)** Localization of 3xmEGFP-myoXIa in a growing protonemal cell. Note the accumulation of fluorescent signal at the cell apex (arrow). Also note that the signal at the apex fluctuates in intensity. **(B)** F-actin distribution in a different cell was visualized by Lifeact-mEGFP. Note the similar accumulation (arrow) and fluctuation to that of myosin XI at the cell apex. In (A) and (B), each time point is a maximal projection of 5 optical sections acquired at 1μm intervals. **(C)** and **(D)** Single focal plane images of 3xmEGFP-myoXIa in an emerging branch (C) and the apex of a chloronemal cell (D). The scale bar is 3 μm and time is indicated in seconds.

CHAPTER 3

THE ROLE OF ROP IN TIP GROWTH

ROP is essential for tip growth

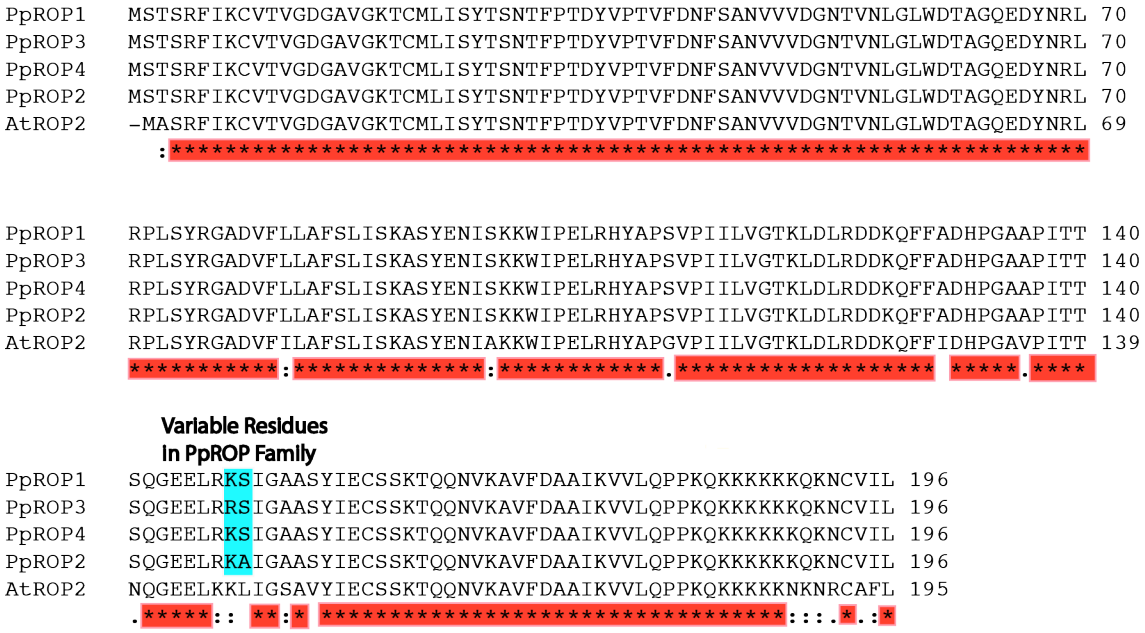

Figure 3.1. Alignment of moss ROP proteins with AtROP2. Identical residues are highlighted in red. Residues 148 and 149 (highlighted in blue) are the only variable residues within the moss ROPs.

Moss *ROP*s are highly similar to *AtROP2* (Figure 3.1). The amino acid sequences of all four *ROP* genes in *Physcomitrella patens* are nearly identical with only 1 residue (148 or 149) differing between any two isoforms. I reasoned that with such high sequence similarity the *ROP* genes were likely functionally redundant. Therefore, I examined their role in tip growth by simultaneously silencing all four *ROPs* using RNA interference (RNAi). Three RNAi constructs targeting different regions of the genes were used. The RNAi constructs contain either a single cDNA fragment with high sequence identity to the other *ROP* genes

(*ROP4* cds and *ROP* cds) or contain multiple cDNA fragments (*ROP* 3'Utr) (Figure 3.2). Specifically, the *ROP4* coding sequence RNAi construct (*ROP4* cds) contains the first 227 bp from the *ROP4* coding sequence. This region is at least 87% identical to the other three *ROP* genes. The *ROP* coding sequence (*ROP* cds) RNAi has 410 bp from the cDNA containing both coding sequence and a portion of the 3' untranslated region of *ROP2*. This sequence region is at least 76% identical to the other *ROP* genes. The *ROP* 3' untranslated region (*ROP* 3'Utr) RNAi contains 190-256 bp from the 3' untranslated regions of *ROP1*, *ROP2* and *ROP4*. The *ROP2* sequence fragment in *ROP* 3'Utr is 85% identical to *ROP3* in this region. With such high sequence identity, I expect that these three RNAi constructs should silence all four *ROP* genes.

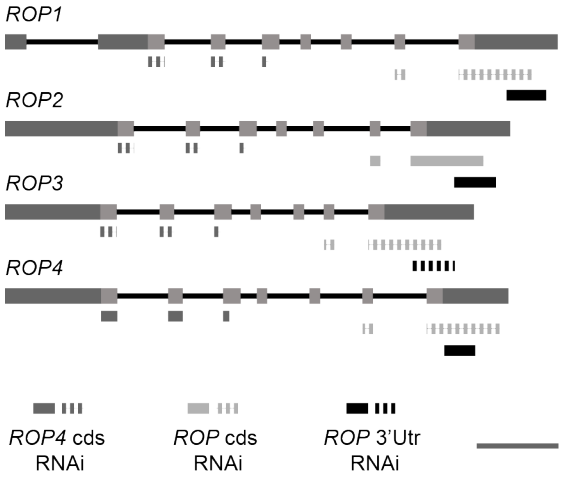

Figure 3.2. Gene models of *Physcomitrella patens ROP* family. *P. patens* has four *ROP* genes. Exons are indicated in light grey, introns in black, and untranslated regions in dark grey. Lines underneath gene models represent sequence regions targeted by various *ROP* RNAi constructs. Solid lines indicate that the denoted sequence was used in the RNAi construct while dashed lines indicate highly similar sequence regions that are targeted by the RNAi constructs: *ROP4* cds RNAi (dark grey), *ROP* cds RNAi (light grey), *ROP* 3'Utr RNAi (Black). Scale bar is 500bp.

I transformed the *ROP* RNAi constructs into moss protoplasts and allowed plants to regenerate for 7 days. Expression of *ROP4* cds and *ROP* 3'Utr RNAi constructs yield plants composed of small spherical cells, while plants expressing the *ROP* cds construct occasionally have a few slightly elongated cells (Figure 3.3A). In contrast, the control RNAi plants have elongated branching protonemal cells observed in normal regenerating moss plants. To quantify the effects of *ROP* RNAi

on plant area and morphology, I measured both plant area and solidity. Silencing with any of the *ROP* RNAi constructs results in a decrease in plant area with a corresponding increase in solidity (Figure 3.3B).

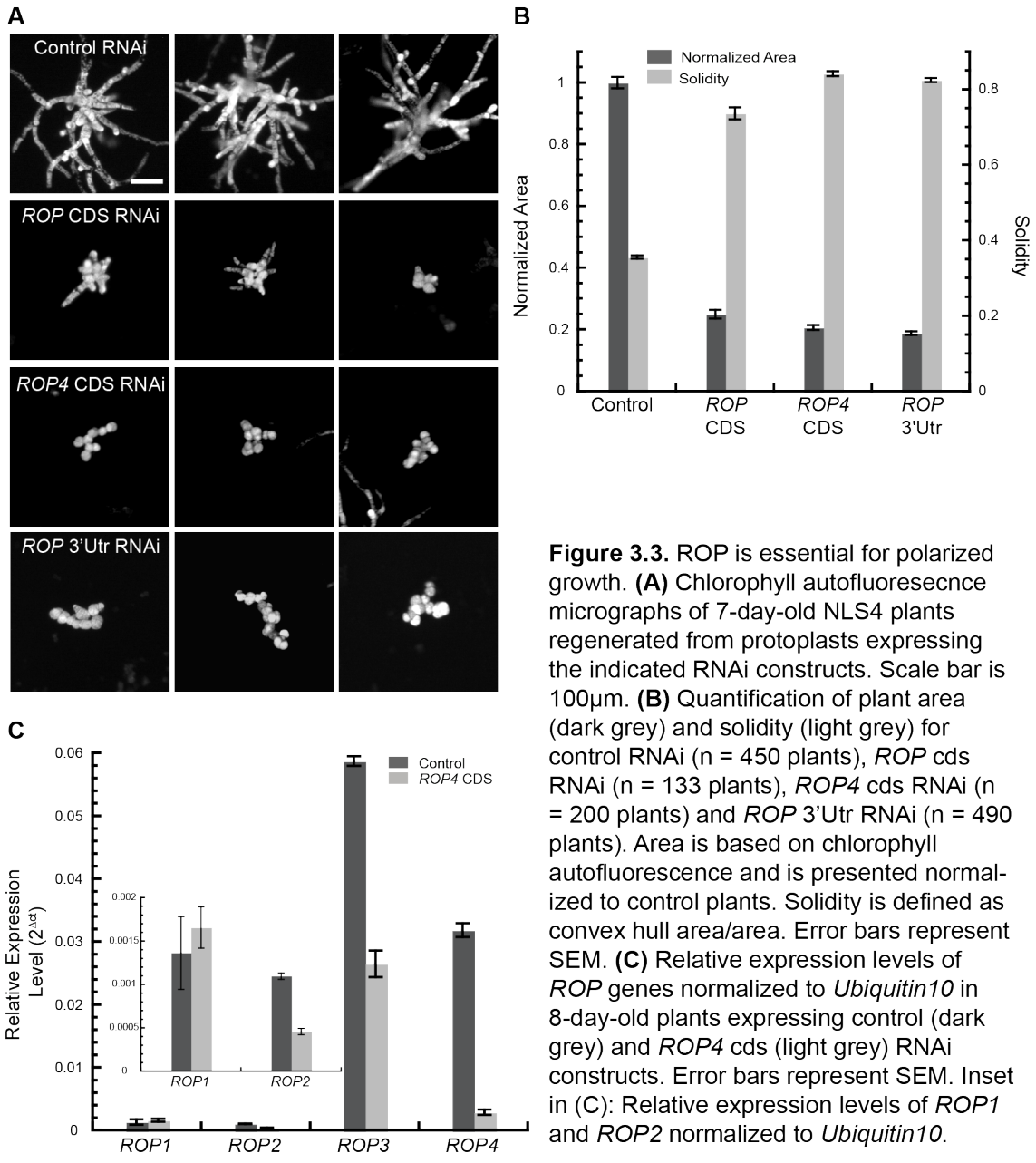

Figure 3.3. ROP is essential for polarized growth. **(A)** Chlorophyll autofluoresecnce micrographs of 7-day-old NLS4 plants regenerated from protoplasts expressing the indicated RNAi constructs. Scale bar is 100μm. **(B)** Quantification of plant area (dark grey) and solidity (light grey) for control RNAi (n = 450 plants), *ROP* cds RNAi (n = 133 plants), *ROP4* cds RNAi (n = 200 plants) and *ROP* 3'Utr RNAi (n = 490 plants). Area is based on chlorophyll autofluorescence and is presented normalized to control plants. Solidity is defined as convex hull area/area. Error bars represent SEM. **(C)** Relative expression levels of *ROP* genes normalized to *Ubiquitin10* in 8-day-old plants expressing control (dark grey) and *ROP4* cds (light grey) RNAi constructs. Error bars represent SEM. Inset in (C): Relative expression levels of *ROP1* and *ROP2* normalized to *Ubiquitin10*.

To confirm that the observed phenotype results from a reduction in ROP function, I measured *ROP* transcript levels. I isolated mRNA from 7-day old control and *ROP* cds RNAi plants and performed quantitative real time RT-PCR (qRT-PCR).

In control plants, *ROP3* and *ROP4* transcripts constitute the majority of the ROP transcripts (97%). In *ROP4* cds RNAi plants, I found that *ROP1* transcript levels were unaltered. However, *ROP2*, *ROP3* and *ROP4* transcripts were reduced by 58%, 55%, and 91%, respectively compared to control RNAi plants, thereby reducing the total transcript pool by 66% (Figure 3.3C). These data demonstrate that ROP is essential for tip growth.

To ensure that the qRT-PCR primers were specific for each *ROP* gene, I generated a stable deletion line for each gene and analyzed the expression levels of the four ROP genes in these lines. Interestingly, I found reductions in plant area as well as transcript levels for all four genes in the stable deletion lines (Figure 3.4A & C). The Δ*rop2* and Δ*rop3* lines have the most severe reductions in transcript levels and also have the smallest areas and increased solidity values. However, *ROP3* and *ROP4* are consistently the most highly expressed when present. Despite some fluctuations in plant size and solidity, all of the stable *ROP* deletion lines performed tip growth (Figure 3.4B), suggesting that *ROP* genes in *P. patens* contribute to overall plant size but are functionally redundant with respect to tip growth.

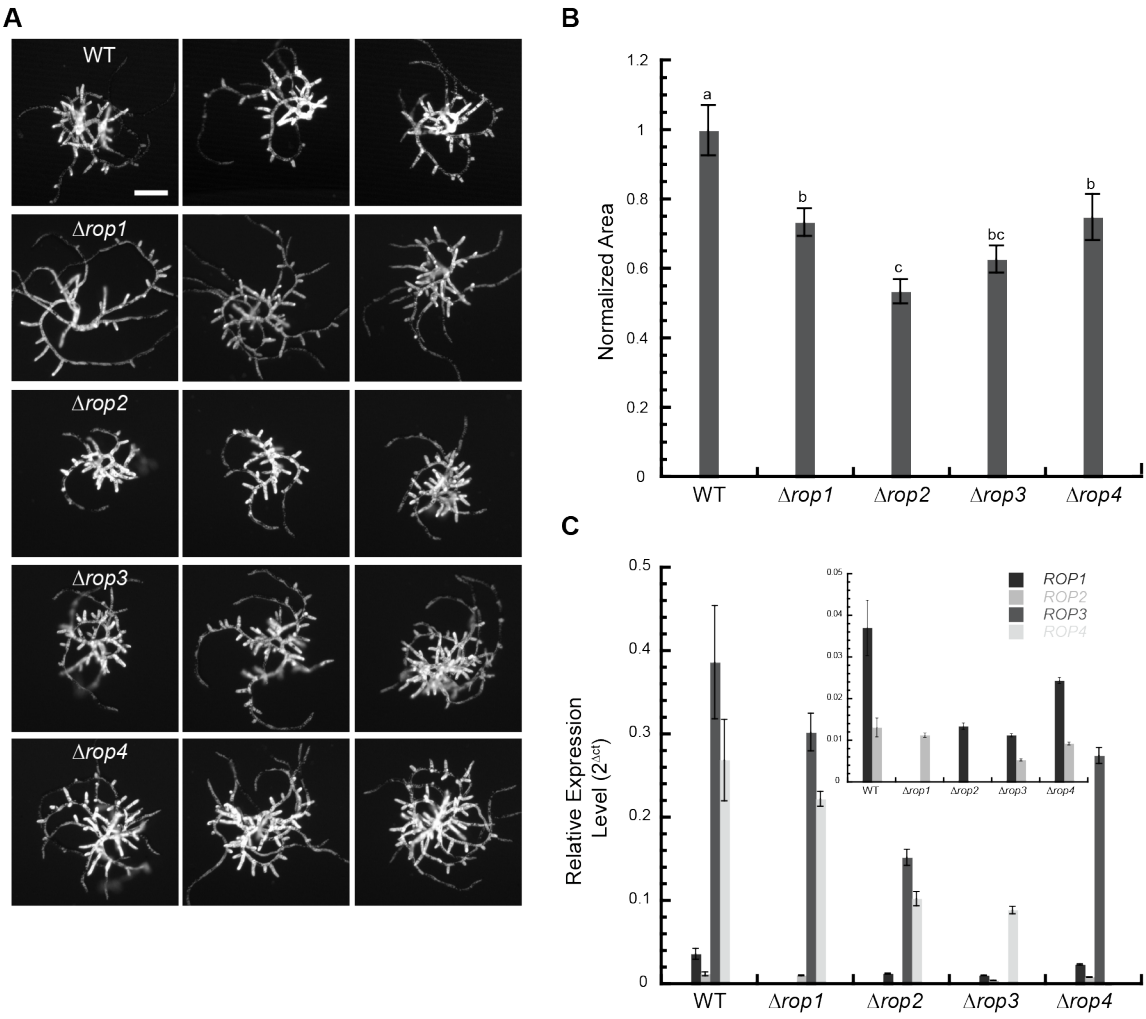

Figure 3.4. Growth phenotypes and expression levels of *ROP* genes in stable single *ROP* deletion lines. **(A)** Chlorophyl autofluorescence micrographs of 6-day old *ROP* deletion and wild type plants regenerated from protoplasts. Scale bar is 200µm. **(B)** Quantification of plant area. Area is based on chlorophyll autofluorescence and is presented normalized to wild type plants. Error bars represent SEM and letters above bars indicate statistical groups with α = 0.05 using ANOVA **(C)** Relative *ROP* expression in single *ROP* deletion lines and wild type, normalized to *Ubiquitin10*. Error bars represent SEM. Inset in **(C)** Relative *ROP1* and *ROP2* expression in single *ROP* deletion lines and wild type, normalized to *Ubiquitin10*. Error bars represent SEM.

Rescue of *ROP* RNAi phenotype

If moss *ROP* genes are functionally redundant, then a single *ROP* gene should be sufficient for tip growth. To investigate this, I first attempted rescue *ROP* RNAi by generating expression constructs that used the maize ubiquitin promoter to drive

expression of the coding sequences of *ROP2*, *ROP3* and ROP4 (Ubi*ROP2* – Ubi*ROP4*) (Figure 3.5) *ROP1* was not used, as it is identical to *ROP4* at the amino acid level. These constructs were then co-expressed with the *ROP* 3'Utr RNAi contstruct. Since the expression constructs lack the 3'Utr, they will be insensitive to the *ROP* 3'Utr construct. As our lab has demonstrated (Augustine et al., 2008; Vidali et al., 2007; Vidali et al., 2009b; Vidali et al., 2010), plants co-transformed with an RNAi and expression construct receive both plasmids and are easily identified as plants that lack nuclear GFP. After co-transformation of ROP expression constructs with *ROP* 3'Utr RNAi construct, the number of silenced plants was severely reduced compared to transformation of the RNAi construct alone. The few silenced plants that were recovered did not have a consistent phenotype: some were completely unpolarized while others showed varying degrees of polarization. Thinking that perhaps moss is sensitive to the level of ROP expression, I tried using successively lower amounts of the expression constructs to see if I could recover more transformants. But I was not able to recover more plants, suggesting that ROP expression from the maize ubiquitin promoter might be lethal in moss.

The maize ubiquitin promoter is a strong, constitutive promoter and results in a large increase in ROP expression (Figure 3.5B). In addition to the expected increase in the expected band at ~21 kDa, there is also a very intense band just below it not found in the control transformation with an empty vector (Figure 3.5B). A similar shift has been reported when geranylgeranylation of the CaaX motif in the small Rho GTPase RhoA is inhibited in mouse embryo fibroblasts (Allal, et al., 2000). These results suggest that at wild type levels in moss a majority of ROP protein has

been geranylgeranylated. While the amount of modified ROP can be increased to a point, strong expression of *ROP3* results in a larger population of ROP lacking the lipid modification (Figure 3.5B). These unmodified ROPs are unable to localize to the membrane, but might still be capable of interacting with ROP regulators and effectors. This could result in titrating out the effect of the endogenous ROPs. However, instead of simply not rescuing the *ROP* RNAi phenotype there is lethality with strong expression of ROP, so perhaps these unmodified ROPs are titrating out a ROP effector for another essential cell process.

To more accurately mimic the native *ROP* expression levels, I generated expression constructs that used the promoter regions and the genomic sequences of *ROP1*, *ROP2* and *ROP3*, excluding the 3'Utrs (Figure 3.5A). I attempted varying amounts of each construct individually as well as in combination to rescue the RNAi phenotype. While I was able to recover more transformed plants, there was little to no rescue of polarized growth. The results of these complementation studies suggest that moss is highly sensitive to ROP expression levels and as a result, transient complementation is an ineffective method to ameliorate the *ROP* RNAi phenotype.

A single *ROP* gene is sufficient for tip growth to occur

As an alternative approach, I altered a *ROP* locus removing the 3' untranslated region from the genomic locus using homologous recombination, thereby rendering the locus insensitive to the *ROP* 3'Utr RNAi construct. If the engineered *ROP* locus is

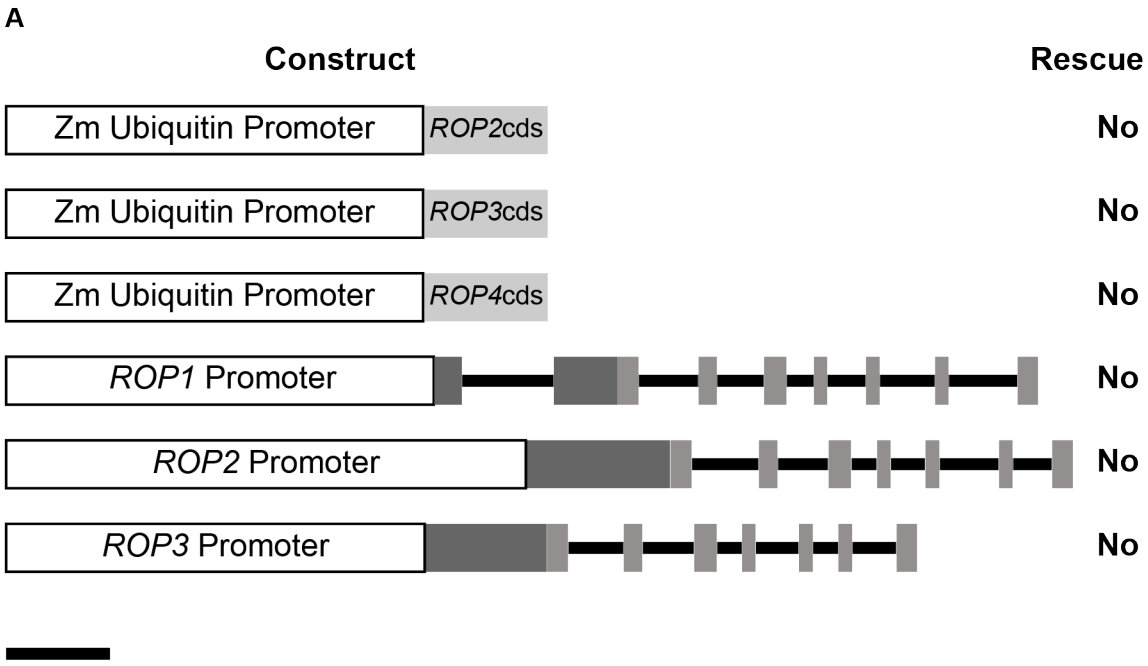

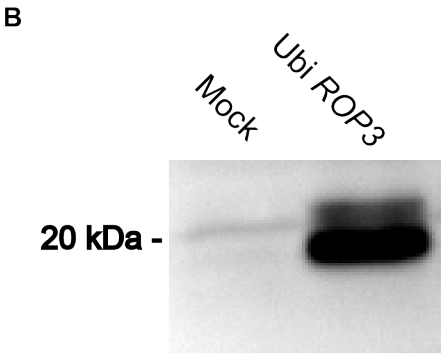

Figure 3.5. Transient complementation of *ROP* RNAi. **(A)** Schematics of complementation constructs using a strong (Zm ubiquitin) or native promoters. Scale bar is 500bp. **(B)** Immunoblot of protein extracts from protoplasts expressing either an empty vector (Mock) or a ubiquitin driven coding sequence of *ROP3*. The immunoblot was probed with an antibody raised to AtROP2.

sufficient for tip growth, then transformation with the *ROP* 3'Utr RNAi construct should result in polarized plants. I generated two lines, NLS4/*ROP3* Δ3'Utr and NLS4/*ROP4* Δ3'Utr, with the deletions in the 3'Utrs of *ROP3* and *ROP4*, respectively (Figure 3.6A). As expected, expression of the *ROP4* cds RNAi construct in these lines still results in small, unpolarized plants, but plants expressing the *ROP* 3'Utr RNAi construct have elongated polarized cells (Figure 3.6B). While these plants show almost complete rescue in terms of solidity, they are only ~49% (NLS4/*ROP3*

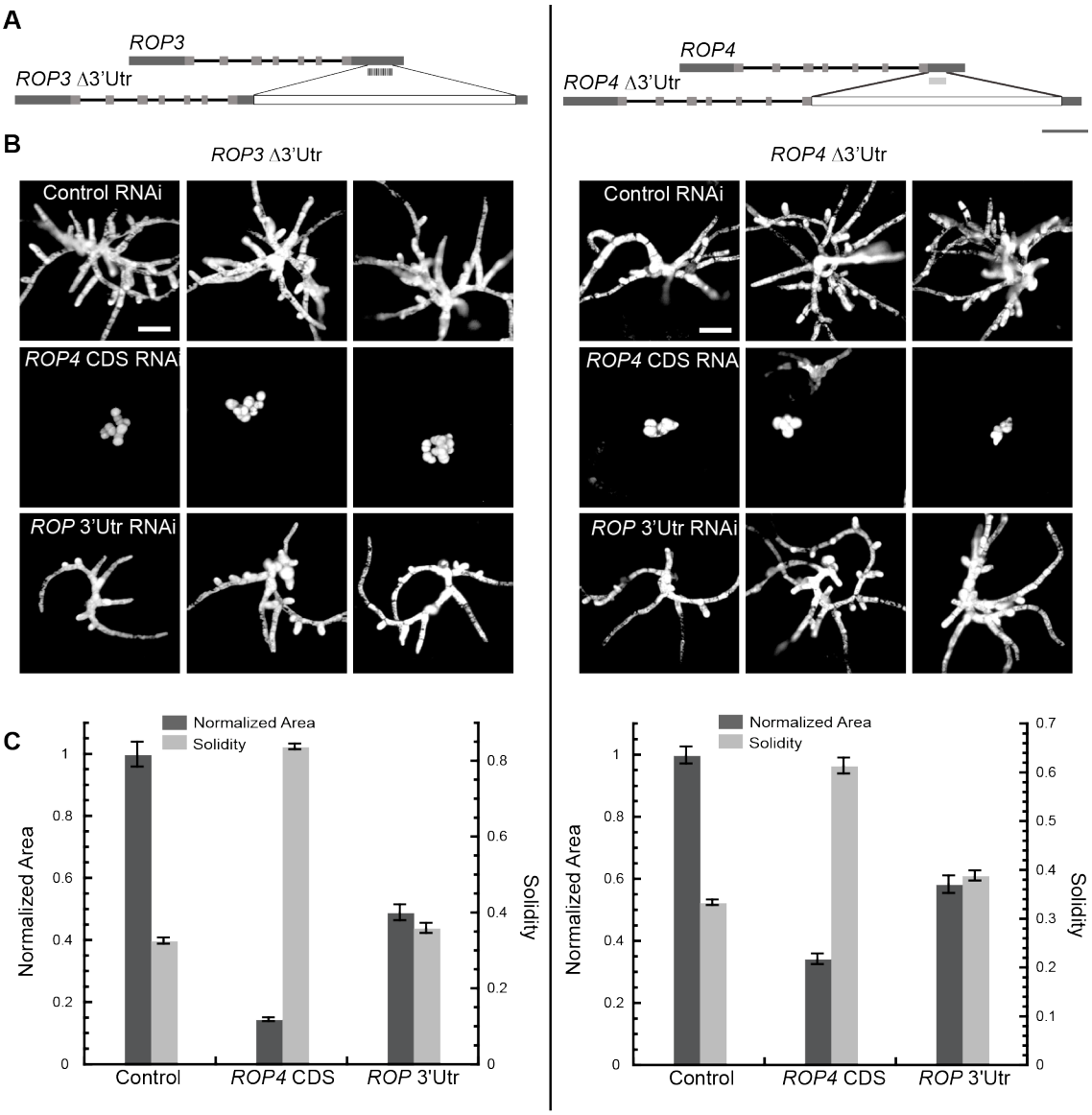

Figure 3.6. A single *ROP* gene is sufficient for polarized growth. **(A)** Diagram illustrating the homologous recombination mediated replacement of the 3'Utrs of the *ROP3* (left) and *ROP4* (right) genes targeted by the *ROP* 3'Utr RNAi construct, generating stable RNAi-insensitive lines. Exons are indicated in light grey, introns in black, untranslated regions in dark grey, and the hygromycin resistance cassette in white. Scale bar is 500bp. **(B)** Chlorophyll autofluore-secnce micrographs of 7-day-old NLS4/*ROP3* Δ3'Utr (left) and NLS4/*ROP4* Δ3'Utr (right) plants regenerated from protoplasts expressing the indicated RNAi constructs. Scale bar is 100μm. **(C)** Quantification of plant area (dark grey) and solidity (light grey) for control RNAi (n = 200/75 (NLS4/*ROP3* Δ3'Utr / NLS4/*ROP4* Δ3'Utr) plants), *ROP4* cds RNAi (n = 180/75 plants) and *ROP* 3'Utr RNAi (n = 177/75 plants). Error bars represent SEM.

Δ3'Utr) and ~58% (NLS4/*ROP4* Δ3'Utr) the size of control RNAi plants (Figure 3.6C). Expression analysis of these silenced plants confirms that the transcript levels of the targeted alleles are unaffected by expression of the *ROP* 3'Utr RNAi construct

(Figure 3.7). However, total ROP transcripts levels were reduced by ~15% (NLS4/*ROP3* Δ3'Utr) and ~43% (NLS4/*ROP4* Δ3'Utr) compared to control RNAi plants. Interestingly, the NLS4/*ROP3* Δ3'Utr line was significantly smaller than NLS4 plants (Figure 3.8), likely correlating with reduced levels of *ROP4* expression (Figure 3.7). Taken together, these results demonstrate that *ROP3* and *ROP4* are each sufficient for tip growth.

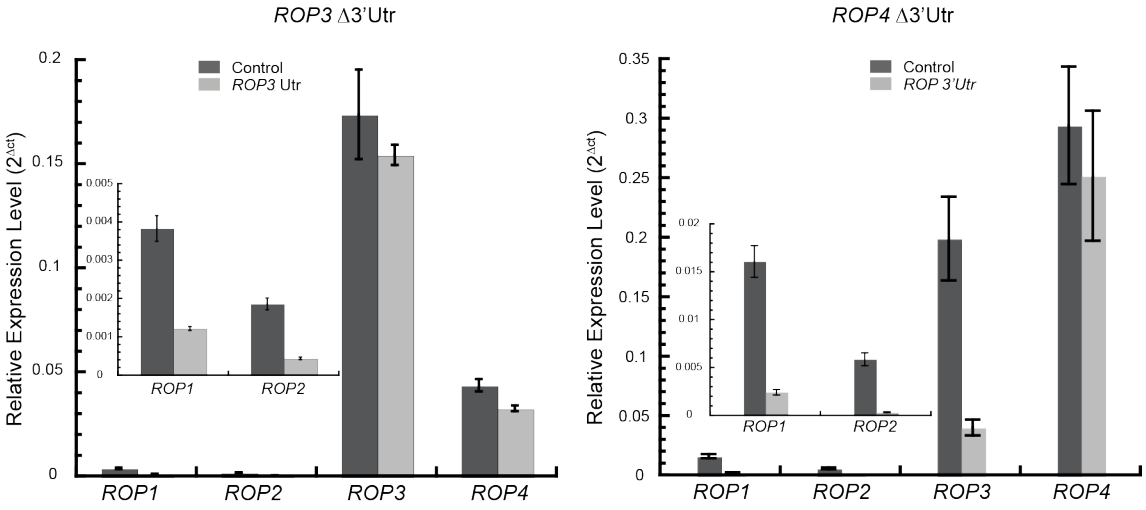

Figure 3.7. Relative expression levels of *ROP* genes normalized to *Ubiquitin10* in 8-day-old NLS4/*ROP3* Δ3'Utr (left) and NLS4/*ROP4* Δ3'Utr (right) plants expressing control (dark grey) and *ROP* 3'Utr (light grey) RNAi constructs. Error bars represent SEM. Insets: Relative expression levels of *ROP1* and *ROP2* normalized to *Ubiquitin10*.

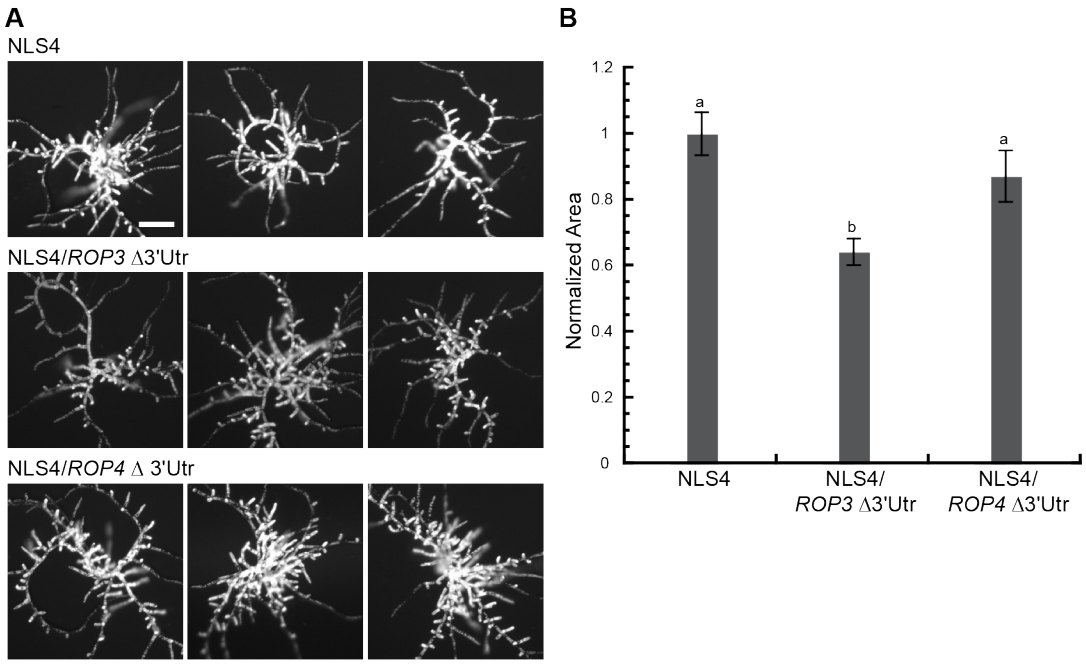

Figure 3.8. Growth assays for stable RNAi insensitive lines. **(A)** Chlorophyl autofluorescence micrographs of 6-day old NLS4, NLS4/*ROP3* Δ3'UTR and NLS4/*ROP4* Δ3'Utr plants regenerated from protoplasts. Scale bar is 200μm. **(B)** Quantification of plant area for NLS4, NLS4/*ROP3* Δ 3'UTR and NLS4/*ROP4* Δ3'Utr. Area is based on chlorophyll autofluorescence and is presented normalized to NLS4 plants. Error bars represent SEM and letters above bars indicate statistical groups with α = 0.05 using ANOVA.

ROP localization

To investigate the subcellular localization of ROP in live cells, I generated a GFP-ROP fusion protein. However, GFP-ROP has not been shown to be functional in any system. The stable RNAi insensitive lines provide the opportunity to express the GFP-ROP fusion protein while silencing the endogenous ROPs and thus test for the functionality. I used homologous recombination to generate a stable line where the endogenous *ROP4* allele, from the start codon through the 3'Utr was replaced with mEGFP fused to the coding sequence of *ROP4* (NLS4/mEGFP-ROP4cds) (Figure 3.9A).

I chose an N-terminal tag to avoid interfering with geranylgeranylation of the C-terminal CaaX motif , as this could mislocalize and affect the functionality of the fusion protein. I also generated a line using three tandem mEGFP molecules fused to *ROP4* (NLS4/3xmEGFP-ROP4cds) as well as a line where only the coding sequence was replaced the genomic sequence (NLS4/ROP4cds). In both GFP tagged lines, I observed apical plasma membrane localization of ROP with the signal progressively weakening from the tip of the cell to the shank (Figure 3.9B), as has been previously observed (Gu et al, 2003; Molendijk et al., 2001). I tested for the functionality of these allele replacement lines by expressing the *ROP* 3'Utr RNAi construct. I found that neither of the GFP tagged lines nor the coding sequence replacement line had polarized plants, indicating that none of the allele replacements rescued tip growth (Figure 3.9A). Since the coding sequence replacement line was also not functional I could not determine if the N-terminal GFP tags impacted ROP function. This result, coupled with the fact that I was unable to rescue the RNAi phenotype with transient or stable constructs expressing the coding sequence but could make RNAi insensitive lines where the genomic sequence was minimally disturbed, suggests that maintaining the genomic intron/exon structure of *ROPs* is critical for function.

I then devised two strategies to generate stable lines where the endogenous *ROP4* allele was minimally altered. These strategies would introduce GFP into the *ROP4* locus and remove the 3'UTR while leaving the intron/exon boundaries unaltered. The first strategy was to use two targeting constructs, one that would insert GFP in frame at the N-terminus of *ROP4* and another that would remove the region of the *ROP4* 3'Utr targeted by the *ROP* 3'Utr RNAi construct to make it

insensitive (Figure 3.9A). Unfortunately, I was not able to recover any stable lines in which both the insertion and the deletion had occurred. This may be due to difficulty in achieving two homologous recombination events in such close proximity to one another in the genome. The second strategy was to insert the GFP tag just in front of the C-terminal CaaX motif of *ROP4*, in an effort to avoid altering prenylation. This also would be an alternate tag if it turned out that the N-terminal GFP tag inhibited ROP function. I generated a construct that included GFP fused to the CaaX motif and used it to replace the CaaX motif and the 3'Utr (Figure 3.9A). I isolated three stable lines, but none of them produced polarized plants when expressing the *ROP* 3'Utr RNAi construct. As these tagged versions were not functional, I did not image them.

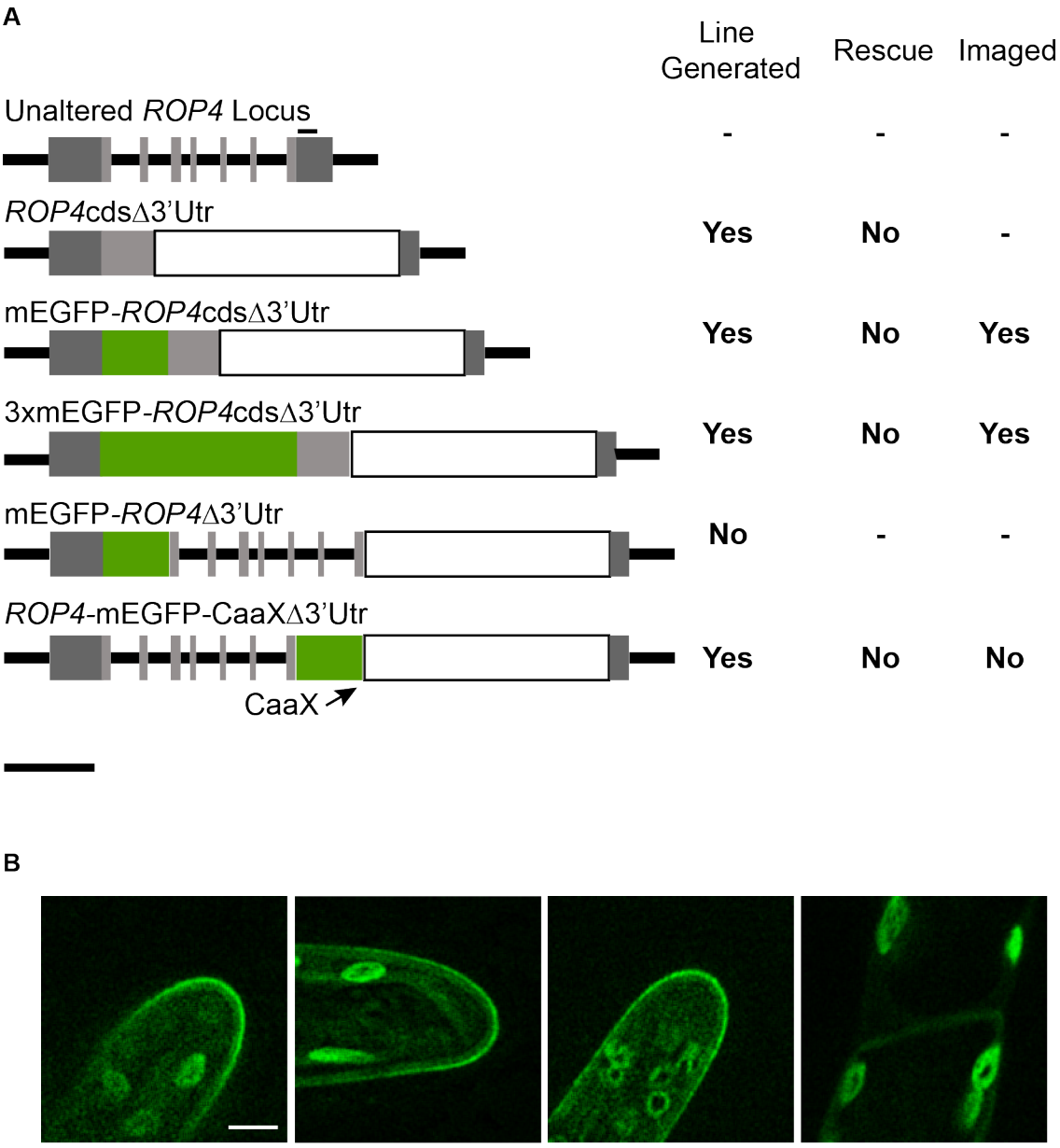

Figure 3.9. Generating GFP-ROP fusions. **(A)** Schematic representations of the *ROP4* locus in various stable lines. Introns are represented in black, untranslated regions are in dark gray, *ROP4* coding sequence is in light grey and GFP coding sequence is in green. On the right, a table indicating if a stable line was successfully obtained, if the fusion protein was functional and if the line was imaged or not. Scale bar is 1000bp. **(B)** Confocal micrographs of the localization of mEGFP-*ROP4cds*Δ3'Utr. Bright bodies are from chlorophyll autofluorescence. Scale bar is 40 μm.

CHAPTER 4

THE IMPACT OF *ROP* RNAi ON CYTOSKELETAL PROTEINS

Actin dynamics and organization are altered in *ROP* silenced cells

To determine how *ROP* affects actin dynamics I examined the cortical actin cytoskeleton using lifeact-mEGFP (Vidali et al, 2009a) in control and *ROP* RNAi plants (for the rest of the work presented in this thesis, *ROP* RNAi will refer to use of the *ROP4* cds RNAi construct described in chapter 3 due to the consistently strong phenotype). Previous studies have suggested that active ROP leads to the generation of actin filaments (Gu et al., 2006; Li et al., 1999; Xu et al, 2010). Therefore, I expected that loss of ROP should reduce filament generation and therefore reduce overall actin dynamics. To quantify changes in actin organization, I imaged the cell cortex of plants expressing lifeact-mEGFP once every second over the course of one minute using spinning disc confocal microscopy (Figure 4.1A). I calculated the correlation coefficient of images over all time intervals in the time-lapse acquisition. This analysis examines the degree of change in the cortical actin cytoskeleton (Vidali et al., 2010). Rapid decay of the correlation coefficient indicates increased cortical actin dynamics. Contrary to expectation, I found that cells expressing the *ROP* RNAi construct have increased actin dynamics compared to control RNAi cells (Figure 4.1B).

In arabidopsis, active *ROP2*, through the effector *RIC4,* causes diffuse actin accumulation in the cortex of the lobed regions of leaf pavement cells (Xu et al., 2010). Therefore a reduction of ROP activity may reduce the density of filamentous

actin in moss. I measured filament density at the cell cortex in both control and *ROP* RNAi cells and found that as predicted filament density was reduced by ~27% as compared to control RNAi plants (Figure 4.1C). To investigate whether a reduction in filament density together with an increase in actin dynamics affected the state of bundled actin filaments, I quantified the degree of actin bundling by analyzing skewness (Higaki et al., 2010). This analysis assumes a normal distribution in the intensity of individual filaments and the degree to which this distribution is skewed to the right as compared to a normal distribution in the analyzed images reflects higher degrees of bundling (Higaki et al., 2010). *ROP* RNAi cells have a similar degree of bundling as control cells; suggesting that changes in density and dynamics has not affected bundling

ROP is a negative regulator of class II formin mediated actin elongation

Since loss of ROP increases cortical actin dynamics, I reasoned that ROP might impact regulators of actin polymerization. Class II formins localize to the cell cortex by binding $PI(3,5P)_2$ (van Gisbergen et al., 2012). Once at the cell cortex, a population of formins generates new actin filaments. Formin molecules that generate new actin filaments move in linear trajectories along the cell cortex (van Gisbergen et al., 2012). If ROP affects formin activity, it is possible that loss of ROP might impact formin localization and activity at the cell cortex.

To test this, I imaged For2A-3XmEGFP (hereafter named For2A-GFP) in control and *ROP* RNAi plants using variable angle epifluorescence microscopy (VAEM) (Figure 4.2A). I found that there was a ~36% reduction in the density of

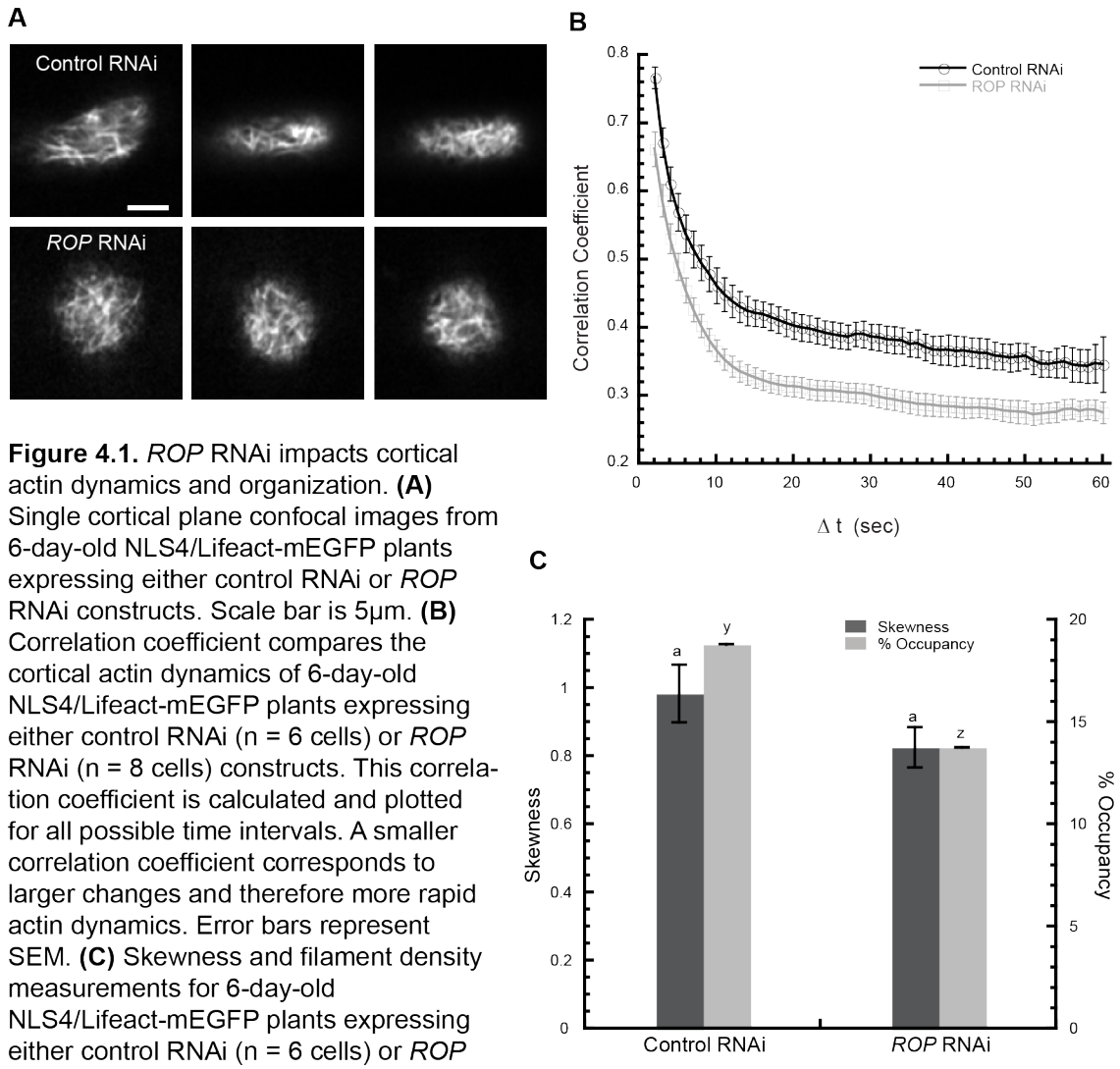

Figure 4.1. *ROP* RNAi impacts cortical actin dynamics and organization. **(A)** Single cortical plane confocal images from 6-day-old NLS4/Lifeact-mEGFP plants expressing either control RNAi or *ROP* RNAi constructs. Scale bar is 5μm. **(B)** Correlation coefficient compares the cortical actin dynamics of 6-day-old NLS4/Lifeact-mEGFP plants expressing either control RNAi (n = 6 cells) or *ROP* RNAi (n = 8 cells) constructs. This correlation coefficient is calculated and plotted for all possible time intervals. A smaller correlation coefficient corresponds to larger changes and therefore more rapid actin dynamics. Error bars represent SEM. **(C)** Skewness and filament density measurements for 6-day-old NLS4/Lifeact-mEGFP plants expressing either control RNAi (n = 6 cells) or *ROP* RNAi (n = 9 cells) constructs. Error bars represent SEM and letters above bars indicate statistical groups with α = 0.05 using ANOVA.

cortical formin spots in *ROP* RNAi as compared to control plants (Figure 4.2B). This is consistent with the decrease in actin filament density I observed when *ROP* is silenced. Since ROPs have a C-terminal CaaX motif for lipid anchoring and are thought to be active on the membrane (Sorek et al., 2007), it is possible that loss of ROP alters the cortical environment. To investigate whether cortical formin molecules were active in *ROP* RNAi plants, I quantified the number of formin

particles that traversed the cell cortex in a linear trajectory, an indication that the formin is generating an actin filament (van Gisbergen et al., 2012). If ROP activates formin activity, I would expect to observe a significant decrease in the number of linear trajectories in *ROP* RNAi plants. Surprisingly I observed just as many linear trajectories in *ROP* as in control RNAi plants. In fact, after normalizing to particle density, I discovered the formin linear trajectories occurred twice as often in *ROP* RNAi cells compared to control cells (Figure 4.2C) To determine whether there were any significant differences between the linear trajectories in *ROP* versus control RNAi plants, I quantified the duration and the rate of linear trajectories. I found that the formin linear trajectories have similar durations on the cortex (Control 1.2 sec +/- 0.16 (SEM), *ROP* RNAi 1.0 sec +/- 0.05) and similar elongation rates (Control 2.1 μm/sec +/- 0.18, *ROP* RNAi 2.1 μm/sec +/- 0.08). Thus, loss of cortical ROP activity reduces the number of cortical formin particles, but does not affect formin behavior at the cortex. However the percent of cortical formin that generates actin filaments is higher in *ROP* RNAi plants, supporting our earlier observation of increased actin dynamics in *ROP* RNAi cells. It seems that once the formin is active it behaves the same in *ROP* RNAi as control cells. However, a higher fraction of the cortical formin is active in *ROP* RNAi cells. Thus while ROP may normally function to produce a membrane domain that recruits formin, ROP nonetheless limits cortical formin activity.

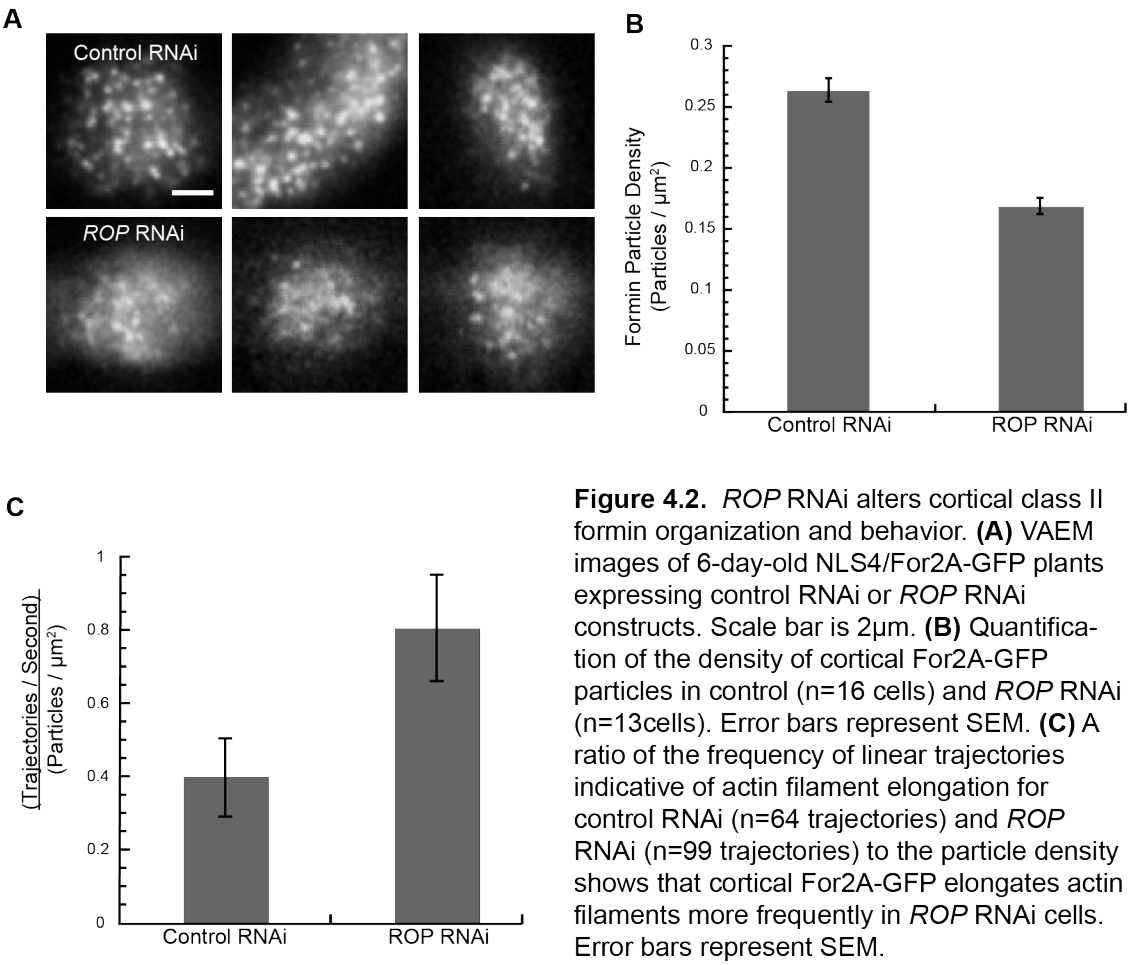

Figure 4.2. *ROP* RNAi alters cortical class II formin organization and behavior. **(A)** VAEM images of 6-day-old NLS4/For2A-GFP plants expressing control RNAi or *ROP* RNAi constructs. Scale bar is 2µm. **(B)** Quantification of the density of cortical For2A-GFP particles in control (n=16 cells) and *ROP* RNAi (n=13cells). Error bars represent SEM. **(C)** A ratio of the frequency of linear trajectories indicative of actin filament elongation for control RNAi (n=64 trajectories) and *ROP* RNAi (n=99 trajectories) to the particle density shows that cortical For2A-GFP elongates actin filaments more frequently in *ROP* RNAi cells. Error bars represent SEM.

Microtubule dynamics and organization are altered in *ROP* silenced cells

While microtubules are not critical for tip growth, there is evidence for ROP mediated regulation of the microtubule cytoskeleton. In arabidopsis ROP6 and its effector RIC1 cause accumulation of microtubules in the indentation regions of leaf pavement cells (Xu et al., 2010; Sorek et al., 2011). Active AtROP11 induces disassembly of cortical microtubules during the formation of secondary cell walls in xylem cells (Oda and Fukuda, 2012). Since moss ROPs are essentially identical and likely functionally redundant, I hypothesized that moss ROPs might impact both actin and microtubules.

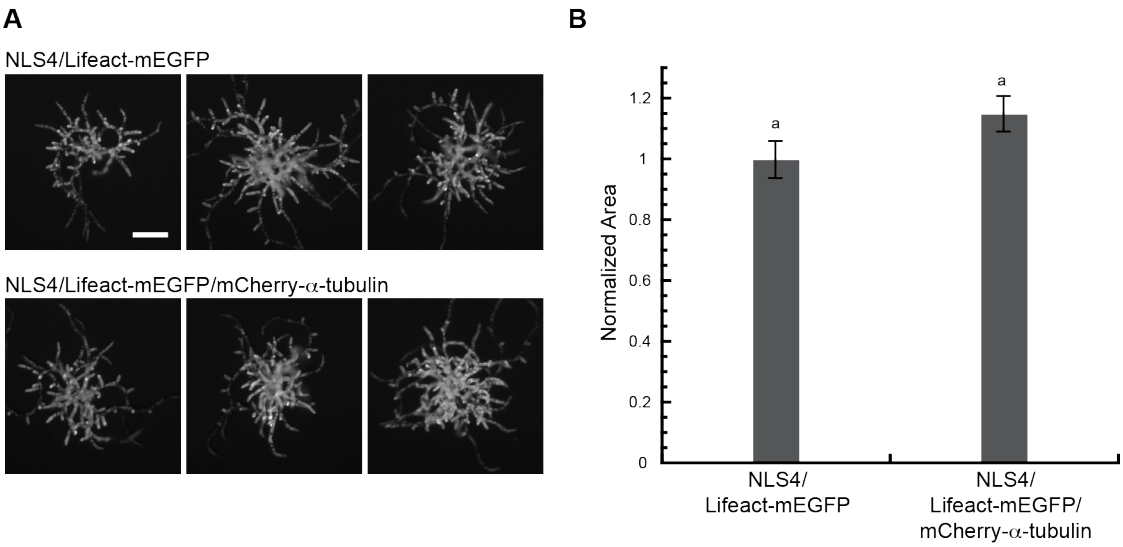

Figure 4.3. Growth assays for the stable line expressing mCherry-α-tubulin. (A) Chlorophyl autofluorescence micrographs of 6-day old NLS4/Lifeact-mEGFP and NLS4/Lifeact-mEGFP/ mCherry-α-tubulin plants regenerated from protoplasts. Scale bar is 200μm. (B) Quantification of plant area (dark grey) and solidity (light grey) for NLS4/Lifeact-mEGFP and NLS4/Lifeact-mEGFP/ mCherry-α-tubulin. Error bars represent SEM and letters above bars indicate statistical groups with α = 0.05 using ANOVA.

To investigate this, I generated a moss line where one of the moss α-tubulin isoforms (Pp1s215_51V6 locus) is replaced with a mCherry-coding sequence fusion at the endogenous locus in the NLS4/lifeact-mEGFP line (NLS4/lifeact-mEGFP/mCherry-α-tubulin). I checked this line for growth phenotypes but found that plant area and solidity was similar to the NLS4/lifeact-mEGFP line (Figure 4.3). I acquired images of the tubulin line every 2 seconds over the course of 1 minute using spinning disc confocal microscopy (Figure 4.4A), and quantified microtubule dynamics using the correlation coefficient analysis. I found that *ROP*-RNAi plants have significantly reduced microtubule dynamics as compared to control plants (Figure 4.4B). To investigate if this reduction is specific for loss of ROP function, I measured microtubule dynamics in plants expressing the myoXIa+b5'UTR described in chapter 2 (referred to as *MyoXI* RNAi for the rest of the work in this thesis) which

exhibit a similar morphological defect, but have little impact on actin dynamics (Vidali et al., 2010) as compared to *ROP* RNAi plants. In addition, I also treated control cells with 13 μM latrunculin B, which also have a similar polarized growth phenotype, or with 50 μM taxol to stabilize microtubules. Initially 10 μM taxol was used, but did not inhibit microtubule dynamics (data not shown). I found that similar to *ROP* RNAi, both drug treatments as well as *MyoXI* RNAi inhibited microtubule dynamics. Surprisingly the Latrunculin B treatment had the largest inhibitory effect on microtubule dynamics (Figure 4.4B).

To identify if *ROP* RNAi had a specific effect on a particular aspect of microtubule dynamics, I measured rates of polymerization and depolymerization (Figure 4.4C). I found that both the *ROP* and *MyoXI* RNAi had reductions in polymerization rates. As expected, both polymerization and depolymerization rates were significantly reduced with the taxol treatment. Surprisingly, latrunculin B treatment was very similar to the taxol treatment. These data show that reduction in microtubule dynamics is likely a consequence of reduced tip growth, not loss of ROP specifically; suggesting that in moss ROP does not directly affect microtubule dynamics during tip growth. However, the latrunculin B data suggests that the actin and microtubule cytoskeletons impact each other.

To determine if loss of ROP affected the microtubule architecture in the cell, I quantified the filament bundling and density. I hypothesized that loss of ROP would lead to a decrease in filament density. However, I found that only the taxol treatment was significantly reduced in filament density, while bundling was not

significantly different for any of the five conditions (Figure 4.4D). This further supports that moss ROPs are not involved in the regulation of microtubules.

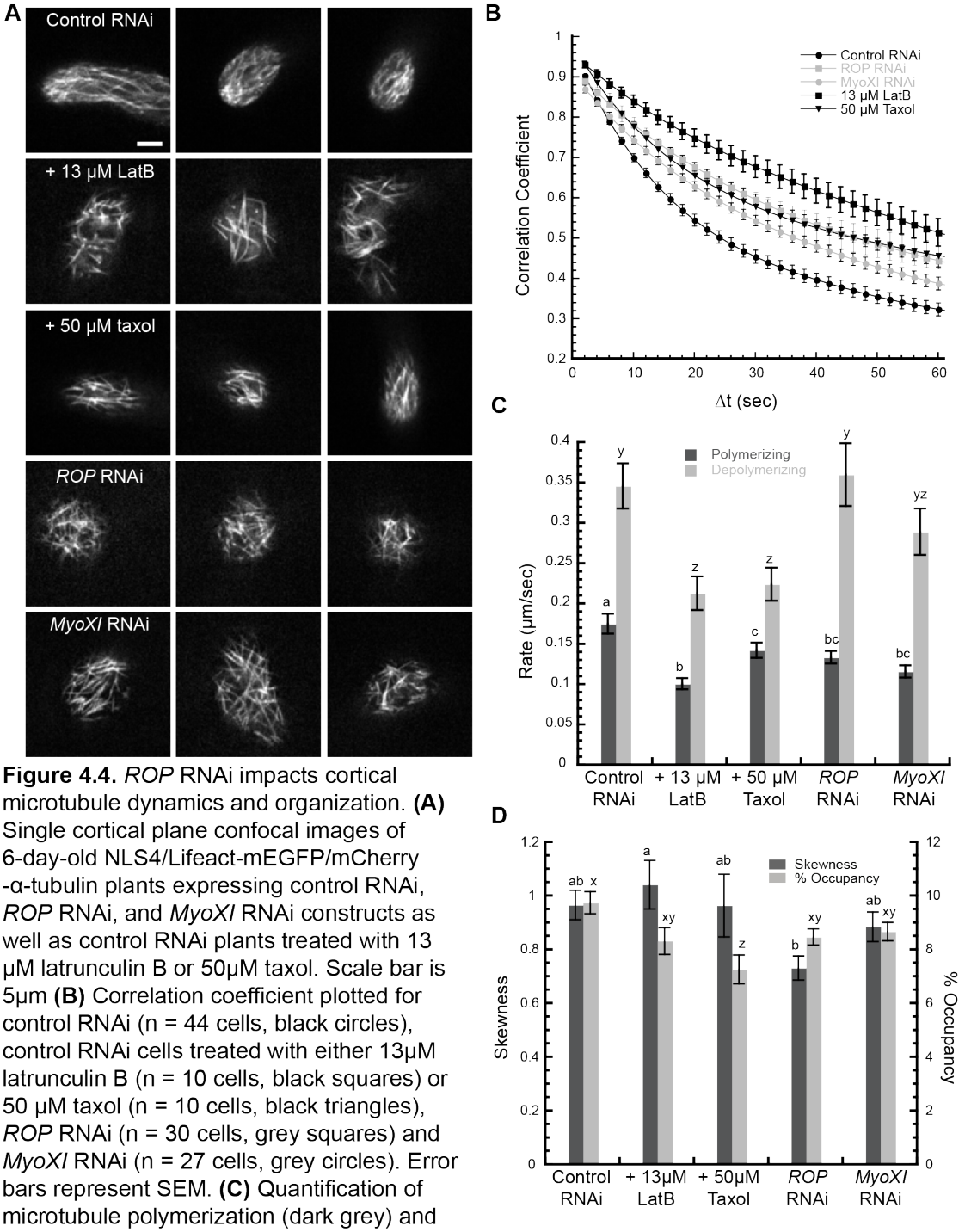

Figure 4.4. *ROP* RNAi impacts cortical microtubule dynamics and organization. **(A)** Single cortical plane confocal images of 6-day-old NLS4/Lifeact-mEGFP/mCherry -α-tubulin plants expressing control RNAi, *ROP* RNAi, and *MyoXI* RNAi constructs as well as control RNAi plants treated with 13 μM latrunculin B or 50μM taxol. Scale bar is 5μm **(B)** Correlation coefficient plotted for control RNAi (n = 44 cells, black circles), control RNAi cells treated with either 13μM latrunculin B (n = 10 cells, black squares) or 50 μM taxol (n = 10 cells, black triangles), *ROP* RNAi (n = 30 cells, grey squares) and *MyoXI* RNAi (n = 27 cells, grey circles). Error bars represent SEM. **(C)** Quantification of microtubule polymerization (dark grey) and depolymerization (light grey) rates. 12 - 15 elongating and 12 – 15 shrinking microtubules were measured for each of the conditions in (B). Error bars represent SEM and letters above bars indicate statistical groups with α = 0.05 using ANOVA. **(D)** Skewness and filament density measurements of 6-day-old NLS4/Lifeact-mEGFP/mCherry-α-tubulin plants expressing control RNAi (n = 15 cells), *ROP* RNAi (n = 15 cells), and *MyoXI* RNAi (n = 11 cells) constructs in addition to control RNAi plants treated with either 13 μM latrunculin B (n = 10 cells) or 50μM taxol (n = 10 cells). Error bars represent SEM and letters above bars indicate statistical groups with α = 0.05 using ANOVA.

CHAPTER 5

THE IMPACT OF *ROP* RNAi ON THE CELL WALL

ROP RNAi plants have a cell adhesion defect

To obtain material for the expression analyses in previous chapters, I picked 7-day old RNAi plants using a fine metal needle. In doing so, I noticed that *ROP* RNAi plants broke apart easily. To further investigate, I picked 8-day old plants into a small drop of water in a Petri dish and then placed the dish on the surface of the water in a sonication bath. Since *ROP* RNAi plants are composed of small spherical cells, I used *MyoXI* RNAi plants as a control for plants with a similar phenotype. Interestingly, I found that *ROP* RNAi plants broke apart into smaller clumps of cells or into individual cells; in contrast, control and *MyoXI* RNAi plants remained intact (Figure 5.1A). In a larger trial, where 30 plants were isolated and subjected to the same sonication treatment, 26 *ROP* RNAi plants broke apart whereas only one of 30 control plants and three of 30 *MyoXI* RNAi plants broke apart (Figure 5.1B).

Based on the sonication data, I hypothesized that the reduced cell adhesion in *ROP* RNAi plants is due to a cell wall component that is reduced or over-represented. Since pectin is known to underlie cell adhesion in plants (Lord and Mollet, 2002); I tried staining control, *ROP* and *MyoXI* RNAi plants with various pectin stains including ruthenium red, toluidine blue and propidium iodide. However none of these stains showed a consistent difference in pectin (data not shown). I also incubated control and *MyoXI* RNAi plants in excess EGTA to chelate the calcium in the cell wall. If pectin is the basis for the *ROP* RNAi adhesion defect,

this treatment should destabilize pectin in the cell wall causing control and *MyoXI* RNAi plants to fall apart easier with mild sonication. I also incubated *ROP* RNAi plants in excess calcium to determine if I could stabilize the pectin in the wall, and strengthen the cellular adhesion. However, neither treatment differed from controls (data not shown). This suggests that pectin plays a minor role in cell adhesion in moss.

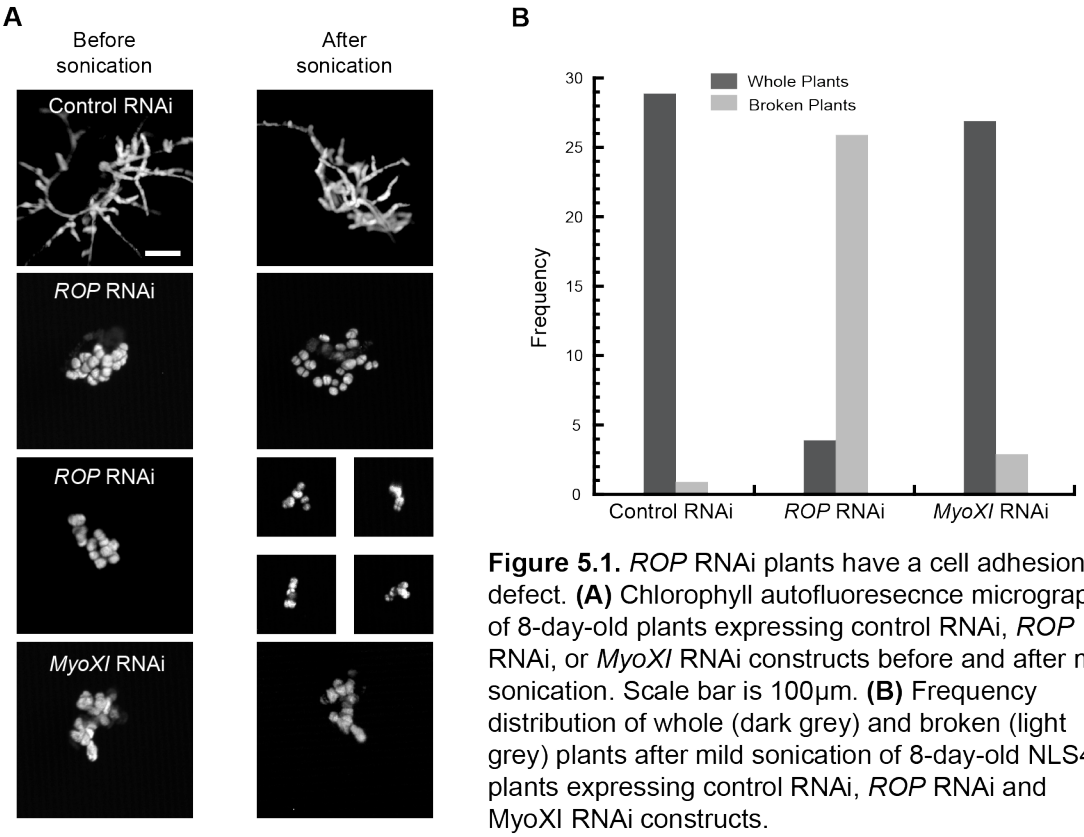

Figure 5.1. *ROP* RNAi plants have a cell adhesion defect. **(A)** Chlorophyll autofluoresecnce micrographs of 8-day-old plants expressing control RNAi, *ROP* RNAi, or *MyoXI* RNAi constructs before and after mild sonication. Scale bar is 100µm. **(B)** Frequency distribution of whole (dark grey) and broken (light grey) plants after mild sonication of 8-day-old NLS4 plants expressing control RNAi, *ROP* RNAi and MyoXI RNAi constructs.

It is possible that other cell wall components play a more predominate role in cell adhesion in moss. Since cellulose and callose are major components of the moss cell wall (Roberts et al., 2012), I investigated whether there were differences in cellulose and callose levels between control, *ROP*, and *MyoXI* RNAi plants. I isolated and stained plants with the following dyes: calcofluor white (stains cellulose and

callose), aniline blue (stains callose), and Pontamine fast scarlet 4B (stains cellulose). To quantify, I ensured that plants were stained for equivalent amounts of time and excess dye was removed by washing. I found that the fluorescence intensity was reduced for all three dyes in *ROP* RNAi plants compared to control plants, while *MyoXI* RNAi plants were similar to control levels for both calcofluor white and aniline blue, but slightly reduced for fast scarlet 4B (Figure 5.2A-D).

Because the intensity of a cell wall stain also depends on whether the dye can penetrate the wall, I used polarized light microscopy to look at birefringent cellulose in the cell wall (Figure 5.3A). Using line scans across the cell walls of control, *ROP* and *MyoXI* RNAi plants, I quantified the degree of light retardance. In contrast to the dye results, I found that *ROP* RNAi cells had the highest average retardance (10.7 nm, +/-0.44), while *MyoXI* RNAi cells had the lowest value (6.0 nm, +/- 0.35) (Figure 5.3B).

These data show that *ROP* RNAi cells have more cellulose in their walls, and *MyoXI* RNAi cells have less cellulose as compared to control RNAi plants. It is possible that the discrepancy between the dyes and polarized light microscopy results from an alteration in the organization of the cell wall, reducing dye accessibility. This alteration might be the underlying cause for the cell adhesion defect. The increase in cellulose in *ROP* RNAi plants suggests that secretion of cell wall material is not inhibited. In the absence of ROP, delivery of cell wall material may be distributed evenly around the entire membrane and the excess material and altered organization could make the cell unable to expand any more.

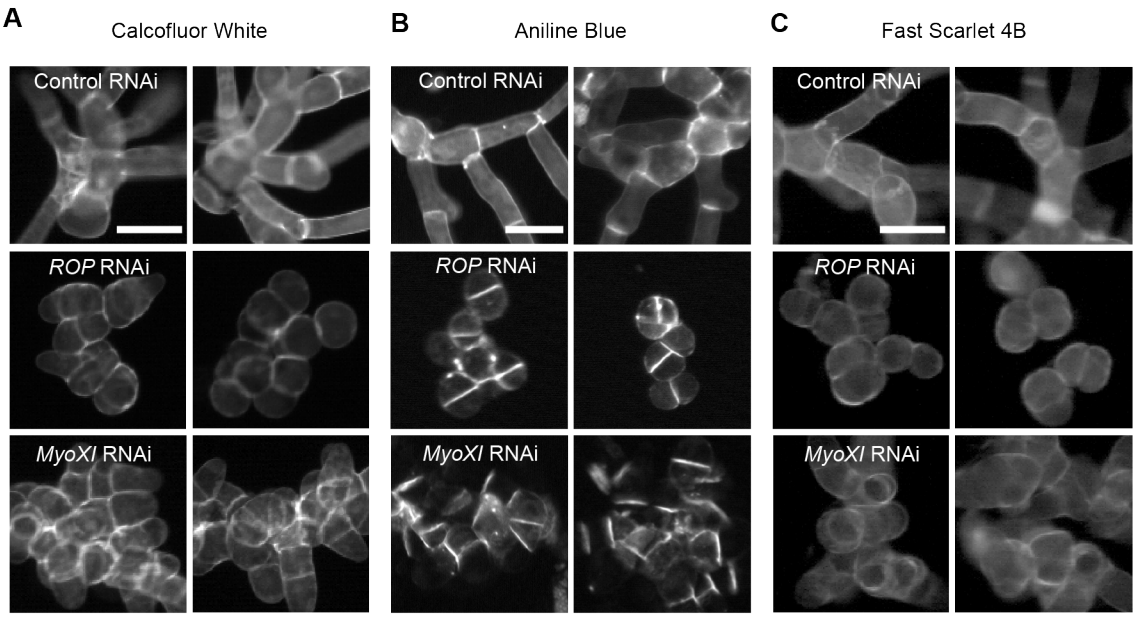

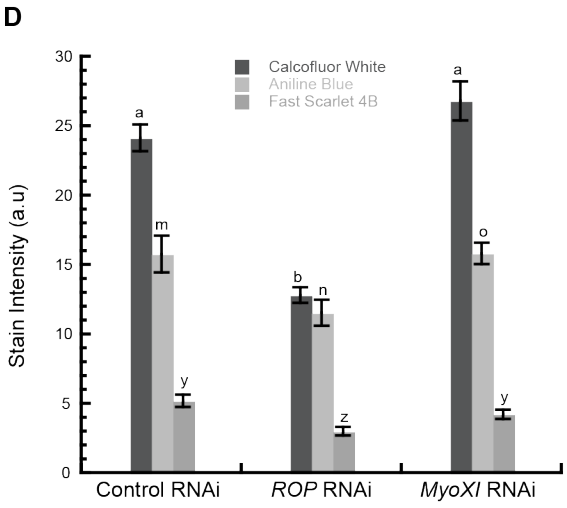

Figure 5.2. Cell walls stains indicate decreased polysaccharide content in *ROP* RNAi plants. **(A,B,C)** Flourescence micrographs of 6-day-old NLS4 plants expressing control RNAi, *ROP* RNAi, and *MyoXI* RNAi constructs stained with calcofluor white **(A)**, aniline blue **(B)** and fast scarlet 4B **(C)**. Scale bars are 50µm. **(D)** Fluorescence intensity quantification of calcofluor white (dark grey) and aniline blue (light grey) staining of 6-day-old NLS4 plants expressing control RNAi (n = 60/15/23 plants (calcofluor white/aniline blue/fast scarlet 4b)), *ROP* RNAi (n = 61/15/18 plants) and *MyoXI* RNAi (n = 25/19/22 plants) constructs. Error bars represent SEM and letters above bars indicate statistical groups with α = 0.05 using ANOVA.

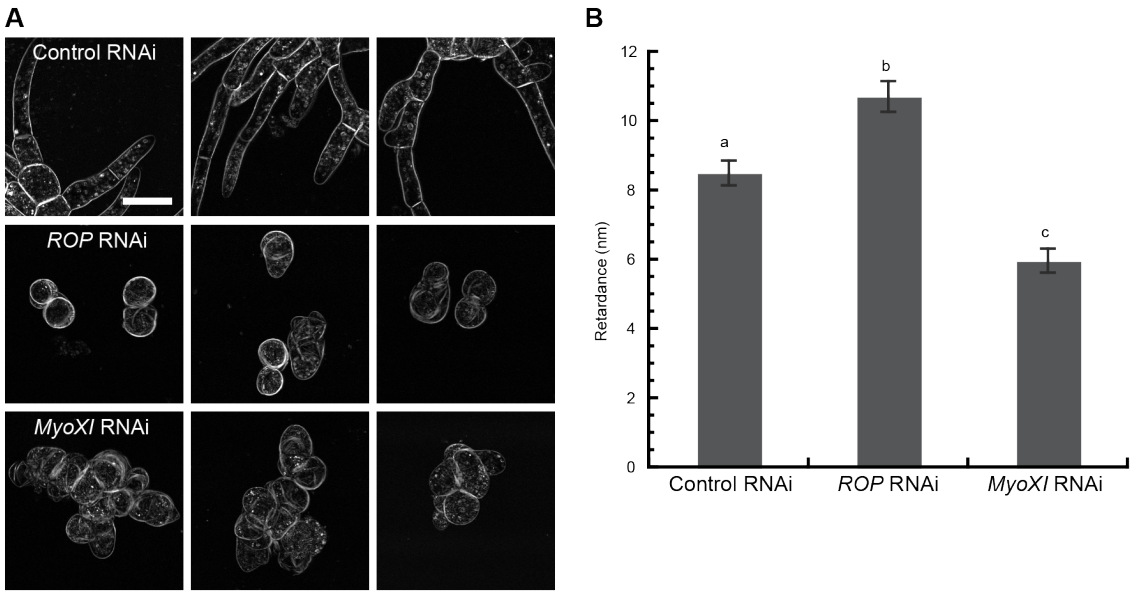

Figure 5.3 Cellulose deposition is not impaired in *ROP* RNAi plants **(A)** Polarized light retardance micrographs of 7-day-old NLS4 plants expressing control RNAi, *ROP* RNAi, and *MyoXI* RNAi constructs. Scale bar is 50µm. (F) Light retardance of cell walls based on polarized light images using at least 3 external cell walls from 8 – 10 images for each RNAi construct. Error bars represent SEM and letters above bars indicate statistical groups with α = 0.05 using ANOVA.

CHAPTER 6

CHARACTERIZING THE ROLE OF ROP REGULATORY PROTEINS

Establishing a bimolecular fluorescence complementation assay in moss

Small GTPases act as molecular switches and regulate cellular processes through effector proteins. To identify how ROP regulates tip growth, actin dynamics and cell adhesion, it is necessary to identify proteins that interact with ROP. To verify interactions in moss, I wanted to establish a bimolecular fluorescence complementation assay, which uses reconstitution of a split YFP molecule to signal interaction between two proteins (Hu et al., 2002). RNAi of positive interactors in this assay would then help determine how they interact with ROP. I chose *RopGAP6* and *RopGEF6* as positive controls for the assay because these families have previously been shown to interact with ROP in arabidopsis and these genes have the most expressed sequence tags for the respective families (Gu et al., 2006; Wu et al., 2000).

I generated vectors for the assay that would express ROP4 with an N-terminally fused fragment of eYFP (nEYFP-ROP4 and cEYFP-ROP4) (Figure 6.1A). Tagging at the C-terminus was not attempted in order to avoid interfering with the geranylgeranylation of ROP4. I generated similar vectors expressing RopGAP6, tagged N-terminally or C-terminally with either nEYFP or cEYFP (Figure 6.1A). I made similar constructs for RopGEF6 as well as control vectors that only expressed the EYFP fragments. I introduced the BiFC constructs in to moss by both PEG-mediated transformation of moss protoplasts and particle bombardment of moss

tissue, but I never saw a positive interaction using either method, even for control plasmids. In an attempt to strengthen the interactions, I used site directed PCR mutagenesis (Weiner et al., 1994) to create constitutively active (G15V) and dominant negative (T20N) isoforms of *ROP4*. As these mutant versions are locked in either the GTP bound (G15V) or GDP bound (T20N), interaction with RopGAPs and RopGEFs may be respectively enhanced. However I still did not observe any positive interactions.

Thinking that perhaps the constructs were not expressing, I extracted proteins from transformed protoplasts and performed an immunoblot using GFP antibodies. Almost all of the constructs were expressed and no cleavage of the GFP was evident (Figure 6.1B). I also tried using myosin XI tails, which dimerize via a coiled-coil domain, as alternative positive controls but no positive interactions were observed once again. These difficulties caused me to abandon a bimolecular fluorescence complementation approach to identifying effectors in moss. However, I still wanted to verify the regulation of ROPs by moss RhoGAPs and RhoGEFs, so I used RNAi of each gene family to investigate if the resulting phenotype was consistent with the reported role of the regulator.

Silencing moss RopGAPs

In arabidopsis and tobacco, the RopGAP/RhoGAP genes were identified through a yeast two-hybrid screen (Wu et al., 2000). In addition to a GAP domain these proteins have a cdc42/Rac interactive binding (CRIB) motif, which has been reported to increase interaction with active ROP and stimulates ROP GTPase

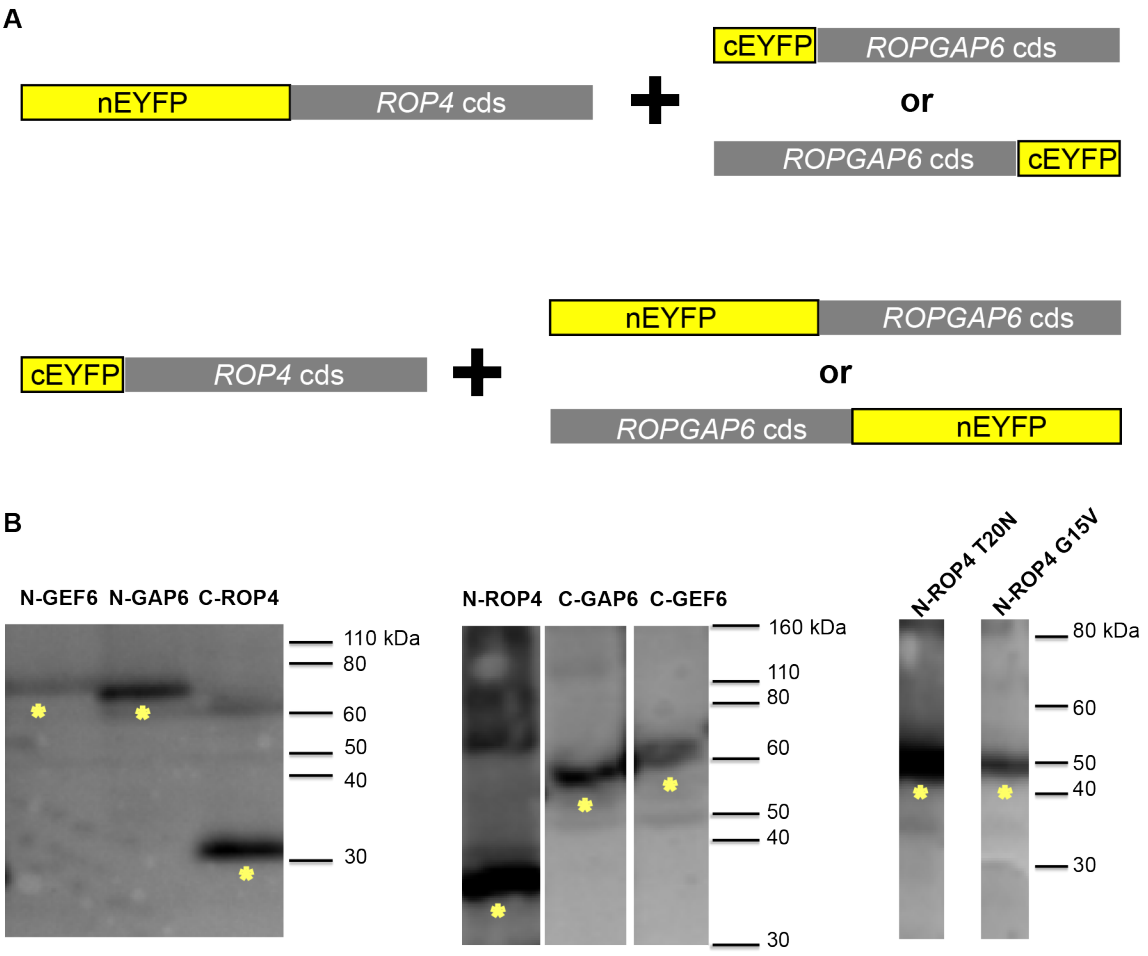

Figure 6.1. Establishing a bimolecular fluorescence complementation assay in moss. **(A)** Examples of BiFC construct combinations used to test for protein interaction in moss. All constructs were expressed under the maize ubiquitin promoter. **(B)** Immunoblot of protein extracts from protoplasts expressing various BiFC constructs. Yellow stars are placed below the band representing the expressed construct. No cleavage of YFP was evident and all bands sizes were as predicted. The immunoblot was probed with an antibody raised to GFP.

activity (Wu et al., 2000). In tobacco pollen tubes, NtRhoGAP1 localizes to the flanks of the cell tip and this localization is dependent on the N-terminus and CRIB domain (Klahre and Kost, 2006). This localization keeps active ROP restricted to the very tip of the cell.

There are five *RopGAP* genes and one *RopGAP*-like gene in arabidopsis (Wu et al., 2000). Similarly, moss has six *RopGAP* genes. Silencing of the *RopGAP*s in moss

should inhibit the deactivation of ROP leading to an accumulation of active ROP. This would be similar to over-expression of ROP. To silence the *RopGAP*s in moss, 216 – 240 bp from the coding sequences of *RopGAP* 1, 3, 4 and 5 were used to generate a *RopGAP* RNAi construct (Figure 6.2A). The sequences of *RopGAP* 1 and 3 are ~86% identical to *RopGAP* 6 and 2 over these regions, respectively. Expression of the *RopGAP* RNAi construct yielded significantly fewer silenced plants, approximately 40% the yield of *ROP* RNAi silenced plants in parallel transformations, varying both in size and the degree of solidity (Figure 6.2B & C). This is similar to what I observed when I attempted to rescue the *ROP* RNAi phenotype using the maize ubiquitin promoter to drive expression of a complementation construct. This suggests that these moss RopGAPs do indeed act as negative regulators of ROP activity.

Silencing RopGEF and SPK families

RopGEFs contain a novel PRONE (plant-specific ROP nucleotide exchanger) domain, which appears to be sufficient for both apical membrane localization of the GEF as well as activation of ROP (Gu et al., 2006; Berken et al., 2005; Zhang and McCormick, 2007). This PRONE domain is unique to the RopGEF protein family. Transient over-expression of a single arabidopsis RopGEF fused to GFP shows localization to the apex of tobacco pollen tubes (Berken et al., 2005; Gu et al., 2006). Over-expression of *RopGEF*s causes arabidopsis pollen tube tips to swell (Gu et al., 2006). It is thought that RopGEFs are regulated by autoinhibition, which is released when the C-terminus of RopGEF is phosphorylated by receptor like kinases (Eklund

et al., 2010). This regulation has been demonstrated by deletions and phosphomimetic mutations of *AtRopGEF12*, which causes tip swelling while the full-length protein does not (Zhang and McCormick, 2007).

There are only six *RopGEF*s in moss compared to the 14 identified in arabidopsis (Berken et al., 2005; Gu et al., 2006). By silencing *RopGEF* genes, the amount of active ROP should be reduced, so RNAi of *RopGEF*s would have a similar phenotype to *ROP* RNAi. To generate a *RopGEF* RNAi construct, I used 207 -230 bp of coding sequence from *RopGEF* 2, 4, 5 and 6 (Figure 6.3A). The sequences of *RopGEF* 4 and 6 are 90 and 86% identical to *RopGEF* 3 and 1 over these regions, respectively. Surprisingly, expression of the *RopGEF* RNAi construct had no impact on polarized growth or plant size (Figure 6.3B & C). This suggests that RopGEFs are not involved in regulating ROP activity during tip growth; although it is possible the expression is not silenced sufficiently for a phenotype.

The SPIKE (SPK) family of proteins has been shown to have GEF activity on ROP (Basu et al., 2008). These GEFs are similar to the DOCK 180 family of RhoGEFs found in animals and fungi, containing a DHR2 (Dock homology region) domain responsible for GEF activity as well as a DHR1 domain that interacts with membrane phospholipids $PI(3,5)P_2$ and $PI(3,4,5)P_3$ (Balagopalan et al., 2006). Null mutants of *AtSPK1* do not survive past the seedling stage and have defects in organelle morphology and trichome branching as well as in leaf pavement cell shape and adhesion (Basu et al., 2008, Qiu et al., 2002). *AtSPK1* is highly expressed in the region of the roots where root hairs form, but is not expressed in pollen tubes

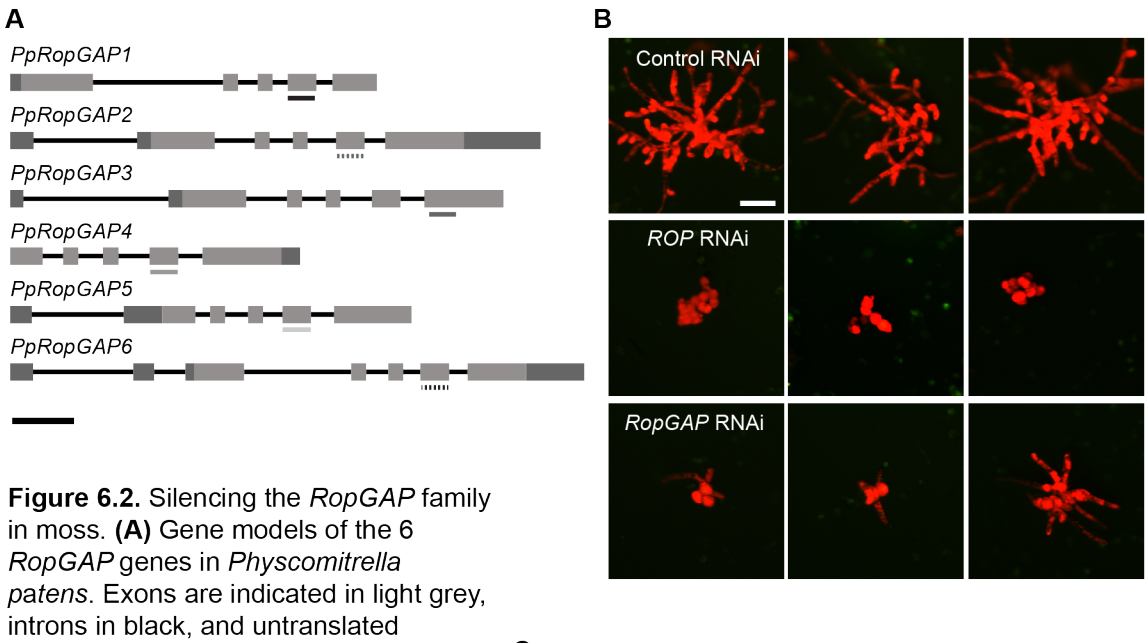

Figure 6.2. Silencing the *RopGAP* family in moss. **(A)** Gene models of the 6 *RopGAP* genes in *Physcomitrella patens*. Exons are indicated in light grey, introns in black, and untranslated regions in dark grey. Lines underneath gene models represent sequence regions targeted by the *RopGAP* RNAi construct. Solid lines indicate that the denoted sequence was used in the RNAi construct while dashed lines indicate highly similar sequence regions that are targeted by the RNAi construct. Scale bar is 500bp. **(B)** Chlorophyll autofluore-secnce micrographs of 7-day-old NLS4 plants regenerated from protoplasts expressing the *RopGAP* RNAi construct. Scale bar is 100µm. **(C)** Quantification of plant area (dark grey) and solidity (light grey) for control RNAi (n = 100 plants), *ROP4* cds RNAi (n = 100 plants) and *RopGAP* RNAi (n = 40 plants). Error bars represent SEM and letters above bars indicate statistical groups with α = 0.05 using ANOVA.

(Eklund et al., 2010). Despite the high expression in root hairs, no defect in tip growth has been reported. To test if loss of SPK results in reduced tip growth in moss, 234 – 251 bp from the coding sequences of *SPK*s 1, 4 and 5 were used to generate a *SPK* RNAi construct (Figure 6.4A). The *SPK1* fragment is 88% identical to *SPK2* over this region while the *SPK5* fragment has 89 and 93% identity with *SPK3*

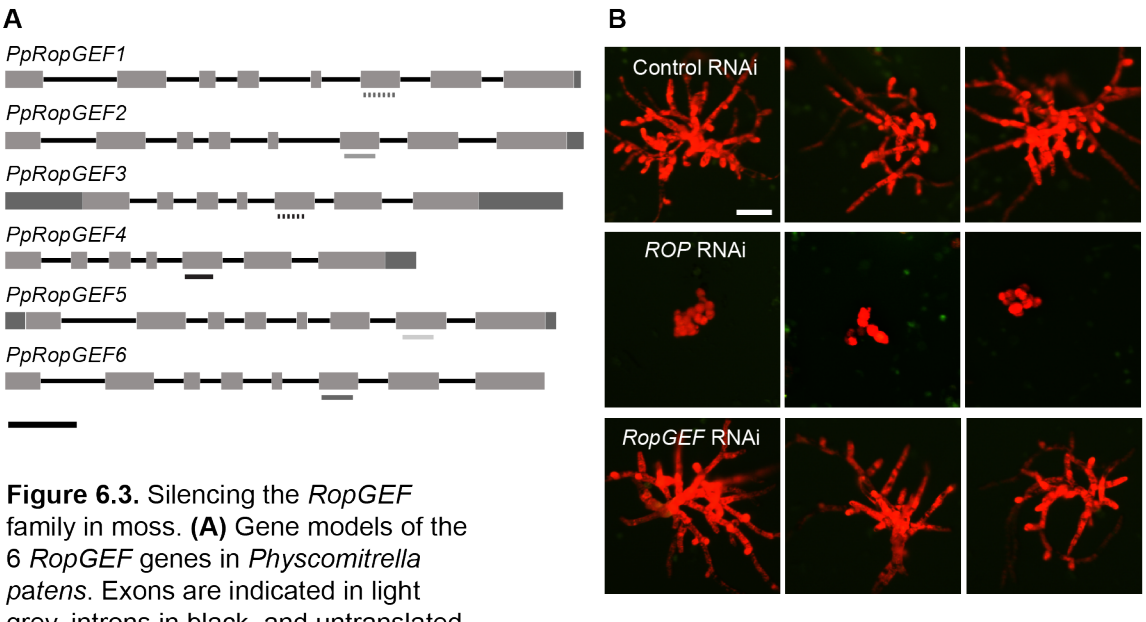

Figure 6.3. Silencing the *RopGEF* family in moss. **(A)** Gene models of the 6 *RopGEF* genes in *Physcomitrella patens*. Exons are indicated in light grey, introns in black, and untranslated regions in dark grey. Lines underneath gene models represent sequence regions targeted by the *RopGEF* RNAi construct. Solid lines indicate that the denoted sequence was used in the RNAi construct while dashed lines indicate highly similar sequence regions that are targeted by the RNAi construct. Scale bar is 500bp. **(B)** Chlorophyll autofluoresecnce micrographs of 7-day-old NLS4 plants regenerated from protoplasts expressing the *RopGEF* RNAi construct. Scale bar is 100µm. **(C)** Quantification of plant area (dark grey) and solidity (light grey) for control RNAi (n = 100 plants), *ROP4* cds RNAi (n = 100 plants) and *RopGEF* RNAi (n = 100 plants). Error bars represent SEM and letters above bars indicate statistical groups with α = 0.05 using ANOVA.

and *SPK6*, respectively. Plants expressing the *SPK* RNAi construct are smaller than control plants and also have increased solidity values (Figure 6.4B & C), although the polarized growth defect is not as severe as in *ROP* RNAi plants. This indicates

that SPK is the GEF for ROP activity in tip growth, which is surprising because no polarized growth defect has been reported for the *SPK1* mutants in arabidopsis.

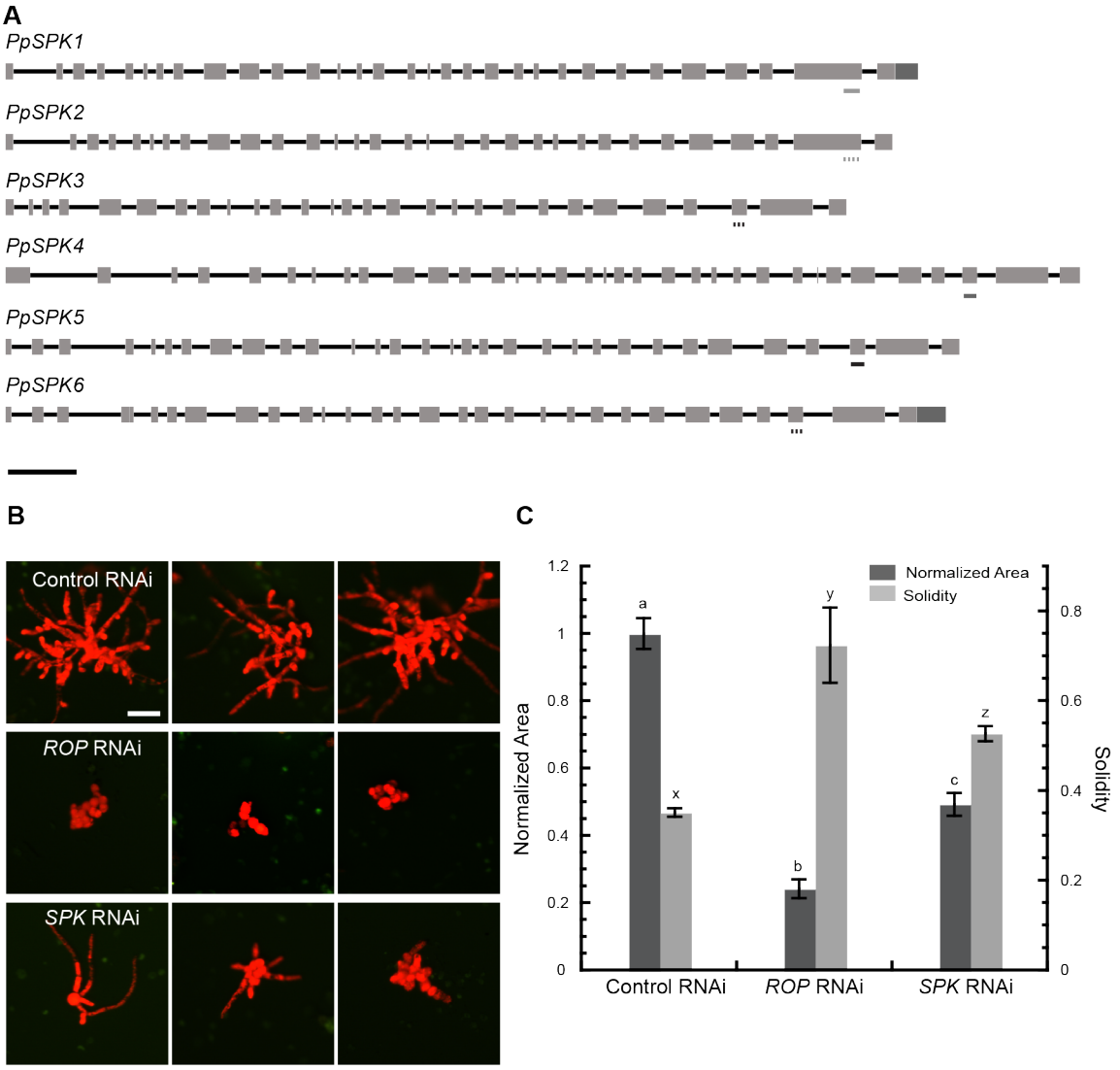

Figure 6.4. Silencing the *SPK* family in moss. **(A)** Gene models of the 6 *SPK* genes in *Physcomitrella patens*.Exons are indicated in light grey, introns in black, and untranslated regions in dark grey. Lines underneath gene models represent sequence regions targeted by the *SPK* RNAi construct. Solid lines indicate that the denoted sequence was used in the RNAi construct while dashed lines indicate highly similar sequence regions that are targeted by the RNAi construct. Scale bar is 1000bp. **(B)** Chlorophyll autofluoresecnce micrographs of 7-day-old NLS4 plants regenerated from protoplasts expressing the *SPK* RNAi construct. Scale bar is 100µm. **(C)** Quantification of plant area (dark grey) and solidity (light grey) for control RNAi (n = 100 plants), *ROP4* cds RNAi (n = 100 plants) and *SPK* RNAi (n = 100 plants). Error bars represent SEM and letters above bars indicate statistical groups with α = 0.05 using ANOVA.

CHAPTER 7

DISCUSSION

Myosin XI in tip growth

I have shown that myosin XI is essential for tip growth. In vascular plants, previous studies altered myosin XI function by either insertional knockouts or dominant-negative constructs (Hashimoto et al., 2005; Ojangu et al., 2007; Peremyslov et al., 2008; Prokhnevsky et al., 2008; Sparkes et al., 2008). Compared to *P. patens*, vascular plants contain more isoforms of myosin XI, significantly complicating functional studies. Single and double insertion mutants in a subset of myosin XI genes from arabidopsis have defects in organelle transport (Peremyslov et al., 2008; Prokhnevsky et al., 2008; Ojangu et al., 2012). Some mutants also have stunted root hairs, although polar outgrowths are still present (Ojangu et al., 2007; Peremyslov et al., 2008; Prokhnevsky et al., 2008). The dominant-negative approach, which relies on over-expression of the tail domain of myosin XI, has been used to investigate global loss of myosin XI function (Sparkes et al., 2008). However, as I discussed in the introduction, localization of either the head or the tail domain alone is often different, so these dominant-negative tails may have interactions with molecules that do not occur in wild type. The RNAi assay I used in my thesis has a key advantage over these other approaches. Namely, I was able to observe the phenotype resulting from silencing of all members of the myosin XI gene family within one week of transformation.

In addition, by using specific RNAi constructs containing UTR sequences together with expression analyses, I have demonstrated that the two expressed myosin XI genes in moss protonemata are functionally redundant, with the myosin XIa gene being the predominantly expressed gene during protonemal growth. Importantly, when both UTR sequences are used in the same RNAi construct, I am able to phenocopy the coding sequence constructs, underscoring the specificity of the constructs. Because the plants are so severely affected when both myosin XI genes are silenced, it may not have been possible to use a knockout approach. In vascular plants, such as arabidopsis, it is plausible that multiple myosin XI isoforms are partially redundant with respect to tip growth and that the appropriate mutant combination has yet to be generated to completely abrogate root hair and pollen tube growth. Additionally, as is the case for moss myosins, the complement of myosins in arabidopsis required for tip growth may also be required for viability and therefore a full loss-of-function mutant may be embryonic lethal.

Using a rapid transient rescue assay, I show that a single myosin XI gene is sufficient for tip growth. Interestingly, an excess amount of the rescuing plasmid does not appear to affect growth area and polarity, suggesting that over-expression of myosin XI does not abrograte growth. However, upon imaging plants containing 3xmEGFP-myosin XI, the fluorescent signal was found to be very weak in comparison with lines overexpressing mEGFP alone. Thus, it is likely that the myosin XI transcript or protein levels, particularly from myoXIa, are regulated. It is possible that the myoXIa transcript variants I found may either contribute to or be a product of this regulation.

Plants lacking myosin XI function closely resemble plants that have been silenced for proteins critical for actin function, such as profilin, ADF and formin (Vidali et al., 2007; Augustine et al., 2008; Vidali et al., 2009b). Loss-of-function of these actin-binding proteins results in severely stunted plants composed of small spherical cells. Silencing of these proteins, like silencing of myosin XI, results in cells with disorganized actin (Vidali et al., 2007; Augustine et al., 2008; Vidali et al., 2009b, Vidali et al., 2010). Whether actin organization relies directly on myosin XI still needs to be examined. However, it is clear that actin dynamics are critical for tip growth. Tip growing cells treated with latrunculin B immediately stop growing (Vidali et al., 2001; Vidali et al., 2009a). It has been shown that myosin XI is not directly involved in regulating actin dynamics (Vidali et al., 2010). This suggests that myosin XI may be involved in either organizing the actin network or moving vesicles to and away from the site of growth.

Consistent with a role in polarized secretion, I found that 3xmEGFP-myoXIa concentrates subcortically at the apex of growing cells. This localization is different from that of mEGFP alone and has been corroborated by other studies using full-length myosins and these studies have also demonstrated myosin XI association with secretory vesicles (Peremyslov et al., 2012; Peremyslov et al., 2013). Additionally, in contrast to previous localization studies, which have analyzed the localization of myosin XI and myosin XI subdomains (Yokota et al., 1995; Hashimoto et al., 2005; Li and Nebenfuhr, 2007; Reisen and Hanson, 2007; Yokota et al., 2008; Sattarzadeh et al., 2011; Sattarzadeh et al., 2013), 3xmEGFP-myoXIa does not localize to organelles. *P. patens* protonemal cells have no cytoplasmic streaming and

show only slow saltatory organelle movements, which is in contrast to the rapid cytoplasmic streaming and organelle motility observed in many vascular plants (Furt et al., 2013). My localization studies are consistent with these slower rates of organelle motility. Future studies will focus on identifying the nature of the subcortical region containing myosin XI and its cargo.

In addition to being localized to the subcortical region of the apex, 3xmEGFP-myoXIa accumulation fluctuates. Time-lapse coupled, three-dimensional imaging has been used to determine that the position of the apical cluster moves in three dimensions in and out of the medial plane of the cell, and it also fluctuates in intensity (Vidali et al., 2010). Similar fluctuations have been observed in apical actin residing in the medial section of moss cells (Vidali et al., 2009a), and these myosin XI fluctuations proceed and those of actin (Furt et al., 2013). In support of this, when cells are treated with jasplakinolide, which stabilizes the actin cytoskeleton, it has been observed that both the apical actin focal point and the myosin XI accumulation dissipate (Vidali et al., 2010). This suggests that dynamic actin is required for myosin XI localization. However, treatment of moss cells with low levels of latrunculin B does not dissipate the apical myosin XI accumulation (Furt et al., 2012). Similar to what has been observed in yeast (Kozubowski et al., 2008), it is possible that these fluctuations might result from a feedback loop regulating the distribution of myosin and its cargo. Moss myosin XI has recently been demonstrated to associate with endomembrane vesicles (Furt et al., 2013). Alterations in this feedback mechanism, at the level of actin dynamics, organization, or secretion, would result in disruption of tip growth. Consistent with this, moss

lacking critical regulators of actin dynamics and organization result in round cells with altered actin organization (Vidali et al., 2007; Augustine et al., 2008; Vidali et al., 2009b; Vidali et al, 2010). This suggests that myosin XI's role in this cycle is to either organize actin or drive secretion to the site of tip growth.

Based on polarized light microscopy, one possible secretory cargo for myosin XI is vesicles containing cellulose synthase molecules. I have shown that plants lacking myosin XI appear to have reduced crystalline cellulose in their walls, suggesting that there may be a defect in the delivery of cellulose synthase. Whether this is due to a lack of one component or many remains to be seen. However the loss of the only other family of myosins, myosin VIII, does not have a polarized growth phenotype (Wu et al., 2011). This suggests that many cell wall components may be delivered in myosin XI transported vesicles.

My studies of myosin XI in tip growth support a role in delivering vesicles for synthesizing new cell wall via actin filaments. Loss of myosin XI results in a disordered actin cytoskeleton, suggesting that myosin XI may be involved in organizing actin. However, this disordered actin cytoskeleton is not specific to the loss of myosin XI and has been observed in *ROP*, *ADF*, profilin and formin RNAi plants when myosin XI is present (Vidali et al., 2007; Augustine et al., 2008; Vidali et al., 2009b). Currently, it is unknown if this disordered actin is a cause of or a result of the loss of polarized growth.

ROP in tip growth

Similar to myosin XI, previous studies of ROP function have used over-expression of constitutively active and dominant negative isoforms in plants that still have many other endogenous *ROP* genes (Li et al., 1999; Jones et al., 2002; Fu et al., 2002; Fu et al., 2001). This has complicated functional studies. However, the swelling of pollen tubes and root hairs over-expressing constitutively active ROP and the cessation of growth when the dominant negative form is over-expressed have lead to the assumption that ROP plays a key role in tip growth. Using RNAi to silence all four *ROP* genes in moss, I have shown that ROP is essential for this process. Deletion of any single moss *ROP* did not result in a loss of tip growth, indicating that no single gene is responsible for regulation. By rendering the alleles of *ROP3* or *ROP4* RNAi insensitive, I demonstrated that either is sufficient to maintain tip growth during the reduction of all other endogenous *ROP*s. These two genes are the most highly expressed, making up 97% of the total *ROP* transcript in wild-type plants, so it is possible that *ROP1* or *ROP2* might not be capable of maintaining tip growth under the same conditions.

Interestingly, the expression of *ROP* genes are affected by alterations in other *ROP* loci, as the deletion of any single gene results in a reduction in expression of the other three compared to wild-type. This was also observed when the expression of *ROP4* was reduced when the 3'Utr region of the *ROP3* locus was removed. Reduction of the overall expression of moss *ROP*s correlates with reduced plant size but plant solidity is unaffected in both the stable deletion lines and the RNAi insensitive lines,

suggesting that a basal level of *ROP* expression is required for tip growth to occur and more *ROP* expression will lead to faster growth.

I also found that *ROP* expressed under a strong promoter is lethal, indicating that an upper threshold for *ROP* expression levels may also exist. However, this apparent lethality may be due to high expression levels of ROP leading to an accumulation of non-geranylgeranylated ROP, which may dilute the pool of functional ROP and compete for interactors. It would be interesting to see if high expression levels of ROP in arabidopsis also result in accumulation of non-geranylgeranylated versions.

I have also shown that ROP function is dependent on the genomic structure of the locus, as stable lines where the genomic *ROP4* locus was replaced with only the coding sequence were no longer capable of maintaining polarized growth in the absence of the other three endogenous ROPs. It would be interesting to look at the *ROP* expression levels in the *ROP4* coding sequence allele replacement stable line to see how levels and growth are impacted. Since the coding sequences are so similar, regulation of *ROP* transcript levels could be mediated by microRNAs. By deleting one *ROP* gene the relative amount of silencing in the other three genes would be increased, which is what I have observed. However, more investigation into the complex regulation of ROP transcription is required.

Previous localization data for ROP in live cells has been acquired by overexpressing GFP-ROP fusion proteins (Gu et al, 2003; Gu et al., 2006). These fusion proteins were never shown to be functional, but the apical plasma membrane enriched localization has also been demonstrated using immunofluorescence

(Molendijk et al., 2001). With my method of generating stable lines with RNAi insensitive ROP alleles, I had a tool to identify functional GFP-ROP fusions. Unfortunately though I was able to isolate stable lines where the coding sequence of *ROP4* was tagged at the N-terminus or the GFP was inserted in the *ROP4* locus prior to the C-terminal CaaX motif, neither fusion proved to be functional. However, the NLS4/mEGFP-ROP4cds line did exhibit the previously observed apical localization. Unfortunately. I was unable to assess if it was functional or not, as the *ROP4*cds gene replacement line was also not functional. These allele replacement lines further support complex regulation of *ROP* expression.

ROP has been linked to the organization and deposition of the actin cytoskeleton in other plant systems (Fu et al., 2001; Fu et al., 2002), causing delocalization or inhibition of apical actin structures. However, there had yet to be a quantitative analysis of how dynamic the actin cytoskeleton is. I investigated how *ROP* RNAi affects the actin cytoskeleton in moss because I can quantitatively measure actin dynamics in a loss-of-function state.

Based on previous research in arabidopsis where *ROP2* activity increases actin deposition through the effectors *RIC3* and *RIC4* (Xu et al., 2010), I hypothesized that the absence of ROP would result in reduced actin dynamics and a less dense actin network. While the actin cytoskeletal density was reduced, I was surprised to find that actin dynamics were actually increased in *ROP* RNAi plants, suggesting that ROP is a negative regulator of this process. It is unlikely that this regulation would be unique to moss, as actin and the proteins involved with it are highly conserved.

As other studies quantify live cell actin dynamics for *ROP* mutants in other systems, I expect similar results.

I discovered that one potential target of ROP signaling that impacts actin is class II formins. Using TIRF microscopy I analyzed the population of cortical formin at the plasma membrane and found that this population is reduced in *ROP* RNAi cells. This is likely an underlying cause for the reduction in actin density that I observed. Interestingly, despite this reduction of cortical formin, the active fraction that elongates actin filaments is about twice that of control cells. This increase in formin activity supports the observed increase in actin dynamics. It seems that once the formin is active it behaves the same in *ROP* RNAi as controls, as elongation rates and the duration of elongation events are similar.

Since the phospholipid $PI(3,5)P_2$ is critical for the localization of class II formins to the plasma membrane (van Gisbergen et al., 2012), ROP may be responsible for generating a membrane domain that recruits formin and perhaps other cell polarity factors. Yeast formins are directly regulated by the Rho GTPase cdc42 via a GTPase binding domain, which will release the formin from an autoinhibitory state (Dong et al., 2003). However plant formins lack this GTPase binding domain (van Gisbergen and Bezanilla, 2013), and no direct interactions between ROPs and formins have been reported, so it is likely that any regulation of formin activity by ROP would be indirect if it exists. Nevertheless, my observations indicate that ROP does not regulate formin activity in plants. Since the population of active formin is what changes when ROP is lost, it is possible that an activator of formin is present at the plasma membrane. If there is no reduction in the activator

while the amount of formin is reduced, then an increase in the fraction of active formin is what should be expected and is what I observed. The observed increase in actin dynamics may also be due to the reduced formin density on the plasma membrane. In control cells, there is a much higher rate of what appear to be collisions between formin spots. This may result in a cessation of actin filament elongation after each collision. This would result in fewer filaments being elongated in controls cells, Meanwhile the lower formin density in *ROP* RNAi cells results in fewer collision events resulting in more actin filaments being elongated and a resulting increase in actin dynamics. This suggests a possible system for ROP regulation of the actin cytoskeleton by defining membrane domains where cell polarity factors are recruited, which then may drive localized secretion of the materials required for tip growth. When this definition is lost due to the absence of ROP, these materials are instead spread throughout the plasma membrane and no polarization can occur.

Despite microtubules not being essential for tip growth, multiple ROPs have been linked to the microtubule cytoskeleton in arabidopsis. Since the moss ROPs are nearly identical, I hypothesized that moss ROPs affected both actin and microtubules. I generated a stable mCherry-α-tubulin expressing line and silenced ROP. While microtubule dynamics, in particular polymerization were significantly reduced, this was not specific to loss of ROP. Plants with similar cell sizes and shapes also had reduced dynamics. This suggests that this reduction may be due to a lack of polarized growth in general and that ROP does not affect microtubules during tip growth. Interestingly, the absence of actin had the greatest impact on

microtubules. This interplay has been observed previously, where recovery of either cytoskeleton after depolymerization is dependent on the presence of the other cytoskeleton (Sampathkumar et al., 2011). It would be interesting to examine the impact of oryzalin or taxol treatments on actin dynamics and organization to see if this codependency also exists in moss.

ROP and cell adhesion

An unexpected finding in my thesis is the reduced intercellular adhesion observed in *ROP* RNAi plants. This cell adhesion phenotype may be unique to ROP and the relevant ROP effectors, as mutants with similar cell shape phenotype such as *MyoXI* RNAi do not exhibit this adhesion defect. While a cellular adhesion phenotype has not been reported for ROP in other systems, perturbation of *ROP2* and *ROP6* activity in arabidopsis leads to malformed lobes in leaf pavement cells (Xu et al., 2010). As a result, the leaf surface has several gaps between cells. Mutants of *SPK1* in arabidopsis have a similar phenotype in pavement cells, especially in the cells surrounding guard cells (Zhang et al., 2010) and in this study they attribute this phenotype to cell adhesion. This phenotype may actually be a combination of both misforming lobes and decreased cell adhesion.

To identify the basis of this cell adhesion defect, I first attempted to characterize the pectin in moss cell walls, because pectin has been widely implicated in plant cell adhesion (Lord and Mollet, 2002). Despite trying multiple stains specific for pectin (including toluidine blue, ruthenium red and propidium iodide), I was unable to obtain consistent staining patterns in either control or *ROP* RNAi cells. I

also tried stabilizing the pectin in the walls of *ROP* RNAi plants with excess calcium but I saw no rescue in cell adhesion. I then tried to destabilize the pectin in the walls of control and *MyoXI* RNAi plants using EGTA to chelate calcium in order to lessen cellular adhesion, but the treatment had no effect. While these results do not rule out alterations in pectin as a possible cause for this adhesion defect, they make it less likely.

I began to look at other cell wall sugars to see if they are altered in *ROP* RNAi plants. Using stains that were specific for cellulose, callose or both, I saw a decrease in staining intensity in *ROP* RNAi plants compared to control or *MyoXI* RNAi plants. On its own, this suggests that these sugars are present in reduced amounts in the absence of ROP. However the polarized light microscopy data tell a different story. Based on retardance, there is evidently an increase in the amount of cellulose in the walls of *ROP* RNAi plants. This discrepancy between the stains and polarized light imply that there might be a difference in cell wall organization in the absence of ROP. Alterations in the cell wall could change the accessibility of stain binding sites or decrease the permeability of the wall to these stains, resulting in lower stain intensities regardless of how much of a particular substrate is present. Since polarized light microscopy does not depend on stain-substrate interactions, it provides a more reliable method for imaging cellulose levels in the wall.

Interestingly, while *ROP* RNAi plants have increased cellulose in the wall compared to control plants, levels in *MyoXI* RNAi plants are lower than controls despite having a similar polarized growth defect. This suggests that these two proteins are involved in different aspects of tip growth. The observation that plants

lacking myosin XI have lower levels of cellulose is consistent with a role in delivering vesicles carrying cellulose synthase. The higher cellulose levels in the absence of ROP suggest that ROP is not involved in regulating how much cell wall material is delivered but perhaps directing where in the cell delivery occurs. If vesicle delivery is global instead of site specific it may result in more isotropic expansion, creating more spherical cells as is observed in *ROP* RNAi plants. If deposition of new cell wall occurs everywhere along the cell and new wall material is constantly being delivered, this could result in the cell wall being denser in the absence of ROP. This could reduce dye penetrance, which is a possible underlying cause in the observed reductions in stain intensity.

My analysis of this cell adhesion phenotype is far from complete. There are other experiments that would aid in identifying what is different in the cell walls of plants lacking ROP. Antibodies that specifically recognize the esterification status of pectins could be used to identify shifts in the populations of methyl-esterified and de-esterified pectins in moss (Lee et al., 2005). I chose not to use this approach due to the discrepancies I observed when staining the cell wall, as limited dye permeability/accessibility might also apply to antibodies. Another approach is to use raman spectroscopy, which can identify and quantify relative amount of polysaccharides in the cell wall based on light scattering patterns (Zeng et al, 2012; Gierlinger et al., 2012). This approach is currently underway.

ROP interactors

Since ROP is a small GTPase, it regulates downstream cellular processes through effector proteins. Work in arabidopsis has identified two plant specific ROP effector families in ICR/RIP and RIC (Lavy et al, 2007; Li et al., 2008; Wu et al., 2001). While arabidopsis has five ICR/RIP genes, there are none in moss. Moss has only one *RIC* gene compared to the eleven found in arabidopsis. The lack of a tip growth phenotype when the lone moss *RIC* is silenced indicates that it is likely not an effector for the regulation of tip growth by ROP, however it may be an effector for another cellular process regulated by ROP. Some key animal and fungal Rho GTPase effectors including p-21 activated kinases (PAKs) and Rho-associated kinases (ROCKs) have no known homologs in plants (Eklund et al., 2010). This suggests that moss ROPs function through unidentified effectors. The RIC and ICR/RIP families as well as the RopGAP and RopGEF families were all first identified via yeast two-hybrid screens, so this would likely be an efficient method to screen for moss ROP effectors. However, positive interactions need to be further verified in moss.

In an attempt to develop live cell verification for ROP-effector interactions in moss, I developed a bimolecular fluorescence complementation assay. Due to the lack of ICR/RIP genes and the uncertainty of the interaction between the lone moss RIC and ROP, I chose to set up positive controls using the two protein families that control the activity of ROP, RopGAPs and RopGEFs. Unfortunately, I was not able to see any positive results using the assay, despite using constitutively active and dominant negative isoforms of ROP in an attempt to strengthen the interaction with RopGAPs and RopGEFs, respectively. Other positive controls also failed, indicating

that there may be issues with performing this assays in moss and that ROP interactions with RopGAPs and RopGEFs may still be occurring. While not testing for direct interaction with ROP, the *RopGAP* and *RhoGEF* families have very specific functions. Through RNAi of these gene families, I can impair either the activation or the deactivation of ROP and determine if the resulting phenotype is predicted by the reported role of each gene family.

Silencing of the moss *RopGAP*s should result in an accumulation of active ROP, similar to increased ROP expression levels. RNAi of the *RopGAP*s resulted in very few transformants with no consistency in plant size or polarity. This is similar to what I observed when I used a *ROP* over-expression construct in an attempt to complement the *ROP* RNAi phenotype. The similarity of *RopGAP* mutant phenotypes and *ROP* over-expression has been observed previously, mutations reducing the GAP activity of NtRhoGAP1 caused ballooning of the pollen tubes, similar to over-expression of the small GTPase *NtRAC5* (Klahre and Kost, 2006)

There are two RhoGEF families in plants, RopGEF and SPK. The RopGEF family is plant specific and features a plant specific PRONE domain that enables interaction and GEF activity with ROP. Most RopGEFs in arabidopsis have a similar apical membrane localization as has been seen for ROP and over-expression results in swelling of pollen tube tips similar to ROP over-expression (Gu et al., 2006;Gu et al., 2003). The *SPK* family is similar to the DOCK 180 family of RhoGEFs found in animals and fungi, but has been demonstrated to have GEF activity on ROP (Basu et al., 2008). While *SPK* is expressed in root hair forming cells in arabidopsis, no tip growth defect has been described for the lone *SPK* gene. This may be because SPK

localizes to the ER exit sites in arabidopsis and not the apical plasma membrane. Surprisingly, silencing of these two families revealed that SPK is the important RhoGEF for tip growth in moss, as *SPK* RNAi yields plants with a combination of polarized and unpolarized cells. RNAi of the RopGEFs are essentially indistinguishable from control plants. Because arabidopsis SPK mutants exhibit a possible cell adhesion phenotype, I did examine if moss plants expressing SPK RNAi had a similar cell adhesion defect similar to ROP RNAi plants. I tested by probing with a fine needle and did not observe SPK RNAi plants coming apart. However I did not test this phenotype via sonication, which may have revealed a milder adhesion defect.

These results raise some interesting questions about the RopGEF family in plants. Since RopGEFs do not appear to be involved in tip growth they likely play a role in another ROP-mediated cellular process. It is interesting that arabidopsis has fourteen *RopGEF*s compared to the six in moss. It is possible that throughout the evolution of the plant lineage the *RopGEF* family has expanded in order to regulate ROP activity in more diverse cellular functions and tissue types found in seed plants, while SPK genes have been lost over time. The spikemoss *Selaginella molendorfii* has four *RopGEF* genes and only one *SPK* gene, so it is possible that an expansion of *SPK* genes occurred in the bryophyte lineage.

Since SPKs are involved in moss tip growth instead of RopGEFs, the subcellular localization of these proteins is intriguing. Perhaps SPK is not at the ER exit sites as it is in arabidopsis, but instead localizes to the apical plasma membrane. It is possible that SPK localization is based on the DHR2 domain, which in animal

and fungal homologs has been found to bind $PI(3,5)P_2$, and that the distribution of this phospholipid varies between arabidopsis and moss. It has already been demonstrated that $PI(3,5)P_2$ is found at the cortical membrane in moss, so DHR2 mediated localization of SPK to this region is certainly a possibility.

A possible mechanism for the regulation of tip growth in moss

The work I have presented in this thesis has revealed some potential connections between proteins essential for tip growth. Since class II formins are localized to $PI(3,5)P_2$ domains of the cortex and their recruitment is reduced in the absence of ROP, the potential localization of SPK to this area could represent a breakthrough in identifying how ROP regulates tip growth. ROP may define $PI(3,5)P_2$ distribution in the membrane and $PI(3,5)P_2$ localized SPK could activate more ROP in these regions, which in turn would recruit class II formins to polymerize actin filaments that deliver more cellulose synthase laden vesicles via myosin XI (Figure 7.1). These vesicles may also deliver more $PI(3,5)P_2$ and SPK which would in turn activate more ROP and recruit more formin, creating a positive feedback loop to establish a site for tip growth to occur. A similar feedback mechanism has been proposed to establish cell polarization in budding yeast (Smith et al., 2013).

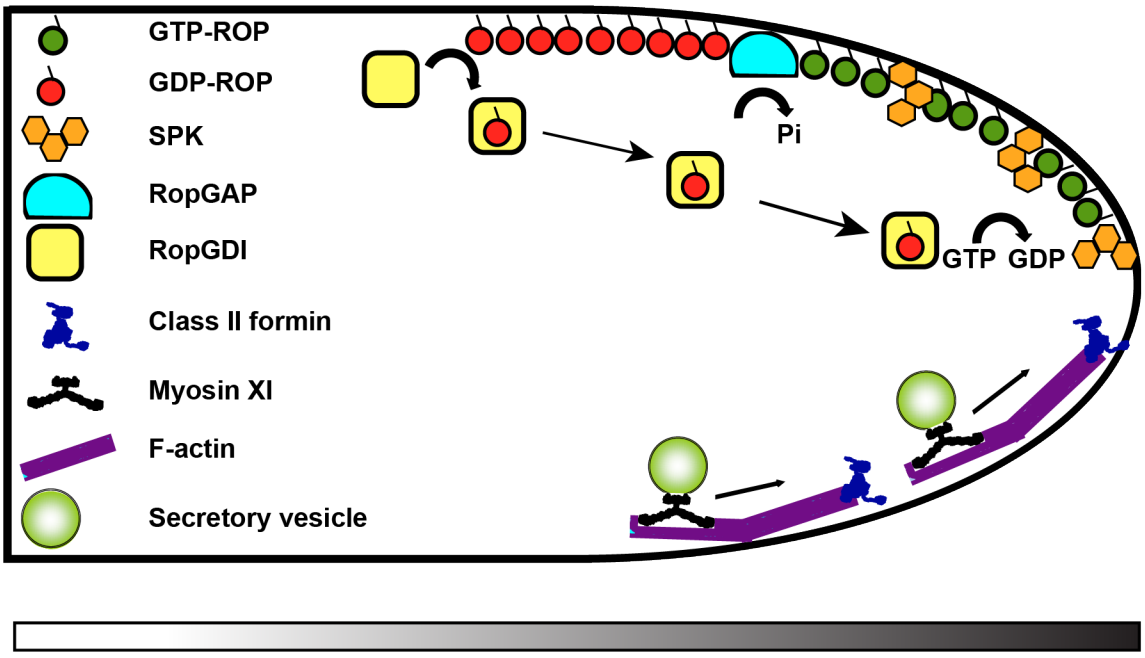

Figure 7.1. A potential model for how ROP and myosin XI are involved in moss tip growth. The model shows a medial section of a tip growing cell. The top half of the model depicts ROP regulation at the tip of the cell while the bottom half depicts myosin XI mediated vesicle delivery at the tip. The gradient below the cell is indicative of the distribution of $PI(3,5)P_2$ in the plasma membrane, with darker shades representing higher concentrations. SPK localizes to $PI(3,5)P_2$ and subsequently activates ROP. Active ROP leads to the recruitment of class II formins to $PI(3,5)P_2$, which nucleate actin filaments. These filaments serve as tracks for myosin XI mediated delivery of secretory vesicles. These vesicles likely contain cellulose synthase molecules and may additionaly contain ROP and SPK, leading to an establishment of polarized exocytosis throught positive reinforcement. Deactivation and recycling of inactive ROP to the tip confines ROP signalling to the cell apex.

However, there are still many unknowns that need to be addressed. $PI(3,5)P_2$ has not been well studied in plants and currently the general abundance and localization have not been shown. If this phospholipid is defining sites for polarized secretion, then I would expect that it would be most concentrated at the cell apex and become more diffuse further back in the cell. While it has been demonstrated that $PI(3,5)P_2$ is in the cortical plasma membrane (van Gisbergen, 2012), the fraction of this phospholipid that is bound by class II formins (or potentially SPKs) is unknown. This makes it difficult currently to determine if $PI(3,5)P_2$ is defining a

region for polarized growth or not. The relationship between ROP, class II formins and PI(3,5)P_2 is also unclear. I have observed less class II formin at the cortex in the absence of ROP, but this could be accomplished in different ways. ROP RNAi may reduce cortical PI(3,5)P_2 levels and in turn reduce the amount of formin on the cortex. Alternatively the phospholipid levels could be unchanged but a ROP effector is no longer recruiting formin. Another possibility is that ROP regulates the accessibility of PI(3,5)P_2 to formin.

My work in this thesis has aided in understanding of polarized growth in plants. Here I have examined how myosin XI and ROP are involved in this process, using a whole gene family loss of function approach to determine that both are essential for tip growth. This approach also allowed me to characterize how these proteins affect the actin cytoskeleton without the complication of other endogenous gene family members or dominant-negative isoforms. I was also able to report on a novel cellular adhesion phenotype that arises when *ROP* is silenced. In investigating the ROP regulators I found that in moss, a different RhoGEF activates ROP for tip growth than has been reported in seed plants. My findings have revealed links between essential polarized growth components and events. Based on this, I have proposed a possible mechanism for how ROP regulates where and when myosin XI mediated vesicle secretion occurs via the actin cytoskeleton. I previously stated that the molecular mechanisms that drive tip growth are not well understood. The work I have presented here has begun revealing some of these mechanisms and has also laid some groundwork for further inquiries.

CHAPTER 8

MATERIALS AND METHODS

Tissue culture and growth media

Moss protonemal tissue was grown on PpNH4 medium (1.03 mM $MgSO_4$, 1.86 mM KH_2PO_4, 3.3 mM $Ca(NO_3)_2$, 2.72 mM $(NH4)_2$-tartrate, 45 µM $FeSO_4$, 9.93 µM H_3BO_4, 220 nM $CuSO_4$, 1.966 µM $MnCl_2$, 231 nM $CoCl_2$, 191 $ZnSO_4$, 169 nM KI, 103 nM Na_2MoO_4) supplemented with 0.7% agar at 25º C. Tissue was harvested, homogenized and plated weekly. Moss protoplasts were regenerated on plates containing PRMB medium (PpNH4 medium supplemented with 6% mannitol, 10 mM $CaCl_2$, 0.8% agar). Prior to plating, protoplasts were re-suspended in either 1 mL top agar (PpNH4 medium supplemented with 6% mannitol, 10 mM $CaCl_2$, and 0.3% agar) or 0.5 mL liquid plating medium (PpNH4 medium supplemented with 8.5% mannitol and 10 mM $CaCl_2$). All growth plates were overlaid with cellophane unless otherwise noted. Agar pads for confocal imaging are made from a 1% agar pad containing modified Hoagland's medium (4 mM KNO_3, 2 mM KH_2PO_4, 1 mM $Ca(NO_3)_2$, 90 µM Fe citrate, 300 µM $MgSO_4$, 9.93 µM H_3BO_3, 220 nM $CuSO_4$, 1.2 µM $MnCl_2$, 231 nM $CoCl_2$, 191 nM $ZnSO_4$, 170 nM KI, 100 nM Na_2MoO_4, and 1% sucrose).

Moss protoplast transformation

One week old protonemal tissue was harvested and placed in 8.5% mannitol with 0.5% driselase (Sigma) for 75 minutes to make protoplasts. Debris was removed from the protoplast solution by passing through a 100 µm mesh. Excess

driselase and ruptured protoplasts were removed by 3 cycles of centrifugation at 250g for 5-7 minutes and resuspension in 8.5% mannitol. Protoplasts were resuspended in 3M (9.1% mannitol, 15 mM $MgCl_2$-$6H_2O$, 0.1% MES, pH 5.6) to a concentration of 1.6 - 2.0 x 10^6 protoplasts/ml. Per transformation, 15-30µg of RNAi or expression plasmid was added to 0.3ml of the protoplast suspension and then combined with 0.3 ml of PEG media (4 g melted PEG 8000 (Sigma) in 10 ml of calcium nitrate solution (100 mM $Ca(NO_3)_2$, 10 mM Tris, pH 8.0 in 8.5% mannitol). After 10 minutes at room temperature, the transformation was heat shocked 45º C for 3 min and then returned to room temperature for 10 minutes. 5ml of 8.5% mannitol was added to each transformation and then kept at room temperature for and additional 0.5–2 hours before centrifugation at 250g for 7 minutes. Protoplasts were then re-suspended in either 5 ml of 8.5% mannitol for protoplast protein extracts, 0.5 ml liquid plating medium for transient experiments, or 1 mL top agar for generating stable lines. For transient and stable experiments, re-suspended protoplasts were plated onto cellophane overlain PRMB medium, and transformed plants were selected for 4 days after transformation on by passing to PpNH4 medium containing the appropriate antibiotic. For complementation studies, the complementing construct was co-transformed with the RNAi construct

Imaging and morphometric analysis of transient moss transformations

Regenerated protoplasts were transferred to selection plates four days after transformation and imaged three days later. Plants lacking the nuclear GFP signal were photographed as 24-bit RGB color images with a 1x objective at 63x zoom

using a stereomicroscope (leica MZ16FA) equipped with a CCD camera (Leica DF300FX). Chlorophyll fluorescence and any nuclear GFP signal are acquired simultaneously using the GFP2 filter set (Leica) with excitation 480/40, dichroic 505 long pass, emission 510 long pass. Exposure settings were maintained constant throughout an experiment. Small adjustments were made in exposure time between experiments.

For morphometric analysis, images were opened in ImageJ (http://rsb.info.nih.gove.ij/). Plants lacking nuclear GFP signal were isolated using the manual selection tool. The red channel is separated from the RGB image, then thresholded using the maximum entropy method and binarized. Plant area is given by the sum of pixels with an intensity of 1. Solidity (the ratio of the area divided by the convex hull area) was calculated from the largest thresholded object in the image. The convex hull, which is the smallest convex polygon that contains the shape under analysis, was calculated using the default function in ImageJ under the Edit/Selection menu. A perfectly solid structure has a solidity of one while more branched structures have lower solidity values.

cDNA preparation, PCR amplification and site directed mutagenesis of *PpMyoXIa*

The full-length cDNA (pdp20423) of *P. patens* myosin XIa was obtained from the Physcobase collection (http://moss.nibb.ac.jp/). The complete open reading frame was amplified and cloned into pENT/D-TOPO generating pdp20423-pENT. The pdp20423 clone contained both the 2-bp deletion and the point mutation near

the 3' end of the gene. To alter these variants to reflect the genomically encoded sequence, cDNA was prepared from total mRNA using myosin XIa specific primers. The first variant site fragment was cloned into pGEM-Teasy (Promega), generating var1-pGEM and the second variant site fragment was cloned into pENT/D-TOPO, generating var2-pENT. Three independent var1-pGEM clones were sequenced and one contained the genomically encoded sequence, var1g-pGEM. We used Bsu36I restriction enzyme sites flanking the site of the first variant from var1g-pGEM to replace the altered sequence in pdp20423-pENT. Eleven var2-pENT clones were sequenced but none contained the genomically encoded sequence. To change the second variant sequence to those present in the genomic sequence, site-directed PCR mutagenesis (Weiner et al., 1994) was performed on var2-pENT, generating var2g-pENT. Changes were verified by sequencing. NdeI and AscI sites flanking the site of the second variant were utilized to insert the corrected sequence from var2g-pENT into the clone in which the first mutation was already altered to match the genomic sequence according to the *P. patens* genome (http://genome.jgi-psf.org/Phypa1_1/Phypa1_1.home.html). The resulting construct, pdp20423g-pENT, was transferred via an LR clonase reaction (Invitrogen) to the destination vectors pTH-UbiGate and pTH-35SGate. This results in the expression constructs pTH-Ubi-myoXIa and pTH-35S-myosXIa. Similar manipulations were used to generate expression constructs containing the sequence variants. Please refer to table 8.1 for a full list of primers used for my thesis work and table 8.2 for a full list of constructs generated.

Generation of myosin XI RNAi constructs

The generation of constructs for RNAi based gene silencing was performed by PCR amplifying segments corresponding to the coding sequence of both myoXIa and myoXIb from cDNA, fused by ligation and cloned into pENTR/D-TOPO (Invitrogen). To generate the individual 5'UTR constructs, a segment of the 5' UTR of myoXIa and myoXIb was amplified from genomic DNA and cloned into pENTR/D-TOPO. Additionally the myoXIa fragment was also cloned into pGEM-Teasy. The myoXIa fragment in pGEM-Teasy was excised with NotI and cloned into the myoXIb-pENT clone digested with NotI generating pENT-myoXIa+b 5'UTR. All constructs were verified by sequencing in the pENT/D-TOPO vector. To generate the RNAi plasmids, constructs were transferred to the RNAi vector pUGGi (Bezanilla et al., 2005) via LR clonase, resulting in myoXIa+bCDS, myoXIa5'UTR, myoXIb5'UTR and myoXIa+b5'UTR. Please refer to table 8.1 for a full list of primers used for my thesis work and table 8.2 for a full list of constructs generated.

Complementation of the myosin XI-RNAi phenotype

30 µg of myoXIa+b5'UTR was co-transformed with various concentrations of a complementing plasmid such as pTH-Ubi-myoXIa or pTH-35S-myoXIa . After four days, the regenerating plants were transferred to hygromycin selection (15 µg/ml) in $PpNH_4$ growth medium. Three days later, the plants lacking nuclear GFP were evaluated for growth by measuring the plant area based on the chlorophyll autofluorescence and the degree of polarization estimated by the plant morphology using solidity.

Realtime RT-PCR analysis of transient RNAi plants

For expression analysis of ROP and myosin XI three-hundred to one-thousand seven to eight day old plants lacking nuclear GFP were manually picked with a fine needle and total RNA was extracted using the RNeasy Plant Mini Kit (Qiagen), followed by DNAse I treatment, according to the manufacturer's protocol. cDNA was synthesized from total RNA using SuperScript II Reverse Transcriptase (for MyoXI studies) or SuperScript III Reverse Transcriptase (for ROP studies) (Invitrogen) and oligo-dT, following the manufacturer's protocol except for the elution volume, which was reduced from 50µl to 25µl. Real-time PCR was performed in triplicate. All real-time PCR reactions used 2-20 ng of cDNA template in a 12.5µl reaction using the Brilliant II SYBR Green QPCR Master Mix (Agilent Tecnologies). The PCR conditions were as follows: 95°C for 10 min, followed by 40 cycles of 95°C for 30 s and 60°C for 1 min, and ending with a melting curve analsysis. The primer sets were designed to have similar amplification efficiencies and are listed in Table 8.1. The *ubiquitin10* gene was used as an internal control for all reactions. Real-time PCR reactions were carried out in an Eppendorf Mastercycler ep Realplex^2 thermal cycler and data were analyzed with the realplex software version 2.2.

Stable expression of 3xmEGFP-myosin XIa

A monomeric version of GFP (mEGFP) was amplified from pmEGFP-C1 (Vidali et al., 2009b) with primers (Table 8.1) that incorporated the appropriate attB sites and an additional BamHI site prior to the start ATG resulting in mEGFP-

L1L5r. The BamHI site at the 5' end allows for cloning of additional mEGFPs with BamHI BglII ends, which digested from the previously described mEGFP-pGEM (Vidali et al., 2009b). The BglII site is lost and additional mEGFPs can be inserted, resulting in 3xmEGFP-L1L5r. pdp20423g-pENT was amplified using the appropriate *att*B primers (Table 8.1) and the resulting fragment was cloned into pDONR P5-P2 via a BP clonase reaction, creating myoXIa-L5L2. Using a 2-fragment gateway recombination reaction, 3xmEGFP-L1L5r and myoXIa-L5L2 were combined and cloned into pTH-UbiGate to generate the expression construct pTH-Ubi-3xmEGFP-myoXIa. This plasmid was transformed into NLS-4 and stable hygromycin resistant plants were isolated. The hygromycin resistance was removed by Cre-mediated recombination of lox-p sites flanking the antibiotic resistance cassette, generating a GFP-myoXI plant.

Quantification of myosin XI protein reduction by confocal microscopy

To determine the extent of protein reduction by the myosin-RNAi constructs, the GFP fluorescence in one-week old GFP-myoXI plants transformed with different RNAi constructs was monitored. Individual transformants undergoing active gene silencing were selected based on the loss of nuclear GFP. The plants were transferred to 1% agar pads on modified Hoagland's medium and mounted for confocal observation under a glass coverslip. Images from several cells from each plant were collected with a water immersion 20X lens (0.75 NA, Nikon) using a laser scanning confocal (C1 - Nikon) exciting with a 488-nm argon laser at 10% power. All acquisition parameters, including laser power, pixel dwell time, and gains were kept

at the same level for all experiments. Single optical sections were collected for comparison, converted to 12 bit TIFF format and imported to ImageJ. For analysis, the cells were thresholded to include all the fluorescence present in the optical section of the cell. Even in cells with very low GFP levels, the background signal provided enough information to delineate the cells. To correct for background levels, wild-type plants not expressing fluorescent proteins were imaged at the same settings and their average intensity values subtracted for the analysis. To reduce possible non-specific signal resulting from residual nuclear GFP-GUS fluorescence, the nuclei were masked before thresholding. I determined that the reduction of nuclear GFP-GUS in actively silencing plants is above 90%, but because of the low signal of 3xmEGFP-myosinXIa, this residual signal could affect further analysis and was therefore removed. The thresholded regions were selected using the automatic select-tool from ImageJ and their average fluorescence intensity recorded. Two transformations were conducted to analyze between 10 and 44 regions from individual plants for each condition.

Analysis of myosin XI subcellular localization

Localization of 3xmEGFP-myoXIa was determined in the stable line, GFP-myoXI. For imaging, regenerated protoplasts were placed on a 1% agar pad in Hoagland's medium with 1% sucrose, covered with a glass coverslip, sealed with VALAP (1:1:1 parts Vaseline, lanoline, and paraffin), and immediately observed at room temperature. To acquire rapid confocal stacks, the imaged area was reduced to 256x256 pixels and sections were generated within one s. For caulonemal cells,

five slices from the apical dome were collected at 1-µm intervals every 5 s using a 488 argon laser with a 515/30 nm bandpass emission filter of a Nikon confocal microscope (Nikon C1), a 60x lens (NA 1.4 – Nikon) and a pixel size of 83 nm. Laser power was maintained at 1% to reduce bleaching. Under these conditions, the cells continue to grow for at least an hour. We subsequently analyzed maximal projections of the five Z-stacks.

For chloronemal cells and branches, which are growing at a slower rate, only single medial optical slices were collected. This reduced laser exposure and allowed for the necessary longer observation periods. For these longer-term observations, plants were cultured on thin agar films surrounded by a thicker layer of agar, to maintain hydration. This was accomplished by creating a hole at the bottom of agar poured onto a glass bottom Petri dish, and adding 50-100 µl of agar to this hole to create a film thin enough for observation with high-resolution optics. Images were collected every 5 s with a 63X lens (NA 1.4 – Leica) with a laser scanning confocal microscope (SP5 Leica) using the 488 nm laser with a 495-525 nm emission filter. These settings were used for all data acquired with the Leica scanning confocal.

Generation of *ROP, RopGAP, RopGEF* and *SPK* RNAi constructs

The sequences used for the RNAi constructs were PCR amplified from *P. patens* cDNA using the appropriate primers (Table 8.1). For constructs containing sequences from more than one gene, the individual PCR products were fused by restriction digest and ligation. The resulting fused sequences were then reamplified by PCR. PCR fragments were cloned in to pENTR/D-TOPO (Invitrogen) and the

resulting plasmids were verified by both restriction digest and sequencing. The RNAi sequences were then inserted into the inverted repeat GUS-Gateway cassette of the destination RNAi expression vector pUGGI (Bezanilla et al., 2005) via LR clonase (Invitrogen) reactions. Restriction digests were used to verify RNAi constructs and compare to the control GUS RNAi vector (Bezanilla et al., 2005). Please refer to table 8.1 for a full list of primers used for my thesis work.

Generation of *ROP* expression constructs

Expression construct sequences were similarly PCR amplified and cloned into pENTR/D-TOPO (Invitrogen) as described for RNAi constructs above. After verification by restriction digest and sequencing, LR clonase (Invitrogen) reactions were used to transfer the sequences to the expression vectors pTH-Ubi-Gate (for transient ROP complementation studies in chapter 3), pMH-Gate (for transient expression of native ROP promoter-ROP genomic sequence constructs in chapter 3) or the four BiFC vectors (pTH-Ubi-nEYFP-Gate, pTH-Ubi-cEYFP-Gate, pTH-Ubi-Gate-nEYFP and pTH-Ubi-Gate-cEYFP). Please refer to table 8.1 for a full list of primers used for my thesis work.

Generation of moss stable lines

Constructs used to make stable lines were generated by multisite gateway recombination (Invitrogen) and cloned into moss via homologous recombination. To target genomic loci for stable ROP deletion constructs targeting the entire gene or the 3' untranslated region, sequences immediately upstream and downstream of

the region to be replaced were amplified and cloned into pDONR P1P4 and pDONR P3P2, respectively, via BP clonase II reactions (Invitrogen). For specific reactions, please refer to table 8.1 for a full list of primers used. These targeting sequences were recombined with L4L3 nos-lox-hygro-lox using a LR Clonase II plus reaction (Invitrogen). Linearized deletion constructs were generated by either PCR amplification (Δ*rop1*-Δ*rop4*) or using restriction sites (*ROP3*Δ3'Utr and *ROP4*Δ3'Utr) flanking the targeting sequences.

To generate stable lines expressing GFP tagged *ROP4*, the *ROP4* sequence was amplified from moss cDNA using primers UM769 and UM770 and cloned into pENTR/D-TOPO (Invitrogen). After verification by sequencing, the coding sequence was then isolated using the restriction sites AscI and SpeI, then inserted into the L5L4-mEGFP or L5L4-3XmEGFPplasmids (modified with restriction sites C-terminal to the mEGFP or 3XmEGFP (L5L4-mEGFP-AscI-SpeI/ L5L4-3XmEGFP-AscI-SpeI) plasmid so as to be in frame with the flourophore, generating L5L4-mEGFP-ROP4cds/ L5L4-3XmEGFP-ROP4cds. A non-tagged version of the ROP4cds was also created (L5L4-ROP4cds). The 5' targeting sequence was amplified using primers UM733 and UM734 and cloned into pDONR P1P5r using BP Clonase II (Invitrogen), generating L1L5-ROP4-5'tarm. Similarly, the 3' targeting sequences was amplified with primers UM634 and UM638 and cloned into pDONR P3P2 using BP Clonase II (Invitrogen), generating L3L2-ROP4-3'tarm. The L1L5-ROP4-5'tarm, L5L4-mEGFP-ROP4cds/ L5L4-3XmEGFP-ROP4cds/ L5L4-ROP4cds and L3L2- ROP4-3'tarm were recombined with L4L3 nos-lox-hygro-lox using LR Clonase II plus (Invitrogen) to

generate the final constructs for homologous recombination in moss, mEGFP-ROP4cds-AR, 3XmEGFP-ROP4cds-AR, and ROP4cds-AR.

The coding sequence of moss α-tubulin (Pp1s215_51V6 locus) was amplified from moss cDNA using primers UM1415 and UM1416 and cloned into pENTR/D-TOPO (Invitrogen). After verification by sequencing, the coding sequence was then isolated using the restriction sites AscI and SpeI, then inserted into the L5L4-mCherry plasmid (modified with restriction sites C-terminal to the mCherry L5L4-mCherry-AscI-SpeI) plasmid so as to be in frame with mCherry, generating L5L4-mCherry- α-tub215-51-1. Sequences upstream and downstream of the locus were amplified as targeting sequences for homologous recombination. The 5' targeting sequence was amplified using primers UM1434 and UM1435 and cloned into pDONR P1P5r using BP Clonase II (Invitrogen), generating L1L5- α-tub215-51-1-5'tarm. Similarly, the 3' targeting sequences was amplified with primers UM1436 and UM1437 and cloned into pDONR P3P2 using BP Clonase II (Invitrogen), generating L3L2- α-tub215-51-1-3'tarm. The L1L5- α-tub215-51-1-5'tarm, L5L4-mCherry- α-tub215-51-1 and L3L2- α-tub215-51-1-3'tarm were recombined with L4L3 nos-lox-hygro-lox using LR Clonase II plus (Invitrogen) to generate the final construct for homologous recombination in moss, mCherry-α- tub215-51-1AR.

Once generated, these targeted construct plasmids are linearized using restriction sites flanking the targeting sequences or PCR amplification. Moss protoplasts are then transformed with 30μg of the linearized plasmids as described above. Transformations were cycled on and off of antibiotics weekly to reduce the number of plants that were transiently expressing the construct. Approximately one

month after transformation live plants were isolated and grown directly on $PpNH_4$ media supplemented with the appropriate antibiotic and then allowed to grow. After two weeks, half the tissue was placed into a microcentifuge tube containing 1.0-2.0 mm diameter ZrSiO beads (Next Advance) and 200μL water. Plants were homogenized in a Bullet Blender (Next Advance) on high speed for 3 minutes, and then mixed with 200 μL of 2X DNA extraction buffer (0.4 M Tris, pH 9.0, 0.8 M LiCl, 50 mM EDTA, 2% SDS). The debris was pelleted by centrifugation and the supernatant was isolated and precipitated with an equal volume of isopropanol, then resuspended in Tris-EDTA buffer. The targeted genomic locus was genotyped by PCR using primers outside of the targeting sequences. Growth assays of stable lines were performed by imaging and analysis of seven-day-old regenerated protoplasts and was performed as described above.

Generation of zeocin resistant RNAi constructs

Since the constructs used to generate the *ROP3*Δ3'Utr and *ROP4*Δ3'Utr stable lines use hygromycin resistance as a selectable marker, the control and ROP RNAi expression constructs described above (expressing hygromycin resistance) will not select specifically for transformed plants expressing the RNAi construct. To generate RNAi constructs with zeocin resistance, pUbi-Nos plasmid was linearized with the SmaI restriction enzyme. The region containing the inverted repeats for RNAi expression was digested out of the control (pUGi), ROP4cds (pUGROP4cdsi) and ROP 3'Utr (pUGROP3'Uti) RNAi constructs as well as the RNAi entry vector pUGGi using restriction enzymes SacI and KpnI, followed by blunting of the ends. These

inverted repeat sequences were then ligated into the linearized pUbi-Nos plasmid. The resulting plasmids were then digested with BglI and Hpa to isolate the dropout of the maize ubiquitin promoter, inverted repeats and the Nos terminator, which was then blunted. These fragments were then ligated into a SacI linearized and blunted pZeo vector, generating pZUGGi, pZUGi, pZUGROP4cdsi and pZUGROP3'Uti.

Confocal microscopy of actin and microtubules

For imaging, regenerated protoplasts were placed on a 1% agar pad in Hoagland's medium with 1% sucrose, covered with a glass coverslip, sealed with VALAP (1:1:1 parts Vaseline, lanoline, and paraffin), and immediately observed at room temperature. Slides were mounted on an inverted microscope (model Ti-E; Nikon) equipped with a spinning disk head (model CSU-X1; Yokogawa Corporation of America) and a 512 Å~ 512 electron multiplying CCD camera (iXON;Andor Technology). Images were collected with a 1.4 NA 60x oil immersion objective (Nikon) at room temperature. Laser power and exposure times varied depending on what fusion protein was imaged, but were kept consistent within experiments. Cytoskeleton images were acquired every second for Lifeact-mEGFP and every 2 seconds for mCherry-α-tubulin for duration of 2 minutes. Image acquisition process was controlled by MetaMorph software (Molecular Devices) and images were further processed with ImageJ as described for specific analyses.

Quantification of cytoskeletal dynamics

Stacks of images were cropped to isolate a region containing actin filaments. Images were processed through a real-space band-pass filter. The size of noise was set to one pixel, and the smallest object is 4 pixels. Correlation maps were calculated from these processed images. The correlation coefficient of a pair of images was calculated using the built-in MATLAB function corr2 defined as:

$$r = \frac{\sum_m \sum_n (A_{mn} - \bar{A})(B_{mn} - \bar{B})}{\sqrt{\left(\sum_m \sum_n (A_{mn} - \bar{A})^2\right)\left(\sum_m \sum_n (B_{mn} - \bar{B})^2\right)}}$$

Here, *A* and *B* denote the matrices of the two images, and *A* and *B* with lines over them are the mean intensity values of each image. The correlation coefficient was computed between all possible temporal spacings (time intervals) to allow for better averaging. The resulting averaged correlation coefficients were plotted as a function of time and compared among treatments.

Measuring cytoskeletal filament bundling and density

Quantification of filament bundling (skewness) and density (% occupancy) was performed as described in Higaki et al., 2010. Confocal images were manually thresholded, skeletonized and binarized before being converted into masks. These masks were then applied to the original images. The skewness macro (ImageJ) (Higaki et al., 2010) measures the intensity distribution of the filament pixels reflects the relative degree of filament bundling. Distributions skewed to the right of normal are indicative of filament bundling. The filament density is given by the

percentage of the total cell area in the focal plane that is occupied by the filament mask.

Analysis of ROP subcellular localization

Localization of ROP was determined in the stable line NLS4/mEGFP-ROP4cds. Slides were mounted on an inverted microscope (model Ti-E; Nikon) equipped with a spinning disk head (model CSU-X1; Yokogawa Corporation of America) and a 512 Å~ 512 electron multiplying CCD camera (iXON;Andor Technology). Images were collected with a 1.4 NA 60x oil immersion objective (Nikon). 30% laser power was used for the 488 laser. The electron gain was 300 and exposure time was 250 msec. Image acquisition
process was controlled by MetaMorph software (Molecular Devices. Five to ten slices from the apical dome were collected at 1-µm intervals. Maximal projections were subsequently created in ImageJ. To increase visibility, enhance contrast and subtract background functions were run on the images.

Variable angle epifluorescence microscopy (VAEM) and analysis

Moss protoplasts were regenerated for 6-7 days. For imaging, protonemal tissue was placed on a 1% agar pad in Hoagland's medium with 1%sucrose, covered with a glass coverslip, sealed with VALAP (1:1:1 parts Vaseline, lanoline, and paraffin), and immediately observed at room temperature. The slide was mounted on an inverted microscope (model Ti-E;Nikon) equipped with a mirror-based T-FL-TIRF illuminator (Nikon) and imaged with a 1.49 NA 100x oil immersion TIRF

objective (Nikon). The 1.5x optivar was used for all images to increase magnification. The laser illumination angle was adjusted individually for each sample to achieve the maximum signal-to-noise ratio. For2A-GFP was excited with a 488 diode laser and GFP emission from the specimen was captured with a 1024 Å~ 1024 electron-multiplying CCD camera (iXON3; Andor Technology). The electronic gain was 300 and exposure time was at 15 msec. Image acquisition process was controlled by NIS-Elements AR 3.2 software (Nikon) and images were further processed with ImageJ, including background coreection, background subtraction and enhanced contrast. Tracking of cortical For2A-GFP dots was performed manually in ImageJ. Quantification of the density of cortical For2A-GFP was performed in ImageJ, using the "Analyze Particles" function. Images were first corrected for uneven illumination using the background correction plug-in, filtered with an FFT bandpass filter, and then binarized using maximum entropy thresholding. 50–60 slices from a time-lapse acquisition were binarized with this method and particles between 8–80 square pixels were counted. The automated counting method was validated by manually counting the dots in at least five frames from a time-lapse acquisition. The total area of the VAEM imaging field was divided by the average number of dots to determine density. The speed of linear dots was measured manually using ImageJ. The rate was calculated by dividing the total distance traveled in a linear trajectory by the trajectory duration.

Polarized light microscopy and analysis

Plants were imaged on an Interphako polarized-light microscope (Zeiss) equipped with an LC Polscope quantification system (Cambridge Research Instruments) implementing the Universal Compensator (Oldenbourg and Mei, 1995). This system generates an image in which the intensity of each pixel is proportional to birefringent retardance. Because the system uses circularly polarized light the retardance data are independent of sample orientation. Retardance was quantified by taking the peak intensities of line scans across the external cell walls of silenced plants using ImageJ. Three to five walls were analyzed per image and 7-10 images per condition were examined. The peak intensities are proportional to retardance with a gray level of 255 = 15 nm. Retardance values for each condition were then averaged and plotted.

Cell wall staining

One-week-old regenerated protoplasts were collected into microfuge tubes and 1ml of stain (10µg/ml calcofluor (fluorescent brightener 28, Sigma), 1% aniline blue or 100µg/ml fast scarlet 4B) was added and incubated for 30 minutes. All liquid was removed and the 1ml of water was added. This was repeated twice for a total of three washes. Plants were then mounted on a slide and pictures of stained silenced plants were captured as 24-bit RGB images with a 5X lens at 30X zoom on the fluorescence stereomicroscope (Leica MZ16FA) equipped with a color camera (Leica DF300FX) and either UV (for calcofluor and aniline blue staining), GFP2 (to identify silenced plants) or dsRed (for fast scarlet 4B) filter sets (Leica). The

fluorescence intensity of the both the plant and a nearby background spot were measured in a 100x100-pixel region of the image using ImageJ. After background subtraction, the intensity values were averaged and plotted.

Sonication assay

Silenced plants were transferred from selection plates to a 0.1ml drop of water in the middle of a 3.5cm petri dish. The dish was then placed on the surface of a sonicating water bath (Sonicor, Ladd Research Industries), filled with 500ml of water at power level 2 for 10 seconds. Plants were imaged before and after sonication using an epifluorescence stereomicroscope (leica MZ16FA) equipped with a CCD camera (Leica DF300FX) with a GFP2 filter (Leica) to capture chlorophyll autofluorescence. The frequency of plant breakage was determined for each treatment.

Bimolecular fluorescence complementation assay

Constructs were generated by PCR amplification of the coding sequence from *P. patens* cDNA and cloning into pENTR/D-TOPO (Invitrogen). After verification, coding sequences were inserted into one or more of the BiFC vectors (nEYFP-Gate, cEYFP-Gate, Gate-nEYFP and Gate-cEYFP) by an LR clonase reaction. Wild type protoplasts were transformed with 200 ng dsRed, 400 ng of an nEYFP construct, and 400 ng of a cEYFP construct, and then plated in top agar. Moss protoplasts were transformed by either particle bombardment using (PDS-1000/He biolistic particle delivery system, Biorad), or PEG-mediated transformation. After 3 days of

regeneration, plants were sequentially imaged with the dsRed and GFP3 filter sets (Leica) with a 1x lens at 115x zoom using an epifluorescence stereomicroscope (leica MZ16FA) equipped with a CCD camera (Leica DF300FX). The green channel representing YFP fluorescence was separated from GFP3 images in ImageJ and the mean fluorescence intensity of the protoplast and a nearby background spot were measured with the elliptical tool using a fixed ellipse size in ImageJ.

Immunoblotting

Moss protoplasts 4 days after transformation were transferred to a microcentrifuge tube and rapidly frozen in in liquid nitrogen. Frozen tissue was ground in the tube using a plastic micropestle, then vortexed in grinding buffer (100 mM sodium phosphate, pH 7.0, 10 mM DTT, 20% glycerol, 5 mM EDTA, 1 mM PMSF, 20 µg/mL Leupeptin). Samples were centrifuged at 4ºC, quantified using a Bradford assay (Biorad) and extractions were concentrated by methanol precipitation prior to separation by SDS-PAGE. The protein separation was transferred to a nitrocellulose membrane and immunoblotted using rabbit anti-*AtROP2* serum (for maize ubiquitin promoter driven expression of moss ROPs) or rabbit anti-GFP antibody (for expression of BiFC constructs). Chemiluminescence emission from horseradish peroxidase fused to polyclonal goat anti-rabbit secondary antibodies was detected on a gel doc system equipped for chemiluminescence detection (Biorad).

Table 8.1 Primers used in these studies.

Primer	Name	Sequence 5'-3')	Use
UM	346	CTAAGAATCTGGTTG TGGCATTAGAAAGTG	Ampification of full-length clone/cDNA preparation
UM	344	CACCATGGCGACAGC AGGGAATG	Ampification of full-length clone
UM	390	TTCGCAATGACAACT CAAGTCG	cDNA preparation/Sequencing
UM	411	CACCTGCTGTCACAT TTGGAAATG	cDNA preparation
UM	401	CACCGACAAGCAGTT GGATTTTTGG	cDNA preparation
UM	464	GGTGATTGCTAACAT GAGAGTTCTAATGAC TGAGG	Mutagenesis to repair 2nd variant
UM	465	CCTCAGTCATTAGAA CTCTCATGTTAGCAA TCACC	Mutagenesis to repair 2nd variant
UM	271	AGAACGGGATACTAG AATCGTCATCTAACA AGAAA	Amplification of MyoXIb cds fragment for RNAi
UM	274	CACCGTTAGCAGAAC TTGAACATTGGATAT ATGAGGCC	Amplification of MyoXIb cds fragment for RNAi
UM	275	TACAGAGAATGGAAT ACTTGAGTCGTCATC TAATAGGAAG	Amplification of MyoXIa cds fragment for RNAi
UM	276	CACCACTTGCAGAAC TAGAGCACTGGATTT ATGAA	Amplification of MyoXIa cds fragment for RNAi
UM	389	CTGTTTGACTGGCTG GTTGACAAGG	Sequencing
UM	391	GCGATGAGAGACTCA AGAGAGC	Sequencing
UM	392	TGGAGGACCCAGAGT TAGCTTGG	Sequencing
UM	394	AGGAGTATGCTGGAG CGTCATGG	Sequencing
UM	395	TCGGTTTTCATTTGC CGAGTTTCC	Sequencing
UM	396	GCTCGTTTCAAGCAA CAATTGGGAGC	Sequencing
UM	397	TGGAGGTGCTCCTCA AAGACG	Sequencing
UM	398	CGAATCAAGGAGGCT GTTATCC	Sequencing
UM	476	GGGGACAACTTTGTA TACAAAAGTTGTGAT GGCGACAGCAGGGAAT	Generation of MyoXIa in 2nd position vector for 2-way gateway recombination

UM	477	GGGGACCACTTTGTACAAGAAAGCTGGGTACTAAGAATCTGGTTGTGG	Generation of MyoXIa in 2nd position vector for 2-way gateway recombination
UM	564	GGGGACAACTTTTGTATACAAAGTTGTGACGGACGACGGCGCCATACGC	Amplification of MyoXIa 5'Utr fragment for RNAi
UM	565	GGGGACAAGTTTGTACAAAAAAGCAGGCTACATTTAAATCCGCGCCCGCCACT	Amplification of MyoXIa 5'Utr fragment for RNAi
UM	566	GGGGACCACTTTGTACAAGAAAGCTGGGTAATTTAAATGGAGCCATCCTCAAT	Amplification of MyoXIb 5'Utr fragment for RNAi
UM	567	GGGGACAACTTTGTATAATAAAGTTGTAGCATGGACTGTGACTGTCCACC	Amplification of MyoXIb 5'Utr fragment for RNAi
UM	471	GGGGACAAGTTTGTACAAAAAAGCAGGCTTAGGATCCATGGTGAGCAAGGGCGAG	Generation of mEGFP in 1st position vector for 2-way gateway recombination
UM	226	GGGGACAACTTTTGTATACAAAGTTGTCTTGTACAGCTCGTCCAT	Generation of mEGFP in 1st position vector for 2-way gateway recombination
UM	893	GGAAGGTTTCAAGGTCACCA	Expression analysis of MyoXIa
UM	896	AGAGCTTGCGAACAAGGAAG	Expression analysis of MyoXIa
UM	894	AACGTGAATGCACAGCAGAC	Expression analysis of MyoXIb
UM	895	CAAGGAAAGGAGGAGCATGA	Expression analysis of MyoXIb
	UbiF2	ACTACCCTGAAGTTGTATAGTTCGG	Expression analysis of Ubiquitin 10 gene
	UbiR	CAAGTCACATTACTTCGCTGTCTAG	Expression analysis of Ubiquitin 10 gene
UM	150	CACCATGAGCACTTCACGGTTTATCAAG	Cloning Full-length cds of ROP4
UM	151	TCACAGAATGACGCAATTCTTTTG	Cloning Full-length cds of ROP4
UM	148	CACCATGAGCACATCTCGGTTTATCAAG	Cloning Full-length cds of ROP2
UM	149	TCAGAGAATAACACAGTTCTTTTGTTTTTTC	Cloning Full-length cds of ROP2
UM	160	AGAAAAGAATACACTACAATTTTAAGTGATCCCAATG	Cloning 3'Utr region of ROP4 for RNAi
UM	161	TACCGGATCCATGTGGCATAGCTTTTATGAGCTGG	Cloning 3'Utr region of ROP4 for RNAi

UM	162	CACCTGAATTGTAGTGTATTCTTTTCTCCTGCTGG	Cloning 3'Utr region of ROP2 for RNAi
UM	163	TACCGGATCCAACACAAGAGATGGTGGAAGTGC	Cloning 3'Utr region of ROP2 for RNAi
UM	533	CACCATGAGCACTTCTCGCTTTATCAAGTGC	Cloning Full-length cds of ROP3
UM	537	TTAGAGAATGACACAGTTCTTTTGCTTCTTTTTCTTC	Cloning Full-length cds of ROP3
UM	621	CACCTAAGAGAGCTACCGATATGCC	amplify Rop2 Genomic DNA plus 2kb upstream
UM	622	CACCGAGTATGACTAGTTTGTTCGC	amplify Rop1 Genomic DNA plus 2kb upstream
UM	623	CACCGGGTTGGAGACATTCAATCACG	amplify Rop3 Genomic DNA plus 2kb upstream
UM	626	GGGGACAAGTTTGTACAAAAAAGCAGGCTCTGGCGCGCCGTCGAACCCTCTACGTTGTAATGC	Generation of ROP4 5'targeting sequence in 1st position vector for 3-way gateway recombination to make ROP4∆3'Utr line
UM	628	GGGGACAAGTTTGTACAAAAAAGCAGGCTCTGGCGCGCCGTAGTTACAGGGGTGCCGATG	Generation of ROP3 5'targeting sequence in 1st position vector for 3-way gateway recombination to make ROP3∆3'Utr line
UM	630	GGGGACAACTTTGTATAGAAAAGTTGGGTGTCAGAGAATGACGCAATTCTTTTG	Generation of ROP4 5'targeting sequence in 1st position vector for 3-way gateway recombination to make ROP4∆3'Utr line
UM	632	GGGGACAACTTTGTATAGAAAAGTTGGGTGTGTTAGAGAATGACACAGTTCTTTTGCTTCTTTTTCTTC	Generation of ROP3 5'targeting sequence in 1st position vector for 3-way gateway recombination to make ROP3∆3'Utr line
UM	634	GGGGACAACTTTGTATAATAAAGTTGTCGGATATGGGGAGATTTTGTAGATGG	Generation of ROP4 3'targeting sequence in 1st position vector for 3-way gateway recombination to make ROP4∆3'Utr line
UM	636	GGGGACAACTTTGTATAATAAAGTTGTCTCGATGTTCGGAGTACCCGAGC	Generation of ROP3 3'targeting sequence in 1st position vector for 3-way gateway recombination to make ROP3∆3'Utr line
UM	638	GGGACCACTTTGTACAAGAAAGCTGGTAGGCGCGCCCCGGTGACTTATTCTAGCGTTACG	Generation of ROP4 3'targeting sequence in 1st position vector for 3-way gateway recombination to make ROP4∆3'Utr line
UM	640	GGGACCACTTTGTACAAGAAAGCTGGTAGGCGCGCCGGGCACATTTTCTAACCCAACC	Generation of ROP3 3'targeting sequence in 1st position vector for 3-way gateway recombination to make ROP3∆3'Utr line
UM	702	CCAAGGTCGAGGTTCTGTAGCTTAGC	Genotype ROP4 ∆3'Utr stable lines

UM	703	TTCGGTCAGTGGTACAGCACCAACC	Genotype ROP4 ∆3'Utr stable lines
UM	733	GGGGACAAGTTTGTACAAAAAAGCAGGCTCTGGATGCTAAGCCAAGCCATTAGAGACTGCC	Generation of ROP4 5'targeting sequence in 1st position vector for 4-way gateway recombination to make ROP4 allele replacement constructs
UM	734	GGGGACAACTTTTGTATACAAAGTTGTGGCTGCGTCCCTACCCACCTAACAC	Generation of ROP4 5'targeting sequence in 1st position vector for 4-way gateway recombination to make ROP4 allele replacement constructs
UM	748	GGCGCGCCATGAGCACTTCACGGTTTATCAAGTGC	Cloning ROP4 cds into 5' gfp tagging vector in 2nd position for 4-way gateway recombination to make mEGFP/3XmEGFP-ROP4cds allele replacement constructs
UM	749	ACTAGTTCACAGAATGACGCAATTCTTTTGTTTTTTC	Cloning ROP4 cds into 5' gfp tagging vector in 2nd position for 4-way gateway recombination to make mEGFP/3XmEGFP-ROP4cds allele replacement constructs
UM	769	GGGGACAACTTTGTATACAAAAGTTGCTATGAGCACTTCACGGTTTATCAAGTGC	Cloning ROP4 cds into 2nd position vector for 4-way gateway recombination to make ROP4cds allele replacement constructs
UM	770	GGGGACAACTTTGTATAGAAAAGTTGGGTGTCACAGAATGACGCAATTCTTTTGTTTTTTC	Cloning ROP4 cds into 2nd position vector for 4-way gateway recombination to make ROP4cds allele replacement constructs
UM	802	GGGGACAAGTTTGTACAAAAAAGCAGGCTCGGTTGTCACCCTTAGCCTCATCTTTCC	Generation of ROP2 5'targeting sequence in 1st position vector for 3-way gateway recombination ∆rop2 line
UM	803	GGGGACAACTTTGTATAGAAAAGTTGGGTGCGCATTTCAAGTACGGTGTAGCATGGC	Generation of ROP2 5'targeting sequence in 1st position vector for 3-way gateway recombination ∆rop2 line
UM	804	GGGGACAAGTTTGTACAAAAAAGCAGGCTCGGCGGAGGTCCTACCGATGG	Generation of ROP4 5'targeting sequence in 1st position vector for 3-way gateway recombination ∆rop4 line
UM	805	GGGGACAACTTTGTATAGAAAAGTTGGGTGCCCTACCCACCTAACACTTCACAGC	Generation of ROP4 5'targeting sequence in 1st position vector for 3-way gateway recombination ∆rop4 line
UM	806	GGGGACAAGTTTGTACAAAAAAGCAGGCTCGGCAGGAGAAGGAGGAGGAGGAGG	Generation of ROP1 5'targeting sequence in 1st position vector for 3-way gateway recombination ∆rop1 line
UM	807	GGGGACAACTTTGTATAGAAAAGTTGGGTGGCGTCCCAGCTCGCTTAACG	Generation of ROP1 5'targeting sequence in 1st position vector for 3-way gateway recombination ∆rop1 line

UM	808	GGGGACAAGTTTGTACAAAAAAGCAGGCTCGCACTTTGTTCGCTACAGTTGATAATCCTCAGG	Generation of ROP3 5'targeting sequence in 1st position vector for 3-way gateway recombination Δrop3 line
UM	809	GGGGACAACTTTGTATAGAAAAGTTGGGTGCCCTGCCCACCGCTATACAG	Generation of ROP3 5'targeting sequence in 1st position vector for 3-way gateway recombination Δrop3 line
UM	825	CACCACGGAATTCTGGTATGTGGACC	Amplification of RopGEF2 cds fragment for RNAi
UM	826	GGATCCTCCATCTCAACCAAAACTTGCGC	Amplification of RopGEF2 cds fragment for RNAi
UM	827	CTTCGGAAGCGAATCCCAATACAC	Amplification of RopGEF4 cds fragment for RNAi
UM	828	CACCCTTCCAAGAGGCGTTCTAGATTCG	Amplification of RopGAP3 cds fragment for RNAi
UM	829	CACCGGATCCTGGTTTCGGGAGTTGCCGC	Amplification of RopGAP1 cds fragment for RNAi
UM	830	TTAGGAGCAAAGACCATTGCAATATTGC	Amplification of RopGAP1 cds fragment for RNAi
UM	833	CACCGGATCCTCAAGGTTGTCTATGCAGAGACAAGAAG	Amplification of RopGEF4 cds fragment for RNAi
UM	834	GGATCCCTGTGTCATGTTCGGAGCAAAAACC	Amplification of RopGAP3 cds fragment for RNAi
UM	858	TAATACCGGATCCCCTACTGTTGATTTGGTGAAGGATATAGG	Cloning 3'Utr region of ROP1 for RNAi
UM	859	TAATACCGGATCCGTAGAACCCACAACACAAAGTGC	Cloning 3'Utr region of ROP1 for RNAi
UM	899	CACCATGAGCACTTCACGGTTTATCAAGTGC	Cloning region of ROP4 cds for RNAi
UM	900	CTGTAACTCAGAGGACGAAGCCTGTTG	Cloning region of ROP4 cds for RNAi
UM	901	CACCGGATCCGCTTGAAAGCTACCATGAGACGG	Amplification of RopGEF6 cds fragment for RNAi
UM	902	CCTTAGGCTTGTGCATTGATAGCCATAGCAGC	Amplification of RopGEF6 cds fragment for RNAi
UM	903	CACCCCTTAGGCGGAATTCTGGTACGTGGACCACG	Amplification of RopGEF5 cds fragment for RNAi
UM	904	GGATCCCCATCTCCGACAAAACTTGCGCG	Amplification of RopGEF5 cds fragment for RNAi
UM	913	CACCGGATCCGCGTGGTTTAGAGAACTTCCAAGAGG	Amplification of RopGAP4 cds fragment for RNAi
UM	914	CCTTAGGGTTTGGGGCAAACACCATAGCG	Amplification of RopGAP4 cds fragment for RNAi

UM	915	CACCCCTTAGGGCGTGGCTTCGAGAACTTCCAACAGG	Amplification of RopGAP5 cds fragment for RNAi
UM	916	GGATCCGCGTCATGTTAGGTGCAAACACCATTGC	Amplification of RopGAP5 cds fragment for RNAi
UM	918	CACCAATCATGTGTGAAAAAGAGC	Genotyping of ∆rop2 lines
UM	919	GGTGTGTAGGGTTTAAGATGTGAGG	Genotyping of ∆rop2 lines
UM	924	GGCATGTGATACGTCATAAATACGGAGG	Genotyping of ∆rop3 lines
UM	925	GGAGGGAGTGTAAGCAAGGGC	Genotyping of ∆rop3 lines
UM	931	CTGCACGCTTTCAGTGACAGC	Genotyping of ∆rop4 lines
UM	932	CTGCATTTGCGGAAGTTAGG	Genotyping of ∆rop4 lines
UM	933	GGTGAAACCACACCGTTAGG	Genotyping of ∆rop1 lines
UM	934	TCATGCTCTTTGAGCTCTTGC	Genotyping of ∆rop1 lines
UM	959	CTGAACAGATGTTAGACGCTCTG	Amplification of moss RIC cds fragment for RNAi
UM	964	CACCCTGAACAGATGTTAGACGCTCTG	Amplification of moss RIC cds fragment for RNAi
UM	1135	GGCGGCCGCTCTAGAACTAGTATGGGCAGCGTGCAGCTCGCC	Generation of Ubi-CeYFP-Gate vector
UM	1136	TCAGCTTTCTTGTACAAAGTGGTGATGGTGAGCAAGGGCGAG	Generation of Ubi-Gate-NeYFP vector
UM	1137	TCAGCTTTCTTGTACAAAGTGGTGGGCAGCGTGCAGCTCGCC	Generation of Ubi-Gate-CeYFP vector
UM	1138	CGAATTCCTGCAGCCCGTATCACTTGTACAGCTCGTCCATGC	Generation of Ubi-Gate-CeYFP vector
UM	1139	GGCGGCCGCTCTAGAACTAGTATGGTGAGCAAGGGCGAG	Generation of Ubi-NeYFP-Gate vector
UM	1140	CGAATTCCTGCAGCCCGTATCAGTCCTCGATGTTGTGGC	Generation of Ubi-Gate-NeYFP vector
UM	1141	CACCATGGTGAGCAAGGGCGAG	Generation of Ubi-NeYFP-Gate vector
UM	1142	CACCATGGGCAGCGTGCAGCTCGCC	Generation of Ubi-CeYFP-Gate vector
UM	1143	TCAGTCCTCGATGTTGTGGC	Generation of Ubi-Gate-NeYFP vector
UM	1144	GTACAAACTTGTGATTACGGGGGATCCGTCCTCGATGTTGTGGCGG	Generation of Ubi-NeYFP-Gate vector

UM	1145	GTACAAACTTGTGATTACGGGGGATCCCTTGTACAGCTCGTCCATGCCGAGAG	Generation of Ubi-CeYFP-Gate vector
UM	1165	CACCATGACAGAGGTTCTCCCAACCC	Amplification of RopGAP6 cds for cloning into BiFC vectors Ubi-NeYFP-Gate and Ubi-CeYFP-Gate
UM	1166	CTATCCTCCACACGTACCAGACAC	Amplification of RopGAP6 cds for cloning into BiFC vectors Ubi-NeYFP-Gate and Ubi-CeYFP-Gate
UM	1167	CACCATGATGAAGGAGAAGTTTGCAAAGCTTCTG	Amplification of RopGEF6 cds for cloning into BiFC vectors Ubi-NeYFP-Gate and Ubi-CeYFP-Gate
UM	1168	CTAGTCGCGCCCCGGAG	Amplification of RopGEF6 cds for cloning into BiFC vectors Ubi-NeYFP-Gate and Ubi-CeYFP-Gate
UM	1219	CAGAATGACGCAATTCTTTTGTTTTTTC	Amplification of ROP4 cds for cloning into BiFC vectorsy Ubi-Gate-NeYFP and Ubi-Gate-CeYFP
UM	1220	GAGTATGACACAGTTCTTTTG	Amplification of ROP1 cds for cloning into BiFC vectorsy Ubi-Gate-NeYFP and Ubi-Gate-CeYFP
UM	1221	GAGAATGACACAGTTCTTTTGCTTCTTTTTCTTC	Amplification of ROP3 cds for cloning into BiFC vectorsy Ubi-Gate-NeYFP and Ubi-Gate-CeYFP
UM	1222	GAGAATAACACAGTTCTTTTGTTTTTTCTTC	Amplification of ROP2 cds for cloning into BiFC vectorsy Ubi-Gate-NeYFP and Ubi-Gate-CeYFP
UM	1223	CACCGGATCCGAATGGATGGCGACCAGGCC	Amplification of SPK1 cds fragment for RNAi
UM	1224	CCTCTTCTCCAATTAACCTAGAATGAACGCG	Amplification of SPK1 cds fragment for RNAi
UM	1225	CACCCATGTGGGGCAAGGAACATGTGG	Amplification of SPK5 cds fragment for RNAi
UM	1226	GGATCCAGTTGTCCGTAGGCACGCCTTGC	Amplification of SPK5 cds fragment for RNAi
UM	1227	CACCGGATCCGAGGTCCTCGTCAACATTCAGTGC	Amplification of SPK4 cds fragment for RNAi
UM	1228	GGATCCGCTCTCCTGCTAAAGCTGCTGTACG	Amplification of SPK4 cds fragment for RNAi
UM	1259	GGGGACAAGTTTGTACAAAAAAGCAGGCTTCATTTAAATTTGGTCCAACAGCTGCACATACG	Amplification of ROP4 5' targeting sequence for GFP-CaaX tag introduction into locus (1st position for 4-way gateway recombination)
UM	1262	GGGGACAACTTTGTATAATAAAGTTGCGCCTGCTGGTAATTTGGTGAAGG	Amplification of ROP4 3' targeting sequence for GFP-CaaX tag introduction into locus
UM	1263	GGGGACCACTTTGTACAAGAAAGCTGGGTACGATGTTAGTTGCACCGGAAATCC	Amplification of ROP4 3' targeting sequence for GFP-CaaX tag introduction into locus
UM	1277	TCCTCCACACGTACAAGACAC	Amplification of RopGAP6 cds for cloning into BiFC vectors Ubi-Gate-NeYFP and Ubi-Gate-CeYFP

UM	1278	GTCGCGCCCCGGAG	Amplification of RopGEF6 cds for cloning into BiFC vectors Ubi-Gate-NeYFP and Ubi-Gate-CeYFP
UM	1309	GTTTAAACTGAGGTTGCAAAAGGAAGGGG	Amplification of ROP4 5' targeting sequence for N-terminal GFP tag introduction into locus (1st position for 3-way gateway recombination)
UM	1310	GTTTAAACATCAGCACCCCTGTAACTCAG	Amplification of ROP4 5' targeting sequence for N-terminal GFP tag introduction into locus (1st position for 3-way gateway recombination)
UM	1314	ATCAGGCACTGAGCAAACATCT	Expression analysis of ROP3
UM	1315	GGTACACCCTGCTACATGATGG	Expression analysis of ROP3
UM	1316	ACTTGCACCATCTCTTGTGTTATTC	Expression analysis of ROP2
UM	1317	AGTGACAAGTAGTGACTGTGACCAA	Expression analysis of ROP2
UM	1318	ACTTTGTGTTGTGGGTTCTACTTTT	Expression analysis of ROP1
UM	1319	TGCACTTCTGAGAGAACAAAACTTA	Expression analysis of ROP1
UM	907	TGATCTTCGCGATGACAAAC	Expression analysis of ROP4 only used for ROP4Δ3'Utr line
UM	908	CTTGATTGCTGCGTCAAAAA	Expression analysis of ROP4 only used for ROP4Δ3'Utr line
UM	911	GACATTATGCGCCATCTGTG	Expression analysis of ROP3 only used for ROP3Δ3'Utr line
UM	912	ATGAGGCTGCTCCAATTGAC	Expression analysis of ROP3 only used for ROP3Δ3'Utr line
UM	1373	GCGGAGGTCCTACCGATGG	Amplification of Δrop4 construct
UM	1374	CCGGTGACTTATTCTAGCGTTACGATTGTAG	Amplification of Δrop4 construct
UM	1375	GCAGGAGAAGGAGGAGGAGGAGG	Amplification of Δrop3 construct
UM	1376	GGAGGGGCCTACTCAGCACAT	Amplification of Δrop3 construct
UM	1380	GACTGTTGGAGATGTAGCTGTAGGGAAGACGTGC	Mutagenesis to create constitutively active version of ROP4 for BiFC assay
UM	1381	GCACGTCTTCCCTACAGCTACATCTCCAACAGTC	Mutagenesis to create constitutively active version of ROP4 for BiFC assay
UM	1382	GCTGTCGGGAAGAATTGTATGCTTATTTCATACACC	Mutagenesis to create dominant negative of ROP4 for BiFC assay
UM	1383	GGTGTATGAAATAAGCATACAATTCTTCCCGACAGC	Mutagenesis to create dominant negative of ROP4 for BiFC assay
UM	1415	ACTAGTTTAGTACTCGTCGTCGTCCTGTCCTCCGTCGGTGGATTCAGC	Cloning alpha-tubulin cds into 5' gfp tagging vector in 2nd position for 4-way gateway recombination to make allele replacement construct

UM	1416	GGCGCGCCATGAGAGAGATCATCAGTATCCATATAGGTCAGG	Cloning alpha-tubulin cds into 5' gfp tagging vector in 2nd position for 4-way gateway recombination to make allele replacement construct
UM	1434	GGGGACAAGTTTGTACAAAAAAGCAGGCTCTGGCGCGCCACTTCATAATCTACCTGTGC	Cloning alpha-tubulin 5' targeting sequence in 1st position vector for 4-way gateway recombination to make allele replacement construct
UM	1435	GGGGACAACTTTTGTATACAAAGTTGTGGAAGAGTACGAGCAGCAGC	Cloning alpha-tubulin 5' targeting sequence in 1st position vector for 4-way gateway recombination to make allele replacement construct
UM	1436	GGGGACAACTTTGTATAATAAAGTTGTGGGCTTTTATTTTGAGGCGGAAACGG	Cloning alpha-tubulin 3' targeting sequence in 1st position vector for 4-way gateway recombination to make allele replacement construct
UM	1437	GGGGACCACTTTGTACAAGAAAGCTGGGTAGGCGCGCCGTTAACTGTGGAGTTCTG	Cloning alpha-tubulin 3' targeting sequence in 1st position vector for 4-way gateway recombination to make allele replacement construct
UM	1510	GGGGACAACTTTTCTATACAAAGTTGCTATGGTGAGCAAGGGCGAG	Amplification of GFP sequence for N-terminal GFP tag introduction into locus (2nd position for 3-way gateway recombination)
UM	1511	GGGGACAACTTTATTATACAAAGTTGTCTTGTACAGCTCGTCCATGCC	Amplification of GFP sequence for N-terminal GFP tag introduction into locus (2nd position for 3-way gateway recombination)
UM	1512	GGGGACAACTTTGTATAATAAAGTTGCTAGCACTTCACGGTTTATCAAGTGC	Amplification of ROP4 3' targeting sequence for N-terminal GFP tag introduction into locus (3rd position for 3-way gateway recombination)
UM	1513	GGGGACCACTTTGTACAAGAAAGCTGGGTAGTTTAAACTTCAAGACGTACTTGAGAAGTAGTTATTGGG	Amplification of ROP4 3' targeting sequence for N-terminal GFP tag introduction into locus (3rd position for 3-way gateway recombination)
UM	1514	GGGGACACCTTTGTATACAAAAGTTGCTGTGAGCAAGGGCGAGGAG	Amplification of GFP sequence for GFP-CaaX tag (2nd position for 4-way gateway recombination)
UM	1515	GGGGACAACTTTGTATAGAAAAGTTGGGTGTCACAGAATGACGCACTTGTACAGCTCGTCCATGCC	Amplification of GFP sequence for GFP-CaaX tag (2nd position for 4-way gateway recombination)
UM	1516	GGGGACAACTTTTGTATACAAAGTTGTATTCTTTTGTTTTTTCTTCTTCTTCTGCTTTGG	Amplification of ROP4 5' targeting sequence for GFP-CaaX tag (1st position for 4-way gateway recombination)
UM	1529	GCAATACAACACACTGTGCTTGGG	Genotyping of mCherry-alpha-tubulin stable lines
UM	1540	TCACTCAAGGAACAGCCTGG	Genotyping of ROP3Δ3'utr lines

UM	1541	GCTAGTCAACGCTTC CTTTGCC	Genotyping of ROP3Δ3'utr lines
UM	1552	CACAGGTCCACAATC TCCTTTCC	Genotyping of mCherry-alpha-tubulin stable lines
UM	1498	CATAGCTTTTATGAG CTGGCTTAGT	Expression analysis of ROP4
UM	1499	TATACGACTGGATTT CAGCAGAGAC	Expression analysis of ROP4

REFERENCES

Allal, C., G. Favre, B. Couderc, S. Salicio, S. Sixou, A. D. Hamilton, S. M. Sebti, I. Lajoie-Mazenc and A. Pradines (2000). RHOa prenylation is required for promotion of cell growth and transformation and cytoskeleton organization but not for induction of serum response element transcription. J Biol Chem **275**(40): 31001-31008.

Augustine, R. C., L. Vidali, K. P. Kleinman and M. Bezanilla (2008). Actin depolymerizing factor is essential for viability in plants, and its phosphoregulation is important for tip growth. Plant J **54**(5): 863-875.

Avisar, D., M. Abu-Abied, E. Belausov and E. Sadot (2012). Myosin XIK is a major player in cytoplasm dynamics and is regulated by two amino acids in its tail. J Exp Bot **63**(1): 241-249.

Balagopalan , L., M.-H. Chen, E. R. Geisbrecht and S. M. Abmayr (2006). The CDM superfamily protein MBC directs myoblast fusion through a mechanism that requires phosphatidylinositol 3,4,5-triphosphate binding but is independent of direct interaction with DCrk. Mol Cell Biol **26**(24): 9442-9455.

Basu, D., J. Le, T. Zakharova, E. L. Mallery and D. B. Szymanski (2008). A SPIKE1 signaling complex controls actin-dependent cell morphogenesis through the heteromeric WAVE and ARP2/3 complexes. Proc Natl Acad Sci **105**(10): 4044-4049.

Berken, A., C. Thomas and A. Wittinghofer (2005). A new family of RhoGEFs activates the Rop molecular switch in plants. Nature **436**(7054): 1176-1180.

Bezanilla, M., P. F. Perroud, A. Pan, P. Klueh and R. S. Quatrano (2005). An RNAi system in *Physcomitrella patens* with an internal marker for silencing allows for rapid identification of loss of function phenotypes. Plant Biol (Stuttg) **7**(3): 251-257.

Cheung, A. Y. and H.-m. Wu (2008). Structural and signaling networks for the polar cell growth machinery in pollen tubes. Annu Rev Plant Biol **59**(1): 547-572.

Craddock, C., I. Lavagi and Z. Yang (2012). New insights into Rho signaling from plant ROP/Rac GTPases. Trends Cell Biol **22**(9): 492-501.

Derksen, J., T. Rutten, I. K. Lichtscheidl, A. H. N. Win, E. S. Pierson and G. Rongen (1995). Quantitative analysis of the distribution of organelles in tobacco pollen tubes: implications for exocytosis and endocytosis. Protoplasma **188**(3-4): 267-276.

Dong, Y., D. Pruyne and A. Bretscher (2003). Formin-dependent actin assembly is regulated by distinct modes of Rho signaling in yeast. J Cell Biol **161**(6): 1081-1092.

Eklund, D. M., E. M. Svensson and B. Kost (2010). *Physcomitrella patens*: a model to investigate the role of RAC/ROP GTPase signalling in tip growth. J Exp Bot **61**(7): 1917-1937.

Era, A., M. Tominaga, K. Ebine, C. Awai, C. Saito, K. Ishizaki, K. T. Yamato, T. Kohchi, A. Nakano and T. Ueda (2009). Application of lifeact reveals F-actin dynamics in *Arabidopsis thaliana* and the liverwort, *Marchantia polymorpha*. Plant Cell Physiol **50**(6): 1041-1048.

Fu, Y., H. Li and Z. Yang (2002). The ROP2 GTPase controls the formation of cortical fine F-actin and the early phase of directional cell expansion during Arabidopsis organogenesis. Plant Cell **14**(4): 777-794.

Fu, Y., G. Wu and Z. Yang (2001). ROP Gtpase–dependent dynamics of tip-localized F-actin controls tip growth in pollen tubes. J Cell Biol **152**(5): 1019-1032.

Fu, Y., T. Xu, L. Zhu, M. Wen and Z. Yang (2009). A ROP GTPase signaling pathway controls cortical microtubule ordering and cell expansion in Arabidopsis. Curr Biol **19**(21): 1827-1832.

Furt, F., Y.-C. Liu, J. P. Bibeau, E. Tüzel and L. Vidali (2013). Apical myosin XI anticipates F-actin during polarized growth of *Physcomitrella patens cells*. Plant J **73**(3): 417-428.

Gierlinger, N., T. Keplinger and M. Harrington (2012). Imaging of plant cell walls by confocal Raman microscopy. Nat Protoc **7**(9): 1694-1708.

Gu, Y., Y. Fu, P. Dowd, S. Li, V. Vernoud, S. Gilroy and Z. Yang (2005). A Rho family GTPase controls actin dynamics and tip growth via two counteracting downstream pathways in pollen tubes. J Cell Biol **169**(1): 127-138.

Gu, Y., S. Li, E. M. Lord and Z. Yang (2006). Members of a novel class of Arabidopsis Rho guanine nucleotide exchange factors control Rho GTPase-dependent polar growth. Plant Cell **18**(2): 366-381.

Gu, Y., V. Vernoud, Y. Fu and Z. Yang (2003). ROP GTPase regulation of pollen tube growth through the dynamics of tip-localized F-actin. J Exp Bot **54**(380): 93-101.

Harries, P. A., A. Pan and R. S. Quatrano (2005). Actin-related protein2/3 complex component ARPC1 is required for proper cell morphogenesis and polarized cell growth in *Physcomitrella patens*. Plant Cell **17**(8): 2327-2339.

Hashimoto, K., H. Igarashi, S. Mano, M. Nishimura, T. Shimmen and E. Yokota (2005). Peroxisomal localization of a myosin XI isoform in *Arabidopsis thaliana*. Plant Cell Physiol **46**(5): 782-789.

Hepler, P. K., L. Vidali and A. Y. Cheung (2001). Polarized Cell Growth In Higher Plants. Annu Rev Cell Dev Biol **17**(1): 159-187.

Higaki, T., N. Kutsuna, T. Sano, N. Kondo and S. Hasezawa (2010). Quantification and cluster analysis of actin cytoskeletal structures in plant cells: role of actin bundling in stomatal movement during diurnal cycles in Arabidopsis guard cells. Plant J **61**(1): 156-165.

Hu, C.-D., Y. Chinenov and T. K. Kerppola (2002). Visualization of interactions among bZIP and Rel family proteins in living cells using bimolecular fluorescence complementation. Mol Cell **9**(4): 789-798.

Jaffe, A. B. and A. Hall (2005). Rho GTPases: biochemistry and biology. Annu Rev Cell Dev Biol **21**(1): 247-269.

Jones, M. A., J.-J. Shen, Y. Fu, H. Li, Z. Yang and C. S. Grierson (2002). The Arabidopsis Rop2 GTPase is a positive regulator of both root hair initiation and tip growth. Plant Cell **14**(4): 763-776.

Justus, C., P. Anderhag, J. Goins and M. Lazzaro (2004). Microtubules and microfilaments coordinate to direct a fountain streaming pattern in elongating conifer pollen tube tips. Planta **219**(1): 103-109.

Klahre, U., C. Becker, A. C. Schmitt and B. Kost (2006). Nt-RhoGDI2 regulates Rac/Rop signaling and polar cell growth in tobacco pollen tubes. Plant J **46**(6): 1018-1031.

Klahre, U. and B. Kost (2006). Tobacco RhoGTPase ACTIVATING PROTEIN1 spatially restricts signaling of RAC/Rop to the apex of pollen tubes. Plant Cell **18**(11): 3033-3046.

Kozubowski, L., K. Saito, J. M. Johnson, A. S. Howell, T. R. Zyla and D. J. Lew (2008). Symmetry-breaking polarization driven by a Cdc42p GEF-PAK complex. Curr Biol **18**(22): 1719-1726.

Lancelle, S. and P. K. Hepler (1992). Ultrastructure of freeze-substituted pollen tubes ofLilium longiflorum. Protoplasma **167**(3-4): 215-230.

Lavy, M., D. Bloch, O. Hazak, I. Gutman, L. Poraty, N. Sorek, H. Sternberg and S. Yalovsky (2007). A Novel ROP/RAC effector links cell polarity, root-meristem maintenance, and vesicle trafficking. Curr Biol **17**(11): 947-952.

Lee, K. J. D., Y. Sakata, S.-L. Mau, F. Pettolino, A. Bacic, R. S. Quatrano, C. D. Knight and J. P. Knox (2005). Arabinogalactan proteins are required for apical cell extension in the moss *Physcomitrella patens*. Plant Cell **17**(11): 3051-3065.

Li, H., Y. Lin, R. M. Heath, M. X. Zhu and Z. Yang (1999). Control of pollen tube tip growth by a Rop GTPase–dependent pathway that leads to tip-localized calcium influx. Plant Cell **11**(9): 1731-1742.

Li, J.-F. and A. Nebenführ (2007). Organelle targeting of myosin XI is mediated by two globular tail subdomains with separate cargo binding sites. J Biol Chem **282**(28): 20593-20602.

Li, S., Y. Gu, A. Yan, E. Lord and Z.-B. Yang (2008). RIP1 (ROP Interactive Partner 1)/ICR1 marks pollen germination sites and may act in the ROP1 pathway in the control of polarized pollen growth. Mol Plant **1**(6): 1021-1035.

Lin, D., L. Cao, Z. Zhou, L. Zhu, D. Ehrhardt, Z. Yang and Y. Fu (2013). Rho GTPase signaling activates microtubule severing to promote microtubule ordering in Arabidopsis. Curr Biol **23**(4): 290-297.

Lord, E. M. and J.-C. Mollet (2002). Plant cell adhesion: A bioassay facilitates discovery of the first pectin biosynthetic gene. Proc Natl Acad Sci **99**(25): 15843-15845.

Lovy-Wheeler, A., L. Cárdenas, J. G. Kunkel and P. K. Hepler (2007). Differential organelle movement on the actin cytoskeleton in lily pollen tubes. Cell Motil Cytoskeleton **64**(3): 217-232.

Lovy-Wheeler, A., K. Wilsen, T. Baskin and P. Hepler (2005). Enhanced fixation reveals the apical cortical fringe of actin filaments as a consistent feature of the pollen tube. Planta **221**(1): 95-104.

Mathur, J., N. Mathur, B. Kernebeck and M. Hülskamp (2003). Mutations in actin-related proteins 2 and 3 affect cell shape development in Arabidopsis. Plant Cell **15**(7): 1632-1645.

Mathur, J., N. Mathur, V. Kirik, B. Kernebeck, B. P. Srinivas and M. Hülskamp (2003). Arabidopsis CROOKED encodes for the smallest subunit of the ARP2/3 complex and controls cell shape by region specific fine F-actin formation. Development **130**(14): 3137-3146.

Molendijk, A. J., F. Bischoff, C. S. V. Rajendrakumar, J. Friml, M. Braun, S. Gilroy and K. Palme (2001). *Arabidopsis thaliana* Rop GTPases are localized to tips of root hairs and control polar growth. EMBO J **20**(11): 2779-2788.

Mooseker, M. S. and R. E. Cheney (1995). Unconventional myosins. Annu Rev Cell Dev Biol **11**(1): 633-675.

Muhlhausen, S. and M. Kollmar (2013). Whole genome duplication events in plant evolution reconstructed and predicted using myosin motor proteins. BMC Evol Biol **13**(1): 202.

Oda, Y. and H. Fukuda (2012). Initiation of Cell Wall Pattern by a Rho- and microtubule-driven symmetry breaking. Science **337**(6100): 1333-1336.

Ojangu, E.-L., K. Tanner, P. Pata, K. Jarve, C. Holweg, E. Truve and H. Paves (2012). Myosins XI-K, XI-1, and XI-2 are required for development of pavement cells, trichomes, and stigmatic papillae in Arabidopsis. BMC Plant Biol **12**(1): 81.

Ojangu, E. L., K. Järve, H. Paves and E. Truve (2007). *Arabidopsis thaliana* myosin XIK is involved in root hair as well as trichome morphogenesis on stems and leaves. Protoplasma **230**(3-4): 193-202.

Oldenbourg, R. and G. Mei (1995). New polarized light microscope with precision universal compensator. J Microscopy **180**(2): 140-147.

Peremyslov, V. V., A. L. Klocko, J. E. Fowler and V. V. Dolja (2012). Arabidopsis myosin XI-K localizes to the motile endomembrane vesicles associated with F-actin. Front Plant Sci **3**: 184.

Peremyslov, V. V., E. A. Morgun, E. G. Kurth, K. S. Makarova, E. V. Koonin and V. V. Dolja (2013). Identification of myosin XI receptors in Arabidopsis defines a distinct class of transport vesicles. Plant Cell **25**(8): 3022-3038.

Peremyslov, V. V., A. I. Prokhnevsky, D. Avisar and V. V. Dolja (2008). Two class XI myosins function in organelle trafficking and root hair development in Arabidopsis. Plant Physiol **146**(3): 1109-1116.

Peremyslov, V. V., A. I. Prokhnevsky and V. V. Dolja (2010). Class XI myosins are required for development, cell expansion, and F-actin organization in Arabidopsis. Plant Cell **22**(6): 1883-1897.

Prigge, M. J. and M. Bezanilla (2010). Evolutionary crossroads in developmental biology: *Physcomitrella patens*." Development **137**(21): 3535-3543.

Prokhnevsky, A. I., V. V. Peremyslov and V. V. Dolja (2008). Overlapping functions of the four class XI myosins in Arabidopsis growth, root hair elongation, and organelle motility. Proc Natl Acad Sci **105**(50): 19744-19749.

Qiu, J.-L., R. Jilk, M. D. Marks and D. B. Szymanski (2002). The Arabidopsis SPIKE1 gene is required for normal cell shape control and tissue development. Plant Cell **14**(1): 101-118.

Reddy, A. and I. Day (2001). Analysis of the myosins encoded in the recently completed Arabidopsis thaliana genome sequence. Genome Biol **2**(7): 1-19.

Reisen, D. and M. Hanson (2007). Association of six YFP-myosin XI-tail fusions with mobile plant cell organelles. BMC Plant Biol **7**(1): 6.

Rensing, S. A., D. Lang, A. D. Zimmer, A. Terry, A. Salamov, H. Shapiro, T. Nishiyama, P.-F. Perroud, E. A. Lindquist, Y. Kamisugi, T. Tanahashi, K. Sakakibara, T. Fujita, K. Oishi, T. Shin-I, Y. Kuroki, A. Toyoda, Y. Suzuki, S.-i. Hashimoto, K. Yamaguchi, S. Sugano, Y. Kohara, A. Fujiyama, A. Anterola, S. Aoki, N. Ashton, W. B. Barbazuk, E. Barker, J. L. Bennetzen, R. Blankenship, S. H. Cho, S. K. Dutcher, M. Estelle, J. A. Fawcett, H. Gundlach, K. Hanada, A. Heyl, K. A. Hicks, J. Hughes, M. Lohr, K. Mayer, A. Melkozernov, T. Murata, D. R. Nelson, B. Pils, M. Prigge, B. Reiss, T. Renner, S. Rombauts, P. J. Rushton, A. Sanderfoot, G. Schween, S.-H. Shiu, K. Stueber, F. L. Theodoulou, H. Tu, Y. Van de Peer, P. J. Verrier, E. Waters, A. Wood, L. Yang, D. Cove, A. C. Cuming, M. Hasebe, S. Lucas, B. D. Mishler, R. Reski, I. V. Grigoriev, R. S. Quatrano and J. L. Boore (2008). The Physcomitrella genome reveals evolutionary insights into the conquest of land by plants. Science **319**(5859): 64-69.

Roberts, A. W., E. M. Roberts and C. H. Haigler (2012). "Moss cell walls: structure and biosynthesis." Front Plant Sci **3**.

Saidi, Y., A. Finka, M. Chakhporanian, J.-P. Zrÿd, D. Schaefer and P. Goloubinoff (2005). Controlled expression of recombinant proteins in *Physcomitrella patens* by a conditional heat-shock promoter: a tool for plant research and biotechnology. Plant Mol Biol **59**(5): 697-711.

Sampathkumar, A., J. J. Lindeboom, S. Debolt, R. Gutierrez, D. W. Ehrhardt, T. Ketelaar and S. Persson (2011). Live cell imaging reveals structural associations between the actin and microtubule cytoskeleton in Arabidopsis. Plant Cell **23**(6): 2302-2313.

Sattarzadeh, A., M. Hanson and E. Schmelzer (2013). Arabidopsis myosin XI sub-domains homologous to the yeast myo2p organelle inheritance sub-domain target subcellular structures in plant cells. Front Plant Sci **4**.

Sattarzadeh, A., E. Schmelzer and M. R. Hanson (2011). Analysis of organelle targeting by DIL domains of the Arabidopsis myosin XI family. Front Plant Sci **2**: 72.

Schaefer, D. G. and J.-P. Zrÿd (1997). Efficient gene targeting in the moss *Physcomitrella patens*. Plant J **11**(6): 1195-1206.

Shimmen, T. and E. Yokota (2004). Cytoplasmic streaming in plants. Curr Opin Cell Biol **16**(1): 68-72.

Singh, M. K., F. Ren, T. Giesemann, C. D. Bosco, T. P. Pasternak, T. Blein, B. Ruperti, G. Schmidt, K. Aktories, A. J. Molendijk and K. Palme (2013). Modification of plant Rac/Rop GTPase signalling using bacterial toxin transgenes. Plant J **73**(2): 314-324.

Smith, S. E., B. Rubinstein, I. Mendes Pinto, B. D. Slaughter, J. R. Unruh and R. Li (2013). Independence of symmetry breaking on Bem1-mediated autocatalytic activation of Cdc42. J Cell Biol **202**(7): 1091-1106.

Sorek, N., O. Gutman, E. Bar, M. Abu-Abied, X. Feng, M. P. Running, E. Lewinsohn, N. Ori, E. Sadot, Y. I. Henis and S. Yalovsky (2011). Differential effects of prenylation and S-acylation on type I and II ROPS membrane interaction and function. Plant Physiol **155**(2): 706-720.

Sorek, N., L. Poraty, H. Sternberg, E. Bar, E. Lewinsohn and S. Yalovsky (2007). Activation status-coupled transient S-acylation determines membrane partitioning of a plant Rho-related GTPase. Mol Cell Biol **27**(6): 2144-2154.

Sparkes, I. A., N. A. Teanby and C. Hawes (2008). Truncated myosin XI tail fusions inhibit peroxisome, Golgi, and mitochondrial movement in tobacco leaf epidermal cells: a genetic tool for the next generation. J Exp Bot **59**(9): 2499-2512.

Tamura, K., K. Iwabuchi, Y. Fukao, M. Kondo, K. Okamoto, H. Ueda, M. Nishimura and I. Hara-Nishimura (2013). Myosin XI-I links the nuclear membrane to the cytoskeleton to control nuclear movement and shape in Arabidopsis. Current Biol **23**(18): 1776-1781.

van Gisbergen, P. A. C. and M. Bezanilla (2013). Plant formins: membrane anchors for actin polymerization. Trends Cell Biol **23**(5): 227-233.

van Gisbergen, P. A. C., M. Li, S.-Z. Wu and M. Bezanilla (2012). Class II formin targeting to the cell cortex by binding PI(3,5)P2 is essential for polarized growth. J Cell Biol **198**(2): 235-250.

Venus, Y. and R. Oelmüller (2013). Arabidopsis ROP1 and ROP6 influence germination time, root morphology, the formation of F-Actin bundles, and symbiotic fungal interactions. Mol Plant **6**(3): 872-886.

Vidali, L., R. C. Augustine, K. P. Kleinman and M. Bezanilla (2007). Profilin is essential for tip growth in the moss *Physcomitrella patens*. Plant Cell **19**(11): 3705-3722.

Vidali, L., G. M. Burkart, R. C. Augustine, E. Kerdavid, E. Tüzel and M. Bezanilla (2010). "Myosin XI Is essential for tip growth in *Physcomitrella patens*. Plant Cell **22**(6): 1868-1882.

Vidali, L., S. T. McKenna and P. K. Hepler (2001). Actin polymerization is essential for pollen tube growth. Mol Biol Cell **12**(8): 2534-2545.

Vidali, L., C. M. Rounds, P. K. Hepler and M. Bezanilla (2009a). Lifeact-mEGFP reveals a dynamic apical F-actin network in tip growing plant cells. PLoS One **4**(5): e5744.

Vidali, L., P. A. C. van Gisbergen, C. Guérin, P. Franco, M. Li, G. M. Burkart, R. C. Augustine, L. Blanchoin and M. Bezanilla (2009b). Rapid formin-mediated actin-filament elongation is essential for polarized plant cell growth. Proc Natl Acad Sci **106**(32): 13341-13346.

Walter, N. and C. Holweg (2008). Head-neck domain of Arabidopsis myosin XI, MYA2, fused with GFP produces F-actin patterns that coincide with fast organelle streaming in different plant cells. BMC Plant Biol **8**(1): 74.

Weiner, M. P., G. L. Costa, W. Schoettlin, J. Cline, E. Mathur and J. C. Bauer (1994). Site-directed mutagenesis of double-stranded DNA by the polymerase chain reaction. Gene **151**(1–2): 119-123.

Win, A. N., B. Knuiman, E. Pierson, H. Geurts, H. P. Kengen and J. Derksen (1996). Development and cellular organization of *Pinus sylvestris* pollen tubes. Sex Plant Reproduction **9**(2): 93-101.

Winge, P., T. Brembu, R. Kristensen and A. M. Bones (2000). Genetic structure and evolution of RAC-GTPases in *Arabidopsis thaliana*. Genetics **156**(4): 1959-1971.

Wu, G., Y. Gu, S. Li and Z. Yang (2001). A genome-wide analysis of Arabidopsis Rop-interactive CRIB motif–containing proteins that act as Rop GTPase targets. Plant Cell **13**(12): 2841-2856.

Wu, G., H. Li and Z. Yang (2000). Arabidopsis RopGAPs are a novel family of Rho GTPase-activating proteins that require the Cdc42/Rac-interactive binding motif for Rop-specific GTPase stimulation. Plant Physiol **124**(4): 1625-1636.

Wu, S.-Z., J. A. Ritchie, A.-H. Pan, R. S. Quatrano and M. Bezanilla (2011). Myosin VIII regulates protonemal patterning and developmental timing in the moss *Physcomitrella patens*. Mol Plant **4**(5): 909-921.

Xu, T., M. Wen, S. Nagawa, Y. Fu, J.-G. Chen, M.-J. Wu, C. Perrot-Rechenmann, J. Friml, A. M. Jones and Z. Yang (2010). Cell surface- and Rho GTPase-based auxin signaling controls cellular interdigitation in Arabidopsis. Cell **143**(1): 99-110.

Yokota, E., A. R. McDonald, B. Liu, T. Shimmen and B. A. Palevitz (1995). Localization of a 170 kDa myosin heavy chain in plant cells. Protoplasma **185**(3-4): 178-187.

Yokota, E., S. Ueda, K. Tamura, H. Orii, S. Uchi, S. Sonobe, I. Hara-Nishimura and T. Shimmen (2009). An isoform of myosin XI is responsible for the translocation of endoplasmic reticulum in tobacco cultured BY-2 cells. J Exp Bot **60**(1): 197-212.

Zeng, Y., M. Himmel and S.-Y. Ding (2012). Coherent Raman microscopy analysis of plant cell walls. Biomass Conversion. M. E. Himmel, Humana Press. **908:** 49-60.

Zhang, C., S. O. Kotchoni, A. L. Samuels and D. B. Szymanski (2010). SPIKE1 signals originate from and assemble specialized domains of the endoplasmic reticulum. Curr Biol **20**(23): 2144-2149.

Zhang, Y. and S. McCormick (2007). A distinct mechanism regulating a pollen-specific guanine nucleotide exchange factor for the small GTPase Rop in *Arabidopsis thaliana*. Proc Natl Acad Sci **104**(47): 18830-18835.